UNIVERSITÁ DEGLI STUDI DI PAVIA
Facoltà di Ingegneria Corso di Laurea Specialistica
in Ingegneria Biomedica

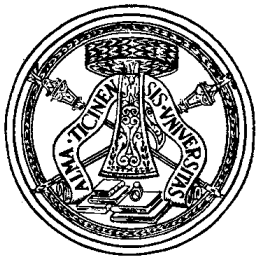

Constitutive modelling of a biodegradable polymer (Poly-L-Lactic Acid) for endovascular applications

Modellizzazione costitutiva di un polimero biodegradabile (Poly-L-Lactic Acid) per applicazioni endovascolari

Supervisor:
Ferdinando Auricchio

Co-Supervisor:
Daniele Dondi

Author:
Carla Masia

Academic Year 2007/08

To my family
a lighthouse always lit and a haven for any storm

Contents

Sommario

Oggetto del seguente lavoro di tesi è la modellizzazione meccanica di un particolare polimero biodegradabile: l'acido poli-L-lattico, anche noto come PLLA. Il polimero possiede caratteristiche chimiche e meccaniche che soddisfano i requisiti necessari per poter essere impiegato in ambito medico. Studi in letteratura hanno evidenziato le peculiarità di tale materiale come buon candidato per la realizzazione di dispositivi biodegradabili impiantabili, quali stents vascolari.

La degradazione di questo particolare poliestere è stata oggetto di studi approfonditi, soprattutto da un punto di vista chimico. Tuttavia, gli studi rivolti alla risposta meccanica dello stesso, quando soggetto a degradazione, sono stati limitati.

Il seguente elaborato è diviso in 6 macro-sezioni:

- Capitolo I: verranno esposte in breve le patologie cui è spesso soggetto il sistema circolatorio e relative modalità di intervento. Si discuteranno i progressi tecnologici che sono stati fatti fino ad oggi per arrivare all'attuale stato dell'arte.

- Capitolo II: verranno descritte le caratteristiche chimiche generali della famiglia di materiali cui il PLLA appartiene.

- Capitolo III: verranno introdotti i concetti generali sulla meccanica del continuo, necessari a comprendere la modellizzazione costitutiva che è stata svolta.

- Capitolo IV: verrà esposto il lavoro di tesi svolto presso il Dipartimento di Meccanica Strutturale dell'Università di Ingegneria di Pavia. Il comportamento del polimero oggetto di studio, verrà modellizzato in termini meccanici sulla base di dati trovati in letteratura.

- Capitolo V: sarà presentato uno studio costitutivo del polimero condotto tramite il codice a elementi finiti Abaqus.
- Capitolo VI: in quest'ultima parte del lavoro di tesi verranno riportati dei risultati preliminari ottenuti in seguito a sperimentazioni sul materiale ed eseguiti presso il Dipartimento di Chimica dell'Università di Pavia. Più precisamente, dati legati alla risposta chimica di film realizzati in PLLA, soggetti a degradazione e deformazione quando siti in un ambiente salino.

Abstract

The purpose of the following thesis is to describe the mechanical modelling of a poly L-lactic acid (PLLA), a particular biodegradable polymer. Such material was chosen because of its peculiar mechanical and chemical properties, that make it suitable for biodegrable implantable devices such as vascular stents.

Most studies regarding the PLLA were mostly focused on its physical response once implanted into the organism. Most analysis and in-depth studies dealt with how the degradation of the material relates to the variation of its molecular weight and loss of mass. On the other hand, studies focusing on its mechanical response to degradation have been very few.

The following script is divided into six parts:

- Chapter I: we will briefly explain the main pathologies affecting the circulation system and how they are treated. We will describe the technologic advances that have been achieved.
- Chapter II: we will discuss the general chemical properties associated with the family of polymers to which the PLLA belongs.
- Chapter III: we will introduce some broad concepts about continuum mechanics, which are required to understand the constitutive modelling developed and the reason behind our choices.
- Chapter IV: we will present the main focus of the present thesis conducted at the Department of Structural Mechanics of the University of Pavia. The behavior of the polymer we have examinated will be mechanically modelled with respect to the literature data.
- Chapter V: we will present a brief excursus summarizing the constitutive analysis of the material performed through Abaqus.

- Chapter VI: in this last part of the thesis we will report some preliminary results we have obtained following the tests performed on PLLA films, at the Department of Chemistry of the University of Pavia.

Acknowledgment

This thesis would not have been possible without the support of many people. I wish to express my gratitude to my supervisor, Prof. Dr. F. Auricchio who was helpful and offered invaluable assistance, support and guidance.

Deep gratitude are also due to the staff of the technicians that have shown an incredible patience to my requests.

Many thanks go in particular to Prof. Dr. A. Faucitano and to his Collaborators, in particular to Daniele Dondi, for their infinite willingness shown during the course of this thesis.

Special thanks also to all my friends, not forgetting my bestfriends who always been present.

Last, and most importantly I wish to express my love and gratitude for my beloved families, for their understanding and endless love, through the duration of my studies.

I have inevitably missed some people but I would like to thank them and let them know that I appreciate their support from the bottom of my heart.

Chapter 1

Introduction

Clinical introduction of coronary stenting dates back to 1987, when Sigwart et al. implanted a stent in humans and described its use for blood vessel scaffolding after balloon angioplasty [53]. Stenting procedure has now become the standard in treating coronary artery diseases [44].

1.1 Vascular system and its main pathologies

The blood vessels are part of the circulatory system and transport blood throughout the body. The most important vessels in the system are the capillaries, arteries and veins. The arteries and veins have the same basic structure: there are three layers, from inside to outside, while the capillaries have only one thick cell layer (Figure 1.1):

- tunica intima (the thinnest layer): delimits the vessel wall towards the lumen of the vessel and comprises its endothelial lining (typically simple, squamous) and associated connective tissue. The endothelial cells are in direct contact with the blood flow.

- tunica media (the thickest layer): is formed by a layer of circumferential smooth muscle and variable amounts of connective tissue. A second layer of elastic fibers, the external elastic lamina, is located beneath the smooth muscle.

- tunica adventila: consists mainly of connective tissue fibres. The tunica adventitia blends with the connective tissue surrounding the vessel. [64].

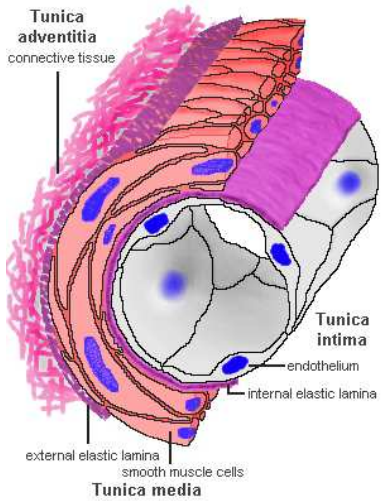

Figure 1.1: Artery wall components

Blood vessels play a role in virtually every medical condition, for example: cancer cannot progress unless the tumor causes angiogenesis (formation of new blood vessels) to supply the malignant cells' metabolic demand; damage, due to trauma or spontaneous, may lead to haemorrhage due to mechanical damage to the vessel endothelium; occlusion of the blood vessel by atherosclerotic plaque, by an embolised blood clot or a foreign body leads to downstream ischemia (insufficient blood supply) and possibly necrosis. In reference to this last condition, vessel occlusion tends to be a positive feedback system: an occluded vessel creates eddies in the normally laminar flow or plug flow blood currents. These eddies create abnormal fluid velocity gradients which push blood elements such as cholesterol or chylomicron bodies to the endothelium. These deposit onto the arterial walls which are already partially occluded and build upon the blockage.

1.1.1 Atherosclerosis

Atherosclerosis is a disease affecting arterial blood vessels, it can start at the age of 20 years and increases with age, it's the prime cause of cardiovascular disease, the main cause of death in the Western world.

Also called the *hardening* of the arteries, atherosclerosis is a condition characterized by accumulation of fatty deposits, platelets, neutrophils, monocytes and macrophages throughout the tunica intima and eventually

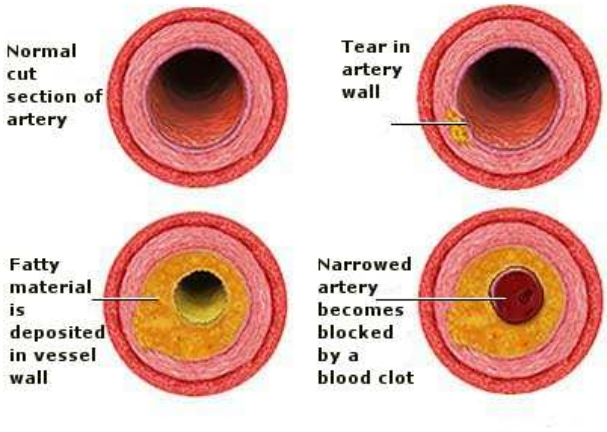

Figure 1.2: Cross-section of an artery subjected to atherosclerosis

into the tunica media (Figure 1.2). These substances create blockages or narrow the vessel in a way that reduces blood flow to the myocardium. Studies indicate that atherosclerosis involves a repetitious inflammatory response to artery wall injury and an alteration in the biophysical and biochemical properties of the arterial walls [55]. Arteries most often affected include the coronaries, the aorta, and the cerebral arteries [5]. It should be noted that not all deposits develop into more advanced lesions. The reason why some fatty deposits continue to develop is unknown, although genetic and environmental factors are involved [55]. Calnan [5] in his book cited that the narrowing of the arteries is, in some respects, a natural product of aging. However, there are more specific theories and two are popular at the moment:

1. fats move into the arterial wall from the blood where they help produce large amounts of scar tissue;

2. blood clots, that form the arterial wall, are integrated into the wall where they degenerate into the fat deposits.

The plaques themselves become the focal point for the formation of more blood clots which can sometimes completely block off an artery. In addition, a piece of plaque may break off and move down the artery until it blocks it. However, the main effect of atherosclerosis is to cause narrowing (stenosys) of the arteries and the severity of the condition is dependent on the location

of these deposits.

Angioplasty and angioplasty with vascular stenting are minimally invasive procedures commonly used to treat conditions that involve a narrowing or blockage of arteries or veins throughout the body.

In the angioplasty procedure, imaging techniques are used to guide a balloon-tipped catheter, a long, thin plastic tube, into an artery or vein and advance it to where the vessel is narrow or blocked. The balloon is then inflated to open the vessel, deflated and removed. In vascular stenting, which may be performed with angioplasty, a small wire mesh tube called a *stent* is placed in the newly opened artery or vein to help it remain open. A typical angioplasty with vascular stenting procedure follows these steps:

1. the cardiologist threads a narrow catheter (a tube) containing a catheter from the groin area into the blocked vessel (Figure 1.3.A);

2. the doctor opens the blocked vessel using balloon angioplasty, in which the surgeon passes a tiny deflated balloon through the catheter to the vessel;

3. the balloon is inflated to compress the plaque against the walls of the artery, flattening it out so that blood can once again flow through the blood vessel freely;

4. to keep the artery open afterwards, doctors use a device called *stent*. (In some cases, a stent may be used as the initial opening device instead of balloon angioplasty (Figure 1.3.B));

5. once in place, the stent pushes against the wall of the artery to keep it open (Figure 1.3.C).

Angioplasty with vascular stenting procedure presents such benefits as:

- they are less invasive and relatively low-risk and low-cost treatments compared to surgical interventions such as bypass surgery;

- no general anesthetic is required in the majority of patients, local anesthesia will usually suffice;

- no surgical incision is needed, just a small nick in the skin that does not have to be stitched closed;

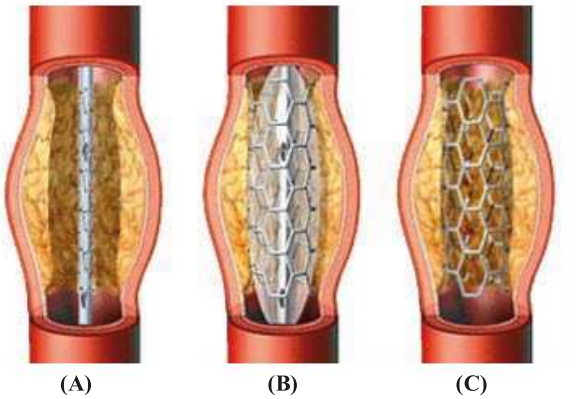

Figure 1.3: (A) Stent insertion, (B) Stent expansion, (C) Stent remain in coronary artery

- the patients are able to return to normal activities shortly after the procedure.

Nevertheless there are some risks:

- the use of metal stents can cause infection, blood clots, or bleeding;
- some other rare complications may occur because of coronary stents: chest pain, heart attacks, or tearing of the blood vessel;
- the stent can move out of place (*stent migration*);
- in some cases, plaques may reappear in the stented artery (*in-stent restenosis* (ISR)).

Before addressing the problem of ISR, we should provide some preliminary concepts.

Restenosis, which is defined as the arterial healing response after injury incurred during transluminal coronary revascularization, is considered to be a local vascular manifestation of the general biologic response to injury. Iatrogenic injuries[1] of the blood vessel lead to the release of numerous vasoactive, thrombogeni, and mitogenic factors which prompt a cascade of molecular and cellular events within the vascular wall, and within this cascade, two major processes can be discerned: arterial remodeling and neointimal hyperplasia [34], [20].

[1] An iatrogenic injury is an injury caused by a medical procedure.

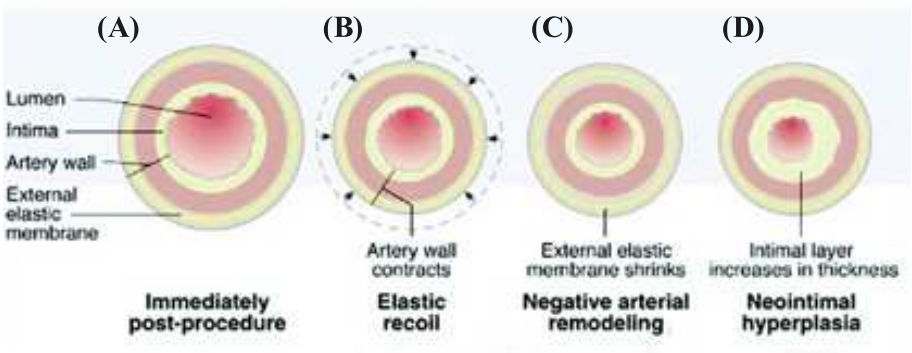

Figure 1.4: Processes of restenosis: (A) Immediately post procedure, (B) Elastic recoil, (C) Negative arterial remodeling, (D) Neointimal hyperplasia

Coronary artery remodeling

This process implies structural changes in the vessel wall in response to various pathophysiologic conditions. Although the classification of remodeling is unclear, it is hypothesized that "the adaptive, positive-outward remodeling is a reactive and compensatory response to stress. The maladaptive negative-inward constrictive remodeling (Figure 1.4.C) is a passive atherosclerotic condition in which the vessel becomes stiffer" [13]. Intravascular ultrasound (IUVS) has demonstrated that negative remodeling is the main component responsible for restenosis in post-PTCA lesions [33]. Stents, providing mechanical scaffolding, have eliminated vessels recoil and restenosis due to long-term negative remodeling following PTCA, however, long-term pressure of the stent struts against the vessel wall is disadvantageous and leads to neointimal tissue proliferation, either focally or diffusely over the length of the stent.

Neointimal hyperplasia

Neointimal tissue proliferation, or "neointimal hyperplasia"[2] (Figure 1.4.D) implies that the new layer of arterial intima, composed principally of smooth cells and extracellular matrix, migrates and proliferates from the *media*.

The second major drawback arising from coronary stenting is called in-stent restenosis (ISR).

[2]Hyperplasia: gradual biological process that leads to growth in the volume of an organ or tissue through an increase in the number of cells that constitute it.

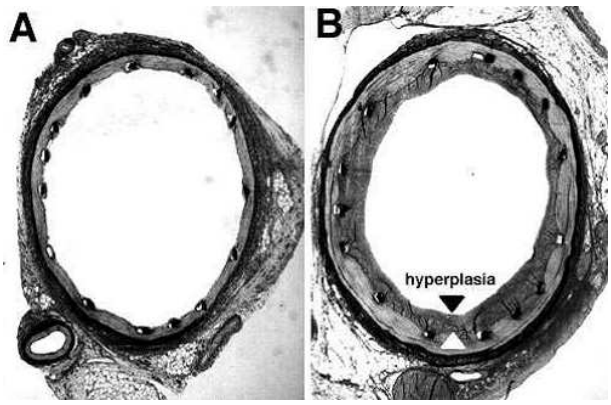

Figure 1.5: In stent restenosis. Pig coronary artery 3 days (A) and (B) 28 days after stenting. Smooth muscle cells have begun to migrate and proliferate in response to stent placement.

1.1.2 In-stent restenosis

ISR is fundamentally different from restenosis associated with PTCA and can be considered as a chronic disease spawned through stenting: tissue repair processes are not only exaggerated due to the high-pressure technique of stent deployment, but also persistently aggravated because the enmeshed wires act as a chronic injury/inflammatory stimulus.

Following the damage incurred on the endothelial barrier at the site of balloon inflation, the extracellular matrix can become exposed. This leads to the hyperproliferation of smooth muscle cells that move into the intima, where they cluster and form a lesion (Figure 1.5.B). The tissue in this region becomes thick and scarred, and the artery undergoes a subsequent remodelling of its structure. The end result is a redevelopment of arterial blockage and obstructed blood flow. A small accumulation of smooth muscle cells is desirable because it allows a thin layer of endothelial cells to accumulate on the inside of the stent and form a smooth cover, incorporating the device into the artery itself and reducing the tendency for clotting. This process, called *endothelialization*, is important in preventing the complication of thrombosis. Patients tipically take an anticlotting drug for six months after stenting.

Although stenting reduces the rate or restenosis, bar metal stent (BMS) can still result in re-blocking (tipically at six-months) in about 25% of cases, necessitating a repeat procedure. The incidence of ISR is particularly high

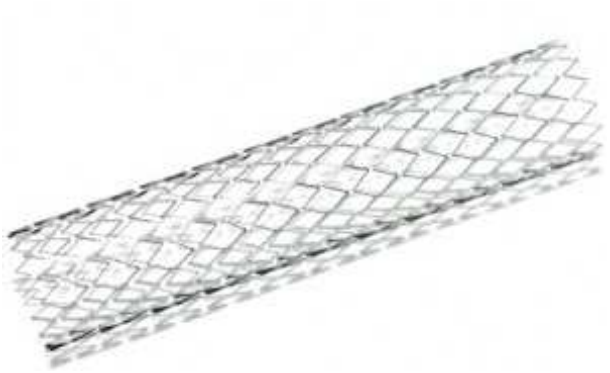

Figure 1.6: Metal stent

in cases where stents are implanted in complex lesions involving bifurcations, long lesions and small vessels or in patients with diabetes. In addition to the obvious clinical complications imposed by ISR, the lesion sites are effectively inaccessible for subsequent surgical revascularization. ISR has seriously impeded the success of stent-based interventional revascularization, and defeating ISR has become as important a challenge as defeating restenosis after angioplasty procedure [38].

1.2 Stents

Vascular stenting has proven to be an effective treatment option for most patients with atherosclerosis. Since the advent of balloon angioplasty, the popularity of the procedure as an alternative to invasive artery bypass graft surgery has grown steadily. Intracoronary scaffolds, or stents are essentially tubular scaffolds (Figure 1.6) comprised of a mesh deployed inside the artery, blood vessel, or other duct (such as one that carries urine) to hold the structure open and restore blood flow. They solve the problem of abrupt closure of arteries following balloon angioplasty and prevent immediate heart attacks.

To function properly and remain in place, stents are designed to be larger in diameter than the healthy artery. As the artery is distended beyond its physiologic limits, pathologic stresses are induced in the artery wall and the artery may be irreversibly damaged. Even in cases wherein acute tissue damage is minimal, cellular response to the new stress environment created by the stent can be problematic [63].

1.2.1 Ideal stent

An ideal stent should posses the physical properties required to perform its mechanical function:

- it should provide adequate support to the wall of a duct;
- it should keep the lumen open during healing;
- after the arterial wall has healed, the body should be able to bioabsorb it and its breakdown products must be biocompatible [71].

The outside diameter of the stent should be small when it is inserted because it will be usually implanted through small ducts, which are liable to damage during the insertion process. The property of self-expansion is thus highly desirable. The outside diameter of an ideal stent is small when it is inserted and after the insertion it expands rapidly against the walls of the duct. Expansion fastens the stent so that migration will not occur. Expansion can be slow or rapid depending on the processing method [69].

Stents are usually made of metals [30], plastics [27], shape memory metal alloys [40] or biodegradable materials [41], [54].

1.2.2 Permanent metallic implants vs. degradable vascular implants (DVI)

Nowadays, permanent metallic implants are key treatment options in cardiovascular intervention but specific drawbacks limit their more widespread use. Once implanted, the stent is expected to remain inside the treated blood vessel for the rest of the patient's life. From a clinical point of view, the permanent implantation is unnecessary since the occluded artery undergoes a 6- to 12- month-long remodelling process [48]. The continued presence of stents may inhibit the ongoing arterial remodelling and provoke in stent-restenosis [19]. Moreover, even though considered as corrosion resistant, stent materials such as austenitic stainless steel and Ni-Ti alloy, are evidently prone to release their metallic ions *in vivo* [36], [52]. Specific metallic ions, such as those potentially released from nickel, chrome and molybdenum, have been categorized as potentially carcinogenic by International Agency for Research on Cancer (IARC) [37]. Other limitations include thrombogenicity, permanent physical irritation, mismatches in mechanical behavior between stented and non-stented vessel areas (the appliance is mechanically more rigid than

surrounding tissue), long-term endothelial dysfunction, inability to adapt to growth, non-permissive or disadvantageous characteristics for later surgical revascularisation, and chronic inflammatory local reactions. Considering those short-term complications with permanently implanted stents, a biodegradable stent could represent the ideal solution [62]. This stent is expected to scaffold the arterial wall until the healing process is completed, then it is supposed to degrad and be expelled from the body.

Biodegradable implants are of special interest in medical applications. They offer more physiological repair, a temporary longitudinal and radial straightening effect, allowing the remodelling of the artery. They allow a late remodelling and are optimum for local drug (or gene) delivery, have a lower risk of late stent thrombosis after brachytherapy, and do not restrict the chance of surgical revascularization. These implants are said to be capable of *"fulfilling the mission and stepping away"*. Biodegradable implants may act as a new biomedical tool satisfying the requirements of compatibility and integration" [73].

1.2.3 Biodegradable stents

Currently, most of the biodegradable implants are polymer based, but metallic ones are also emerging. In respect to the mechanical strength, they provide a better solution but also show problems related to an excessive rate of degradation (or rather corrosion, since we are talking about metals).

Magnesium based alloys stents

As a new generation of biodegradable metallic materials, magnesium and magnesium alloys have gained interest in the recent years, they are generally considered as candidate materials for biodegradable orthopaedic implants [58] and vascular stents.

Magnesium is biocompatible[3] and is also essential to the human metabolism as a cofactor for many enzymes [75]. It has also been reported that magnesium forms soluble and non-toxic oxides in body fluid that are easily excreted with the urine [46]. Magnesium alloys do not have negative influences on the body as long as the concentration of $Mg^{2+}-$ions is in an

[3]Biocompatible materials are intended to interface with biological systems to evaluate, treat, augment or replace any tissue, organ or function of the body [6].

acceptable range [46]. Mechanical properties such as tensile yield strength[4] and Young's modulus[5] are better than those of polymeric implant materials.

Several studies highlighting the potential of different magnesium-based alloys, such as AZ31, AZ91, LAE442 [74], AM60B [29] and WE43 [74] [39], have been reported recently. The implantation of stents prototypes made of AE21 in pigs confirmed the potential of magnesium alloys as biodegradable stent material. Recently, stent prototypes made of WE43 were pre-clinically implanted in lower limb ischemia in adult patients [39] and used to treat congenital heart diseases in newborn babies [77], [49]. However, magnesium alloys still showed rapid corrosion rate both *in vivo* and *in vitro* [74]. This could lead to premature failure of a stent before the arterial remodelling process is completed.

From a material science and engineering point of view, finding the optimal alloy composition for degradable stents is not a trivial task. Among the number of requirements for the selection of the alloy and its specific composition, the following need to be kept into account:

- mechanical properties, including elasticity, ductility, elastic yield and resistance to rupture (in particular after the deployment required by the implantation of the stent). Ideally, these mechanical properties should be as close as possible to these of stainless steel, which today represents the referred standard for clinicians and industrials;

- the mechanical properties as a function of the degradation time. Ideally, the corrosion process will not affect the mechanical properties until the physiological arterial remodeling (after stenting) will be completed;

- the corrosion process that the alloys will undergo *in vivo* should not clinically induce negative side effects on the physiology or the health of the stended patient [29].

Unfortunately, studies on the variation of mechanical properties, following the process of corrosion that occurs within the body, are still very few, so we'll focus on stent made of synthetic polymers.

[4]Tensile yield strength is the stress level at which there is a transition from elastic to plastic deformation.

[5]Young's modulus is a material property that describes its stiffness.

Polymeric stents

Synthetic biodegradable polymers first came into commercial medical use in 1970 with the introduction of a biodegradable suture material (*Dexon*) [47]. Such polymers have seen a steady progression in their development, leading, in more recent years, to a growth in experimental and clinical use in the field of orthopaedics and traumatology, and in the pharmaceutical industry as drug delivery devices. Recent advances have focused on developing biodegradable polymers as scaffolds in the field of tissue engineering [32][8].

Polymers were the first material selected for the development of biodegradable stents, which are not physiologically inert, and will be absorb over time, through the natural mechanisms of the human body [59]. However, the development of biodegradable polymeric stents has been hampered by difficulties in replicating the properties of stainless steel stents [50]. Most biodegradable synthetic polymers stents must have greater bulk to approximate the mechanical performance required in arteries. Many also induce exaggerated acute and chronic inflammatory responses during degradation [70]. Only high molecular weight poly-L-lactic acid (PLLA) has promised acceptable haemocompatibility and hystocompatibility in porcine and human coronary arteries [31].

Among the first polymeric stents to be tested was the PLLA bioabsorbable stent designed and tested by Stack et al [57], and is reported to hold up to 1,000 mmHg crush pressure and maintain its radial strength for 1 month. This stent was almost completely degraded by 9 months with minimal thrombosis, moderate neointimal growth and a limited inflammatory response in porcine coronary arteries. The Igaki-Tamai stent, another polymeric stent, is made of poly-L-lactic acid mono filament (molecular mass = 183 kDa) with a zigzag helical coil design. Another interesting concept is the multilayered biodegradable stent designed by Eury et al. [61], which is made of various polymers such as poly-L-lactic acid, polyglycolic acid, polycaprolactone, polyorthoesters or polyanhydrides. The unique feature of the stent is that one layer addresses the structural requirements of the stent and an additional layer controls the release of different drugs. The laminated construction allows the combination of a plurality of different drugs containing different materials all within a single stent. By appropriate configuration of the layers, drug release characteristics can be adjusted.

The Igaki-Tamai stent was compared with a Palmaz-Schatz stent and showed no stent thrombosis and no significant differences in minimal lumen diameter at 6 months. Histological examination revealed no inflammation and minimal neointimal hyperplasia on poly-L-lactic acid stent struts.

Lincoff et al.[31] demonstrated that poly-L-lactic acid, with a low molecular mass, is associated with an intense inflammatory reaction, whereas a minimal inflammatory reaction occurs with high molecular mass poly-L-lactic acid.

Using a stent made of copolymer L-and D-lactide (L/D ratio 96/4%), Hietala et al. [18] conducted a 34-month study in rabbits. This is the longest known study using a polymer stent, and reported complete endothelialization at 3 months with no inflammatory reaction observed after 6 months. Hydrolyzation of the stent was evident at 12 months and it was completely disintegrated by 24 months. The stent was gradually replaced by fibrosis. The vessel lumen remained patent at all time points. In contrast, the Kyoto University bioabsorbable stent made of polyglycolic acid and polyhydroxybutyrate stents was associated with thrombosis and intensive inflammatory vascular reactions.

Tamai et al. [68] were the first to report immediate and 6-month results after implanting the Igaki-Tamai stent in 15 patients. A total of 25 stents were electively and successfully implanted in 19 lesions. Clinical and angiographic follow-up data at 1 day, 3 months and 6 months were provided. No stent thrombosis or major cardiac event occurred at 30 days. Angiographically, both the restenosis rate and target lesion revascularization rate per lesion were 10.5%, while the rates per patient were 6.75% at 6 months. Even so, the presence of a loss index of 0.48 at 6 months was encouraging. The study showed that the Igaki-Tamai stent might not be associated with more pronounced intimal hyperplasia than stainless steel stents. Interestingly, there was evidence of vascular remodeling at the stented site, with an increase of the stent cross-sectional area from 7.42 mm^2 at baseline to 8.18 mm^2 at 3 months as evaluated by intravascular ultrasound. This persistent expansion was associated with a decrease in the lumen cross sectional area, although after the third month, no further stent expansion was observed. Tsugi et al. [68] reported 1-year follow-up data in a total of 63 lesions in 50 patients who underwent elective stent implantation with the Igaki-Tamai stent. No complications with regard to stent implantation were reported.

Quantitative coronary angiography at 3, 6 and 12 months demonstrated percent diameter stenoses of 12 ± 8, 38 ± 23, and 33 ± 23, respectively. Restenosis rates were 21% at 6 months and 19% at 12 months. The target lesion revascularization rate was 12% at 6 months and 17% at 12 months. A recent report of 4-year follow up on this cohort supported the long-term safety profile of the Igaki-Tamai stent. Further studies in the SFA with this stent demonstrated feasibility and safety in deployment of these stents over a length of 70 mm. Overall, these findings demonstrated feasibility and safety, with acceptable efficacy of the use of biodegradable poly-L lactic acid stents in human coronary arteries.

Chapter 2

Polymer Chemistry

Polymeric materials have been used in medical application for 50 to 60 years [9], often when intimate contact with living tissues is required. The purpose of this chapter is to introduce the chemical properties of polymers, focusing on poly-L-lactic acid (PLLA) because it is used to build most biodebradable stents. Furthermore, we will stress the strong dependence of mechanical properties on the chemical composition and the structure at molecular and supermolecular levels.

2.1 Introduction

Polymers are molecules consisting of thousands of repetitive units (monomers) connected by chemical bonds and arranged in a single (polymer) or more (copolymers) groupings that are repeated to form linear chains, branched or cross-linked structures. The number of repeat units is called *degree of polymerization* (DP) or chain length. Monomers are simple molecules with functional groups[1], able to recursively combine with other molecules - identical to themselves or reactively complementary to themselves - to form macromolecules (polymers).

The fundamental difference between small molecules and polymers lies primarily in their molecular weight, and the behavior that they keep in a solution. Hence, the dissolution of a polymer in a solvent usually generates very viscous solutions (eg paints). Initially, it was believed that such behaviors resulted from the presence of weak interactions between small molecules;

[1]Functional groups are small structural units within molecules at which most of the compound's chemical reactions occur.

only in 1920 Hermann Staudinger showed that these chains were rather large molecular structures, so he coined the definition of "polymers".

2.2 Development of polymers

Polymers were discovered long before anyone understood what they were. During the past several decades, the use of polymers has become so commonplace that it would be nearly impossible to pass a day without coming into contact with a polymer-based product [2].

There are both naturally occurring and synthetic polymers. Among naturally occurring polymers are proteins, starches, cellulose, and latex. Synthetic polymers are produced commercially on a very large scale and have a wide range of properties and uses. The materials commonly called plastics are all synthetic polymers. Most of the organic substances found in living matter, such as proteins, wood, chitin, rubber, and resins, are polymers. Many synthetic materials, such as plastics, fibers (Rayon), adhesives, glass, and porcelain, are also to a large extent polymeric substances.

A comb making company that used natural polymers was probably the first polymer industry in the United States, dating back to 1760. By the turn of the nineteenth century, a new development was about to occur that would change the infant polymer industry dramatically. The change occurred when natural polymers were processed or reacted with chemicals to make them useful substances. These polymers are called *modified natural polymers* or *semi-synthetic polymers*. The first and most famous of these is vulcanized rubber. In 1839, after years of experimentation, Charles Goodyear discovered that the sap of the hevea tree (latex) could be heated with sulfur to permanently alter the physical properties of the latex. Until this discovery, rubber had limited usefulness because it was brittle at low temperatures and melted when the temperatures became warm. Leo Baekeland successfully introduced the first semi-synthetic polymer in 1909, which he called *Bakelite*. Soon after, in 1911, the first semi-synthetic fiber, *Rayon*, was developed as a substitute for silk. Organic chemistry began to flourish and many discoveries were made.

The fact that polymers were large molecules and not colloidal aggregates was first proposed by Staudinger in 1920, but the concept was not fully accepted until the work of Carothers, the inventor of nylon, in 1929.

In the decade of the 1930s, several important new polymers were developed, including polyolefins, polystyrene, polyvinyl chloride, neoprene, and nylon. However, it was not until World War II that a significant change took place in the polymer industry. The technology to produce synthetic polymers from chemicals was developing rapidly, but the applications were not always commercially feasible or profitable. Prior to World War II, natural substances were generally available, therefore synthetics were not as necessary. Once the world went to war, the source of latex was cut off and synthetic rubber became a necessity. Natural fibers such as silk were no longer available for parachutes so nylon became the solution. Since then, the polymer industry has grown, changed, and diversified into one of the fastest growing industries in the United States and in the world.

By 1983, the use of polymers in the United States had surpassed the use of aluminum and steel and this trend continues. In 1996, the plastics industry had total shipments of $274.5 billion, a 55 percent increase since 1991 [12].

2.3 Chemical composition

A polymer can be made up of thousands of monomers. It is the long chains that give polymers their unique properties. Historically, the study of polymers starts from the study of organic compounds: all compounds of carbon.

Carbon atoms can be linked through individual bonds, to form a saturated compound (alkanes: C−C) or through double or triple bonds, to form unsaturated compounds (alkenes: C=C and alkynes: C≡C). The latter two are called unsaturated because the rupture of one of the multiple links can lead to the addition of new atoms and therefore to change the nature of the substance.

Ethane (CH_3-CH_3), for example, is a gas molecule at room temperature. Because of their small size, ethane molecules are very mobile and can run almost anywhere they want without interacting with other molecules. If we double the total number of carbons to four, we get butane, ($CH_3-CH_2-CH_2-CH_3$), which is a liquid fuel. In liquids, atoms or molecules can no longer act as independent units. Because of their larger size, butane molecules are less mobile than ethane molecules. Their lowered mobility allows them

to run into or interact with one another more frequently. When the chain length increases 10 fold, as in paraffin, we get a waxy substance. In this case, the solid-like property of paraffin is a reflection of the entanglement of its long molecules when they move. If we keep increasing the number of repeating carbon units to, say 2000, i.e., ($CH_3(CH_2\text{-}CH_2)_{2000}CH_3$), we have a polyethylene polymer, which is a very hard and brittle solid. The polymer molecules have become so long and so entangled that their movement becomes almost completely restricted. At this point, they appear to be attached to other molecules, which act as "permanent" neighbors.

To get a clear idea of the way polymers are formed, we need to look more closely at the monomer molecules. Let us see some examples:

Tetrafluoroethylene	**Poly-tetrafluoroethylene**
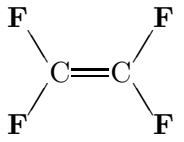	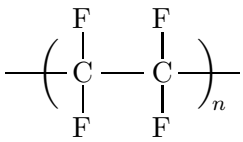
Vinyl chloride	**Poly-vinyl chloride**
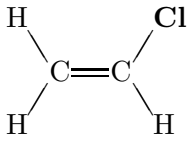	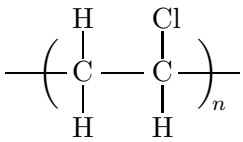
Propylene	**Poly-propylene**
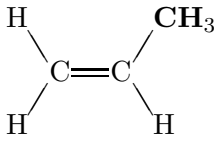	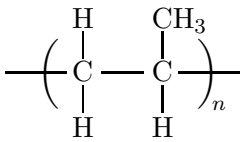

Table 2.1: Examples of monomers and polymers

Each of these monomer molecules seems very different from each other, but they have some common features: carbon-carbon double bonds and side groups. The boldfaced groups (Table 2.1: **F**, **Cl**, **CH_3**) give the polymer chain some of its properties and the double bond is required so that these monomers can form the long polymer chains, as we will see later.

Most of the chemistry of carbon compounds is based on functional groups. The table below shows the main functional groups of which the polymers

are often composed; (R means the "*Rest*" of the molecule).

Organic compounds	Functional groups	General formule
Alcohol	-OH	R-OH
Phenol	-OH	Ar-OH
Ether	-O-	R-O-R'
Aldeayde	-CHO	R-CHO
Ketone	=C=O	R-CO-R'
Carboxylic acid	-COOH	R-COO-R'
Ester	-COO-	R-COO-R'
Amine primary	$-NH_2$	$R-NH_2$
Amine secondary	=NH	R2-NH
Amine tertiary	≡N	R3-N

Table 2.2: Main functional groups of the organic molecules

2.3.1 Mechanisms of polymerization

The processes by which polymers are formed from monomers is called polymerization. Monomers are chemically jointed together in one of two ways: addition polymeryzation or condensation polymerization.

Addition polymerization

Before talking about the mechanism of *polyaddition* (addition polymerization) it is necessary to introduce the "double bond" concept, since this kind of bond is what makes this process possible.

The double bond is made of two pairs of electrons shared by two atoms. This arrangement is fairly strong, but when other molecules that can react with such electrons get close, the bond can be broken. Free radicals are a kind of molecules that may be able to break the bond.

For example, the hydrogen peroxide HO−OH has an easy-to-break O−O single bond and heat or light energy can break it.

$$\text{HO-OH} \rightarrow \text{HO}^{\cdot} +^{\cdot} \text{OH}$$

The single dot $\cdot$ represents one electron from the O−O peroxide bond. The $\text{HO}^{\cdot}$ fragments are the free radicals, and they are very unstable and reactive.

When a free radical gets close to a double bond, one of the bonds is disrupted and one of the electrons in the double bond is attracted to the free radical. The double bond breaks, and a new single bond is formed.

$$HO^{\cdot} + CH_2 - CH_2 \rightarrow HO - CH_2 - \dot{C}H_2$$

Notice that in forming this bond, one electron from the double bond is left alone. Thus, another (larger) free radical has been formed.

The formation of a polymer by polyaddition is an example of a chain reaction. Once a chain reaction gets started, it is able to keep itself going. In addition polymerization, entire monomers are linked together to form a long chain. This reaction develops in three basic steps: initiation, propagation and termination. For example, the polymerization that combines ethylene (ethene) monomers (CH_2 =CH_2), will produce polyethylene:

- Initiation: how the reaction gets started

As we have seen before, in the first part of the initiation step of addition polimarization chain reaction, a peroxide molecule breaks up into two reactive free radicals. It is possible to write an equation for this process:

$$ROOR + \text{Energy} \rightarrow 2RO^{\cdot}$$

where ROOR is the peroxide and $2RO^{\cdot}$ is the free radical initiator.

The second part of initiation occurs when the free radical initiator attacks and attaches to a monomer molecule. This forms a new free radical, which is called the "activated monomer":

$$RO^{\cdot} + CH_2 = CH_2 \rightarrow RO - CH_2 - \dot{C}H_2$$

where $RO^{\cdot}$ is the free radical initiator, CH_2-CH_2 is the ethylene monomer and RO-CH_2-CH_2 is the activated monomer.

- Propagation: how the reaction keeps going

During a chain reaction, most of the time is spent in the propagation phase as the polymer chain grows. In this phase, the newly-formed activated monomer attacks and attaches to the double bond of another monomer molecule. This addition occurs again and again to create a long polymer chain:

$$RO - CH_2 - \dot{C}H_2 + nCH_2 = CH_2 \rightarrow$$

$$\mathrm{RO}\!\left(\!-\mathrm{CH_2}-\mathrm{CH_2}-\right)_n\!\mathrm{CH_2}-\dot{\mathrm{C}}\mathrm{H_2}$$

The "n" stands for any number of monomer molecules, typically in the thousands.

- Termination: how the reaction stops

This chain reaction cannot go on forever, soon or later it must end. A growing polymer chain joins with another free radical. We watched a peroxide break up to form two radicals. It makes sense that two free radicals could join to make a stable bond. The equation representing this step of the chain reaction can be written simply as:

$$\mathrm{R}^{\cdot} + \mathrm{R}_1^{\cdot} \rightarrow \mathrm{R} - \mathrm{R}_1$$

Condensation polymerization

The monomers that are involved in condensation polymerization are not the same as those involved in addition polymerization. The formers have two main characteristics:

- instead of double bonds, these monomers have functional groups (like alcohol, amine, or carboxylic acid groups);
- each monomer has at least two reactive sites, which usually means two functional groups.

Some monomers have more than two reactive sites, allowing for branching between chains, as well as increasing the molecular mass of the polymer. During the chemical reaction a small molecule (often of water) is eliminated as the monomers join together. Since the water is removed, this kind of reactions are called "condensation reactions" (water condenses out). Let us look at one example.

$$\mathrm{HOOC}-\mathrm{CH}=\mathrm{CH}-\mathrm{COOH} \quad + \quad \mathrm{HO\text{-}CH_2}-\mathrm{CH}-\mathrm{OH} \rightarrow$$

$$-\mathrm{OC}-\mathrm{CH}=\mathrm{CH}-\mathrm{CO}-\mathrm{O}-\mathrm{CH_2}-\mathrm{CH_2}-\mathrm{O} \quad + \quad \mathrm{H_2O}$$

When a carboxylic acid and an alcohol react, a water molecule is removed, and an ester molecule is formed. Because of this ester formation, this bond is known as an "ester linkage" and the polymer chain is a polyester.

2.4 Physical characteristics

The means of polymerization will affect the heat reaction of the formed polymer, likewise, the arrangement of the monomers within the molecule will affect the physical characteristics of the formed polymer, that depend on its molecular weight, shape and physical structure.

Molecular weight

Molecular weight can be defined as a sum of the relative atomic masses (A_r)[2] of the constituent atoms of a molecule [6].
The polymer chain at some point stops growing, because of accidental events or depletion of reagents. So, the various chains that form during a polymerization reaction may be of different lengths. Each sample of a polymer contains molecular chains of varying lengths, i.e. of varying molecular mass (M_M)[3]. The mass (length) distribution is of importance in the advent of gel permeation chromatography (GPC)[4] but it could only be determined by tedious fractional procedures. Therefore, most investigations quoted different types of average molecular mass, the commonest being the number average $\overline{M}_n$ and the weight average $\overline{M}_W$ defined as:

$$\overline{M}_n = \frac{\sum N_i M_i}{\sum N_i} \qquad \overline{M}_W = \frac{\sum (N_i M_i) M_i}{\sum N_i M_i} \tag{2.1}$$

where N_i is the number of molecules of molecular mass M_i. The weight average molecular mass is always higher than the number average, as the former is strongly influenced by the relatively small number of very long (massive) molecules. The ratio of the two averages gives a general idea of the width of the molecular mass distribution.
Molecular mass was often deduced from viscosity measurements of either

[2] To consider the masses of atoms measured in grams, for example, would be to deal inconveniently with extremely small numbers. Rather, the mass of an atom is compared with that of an atom of carbon-12. The relative atomic mass of carbon-12 is taken to be 12. Relative masses have no units because they have canceled in their calculation.

[3] Sum of the atomic masses (atomic weights) of the atomic species that constitute the molecule [6]

[4] GPC, also known as size exclusion chromatography (SEC), is a chromatographic method in which molecules are separated based on their size. This method is most widely used in the analysis of polymer molecular weights (or molar mass).

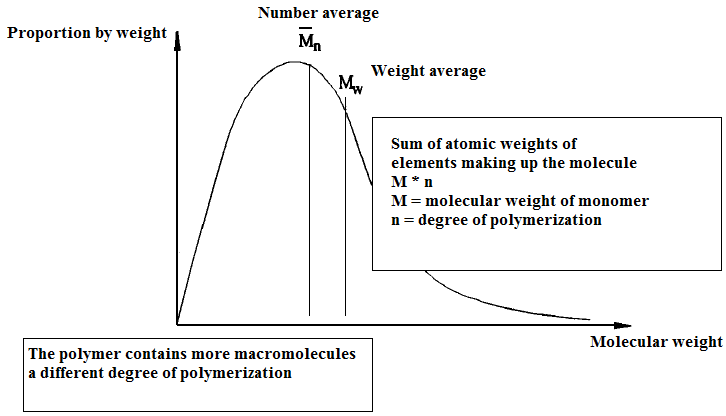

Figure 2.1: The gel permeation chromatograph trace gives a direct indication of the molecular distribution. (Results obtained in mArlex 6009 by Dr T. Williams)

a dilute solution of the polymer (which relates to $\overline{M}_n$) or a polymer melt (which relates to $\overline{M}_W$). Each method yielded a different average value, which made it difficult to correlate specimens characterized by different groups of works.
The molecular mass distribution is important in determining flow properties, and so may affect the mechanical properties of a solid polymer indirectly by influencing the final physical state. Direct correlations of molecular mass to viscoelastic behavior have also been obtained [2].

Shape

The molecules of a polymer chain are not strictly linear, since the zig-zag conformation of atoms of the basic structure should be taken into account (Figure 2.2). The links of one chain are in fact able to rotate into space. Thus, a single molecule of the chain, consisting of many atoms, could take

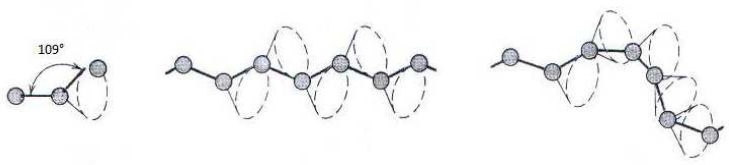

Figure 2.2: Possible orientations of the molecular chain.

a range of bending. It has been observed that the start-end distance, (r),

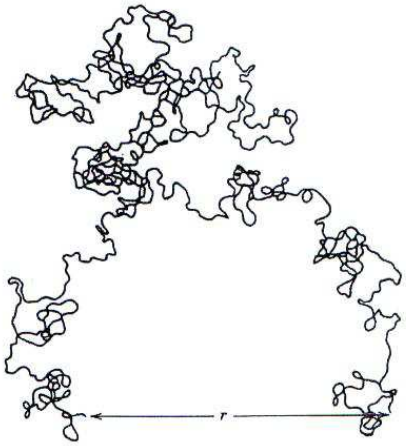

Figure 2.3: Possible structure of a macromolecule

of the chain is much shorter than the total length of the chain (Figure 2.3). Polymers, in turn, are composed of a large number of molecular chains, each of which can tilt, roll and spiral. This leads to a significant entanglement of molecules of adjacent chains, which is the basis of some important characteristics of polymers, including high sensitivity offered by elastic rubber. Some of the mechanical and thermal properties of polymers depend on the ability of segments of the chain to rotate in response to efforts made or thermal fluctuations. The flexibility in the rotation depends on the structure and chemistry of monomers. For example, the part of the chain that is linked by two C=C is hard to turn. Also, the introduction of a bulky side reduces rotational movement. For example, the molecules of polystyrene, which have a lateral phenyl group, are more resistant to rotational stress than the chains of polyethylene (Figure 2.4).

Physical structure

The physical properties of a polymer of a given chemical composition are dependent on two distinct aspects of the arrangement of the molecular chain in space:

1. the arrangement of a single chain without regard to its neighbor: rotational isomerism.

2. the arrangement of chains with respect to each other: orientation and

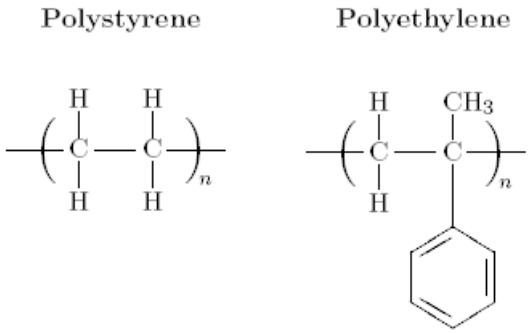

Figure 2.4: Polyethylene and polystyrene molecules. The lateral phenyl group reduces rotational movements.

crystallinity.

The former, (rotational isomerism) arises because of the alternative conformations of a molecule that can result from the possibility of hindered rotation around the many single bonds in the structure. A single conformation is just a single shape that a chain can adopt, so that, for example, when a polyethylene chain is shown as a linear zig-zag, this is just one possible conformation. These chain molecular motions increase in both frequency and amplitude as the temperature is raised, the most important being rotation around single bonds. By contrast, double bonds are rigid and the adjacent atoms are immobile. As a consequence of extra rotational motion, the number of conformations a chain can adopt increases rapidly with increasing temperature. The question then arises whether or not there are any conformations which are more stable than others at any particular temperature, given the chemical structure of the repeat unit.

When we consider the arrangement of molecular chains, with respect to each other, there are again two largely separate aspects, those of molecular orientation and crystallinity. In semicrystalline polymers this distinction may at times be an artificial one.

When cooled from the melt, many polymers form a disordered structure called the *amorphous state*. An amorphous arrangement of molecules has no long-range order or form in which the polymer chains arrange themselves. Amorphous polymers are generally transparent. This is an important characteristic for many applications such as food wrap, headlights and contact lenses. Some of these materials have a comparatively high modulus at room

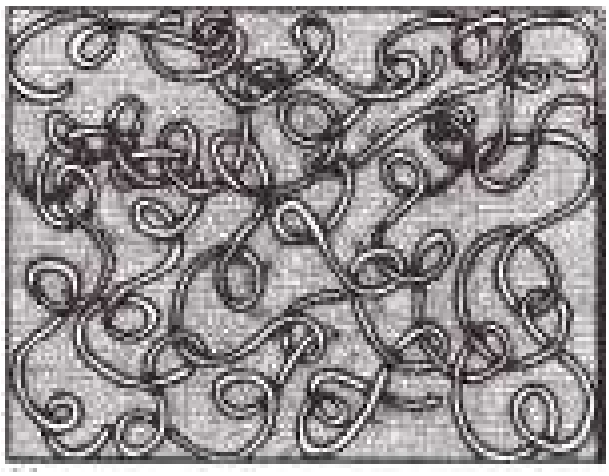

Figure 2.5: Schematic diagram of amorphous polymer.

temperature, but others have a low modulus. These two types of polymer are often termed "glassy" and "rubber-like", respectively, and we shall see that the form of behavior exhibited depends on the temperature relative to a glass-rubber transition temperature (T_g) that is dependent on the material and the test method employed. An amorphous polymer may be modelled as a random tangle of molecules (Figure 2.5) [72]. When an amorphous polymer is stretched, the molecules may be preferentially aligned along the stretch direction. Stretching produces both molecular orientation and small regions of three-dimensional order, termed crystallites. For a polymer to crystallize the molecule must have a regular structure, the temperature must be below the crystal melting point and sufficient time must be available for the long molecules to become ordered in the solid state. Regular structures with little or no branching allow the polymer chains to fit close together, forming a *crystalline structure* (Figure 2.6). By definition, a crystalline arrangement has atoms, ions or molecules in a distinct pattern [6]. Crystalline structures are generally stronger, more brittle, of higher density, more resistant to chemical penetration and degradation, less soluble and have higher melting points. The physical characteristics of a polymer depend not only on its shape and its molecular weight, but also on differences in structural configuration of molecular chains. We will describe the most important ones below.

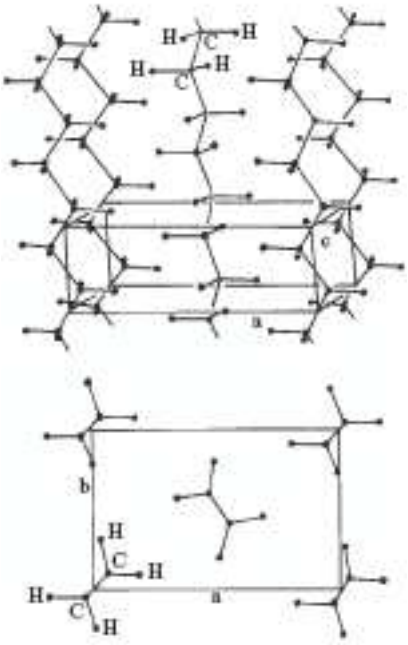

Figure 2.6: Arrangement of molecules in polyethylene crystallites. (From *Fibres from Synthetic Polymers* (ed R. Hill),Elsevier, Amsterdam, 1953)

Linear Polymers

Linear polymers (Figure 2.7.A) consist of long molecular chains of covalently bonded atoms and they are like ropes [2], the units are joined together end to end in a single chain. These long chains are flexible. Some of the common polymers with linear structure are polyethylene, polyvinyl chloride, polystyrene, polymethyl metacrilato, nylon and the fluorocarbons.

Branched Polymers

Polymers may be synthetized as connected to the main ones. These "extensions" are called *branches* (Figure 2.7.B) and affect the polymer's properties. Branches may be long or short, frequent or infrequent. For example, so called *low density polyethylene* (LDPE) has between forty and one hundred short branches for every 1,000 ethylene units, whereas *high density polyethylene* (HDPE) has only one to six short branches for every 1,000 ethylene units. Branching discourages the chains from fitting close together so that the structure will be *amorphous* with relatively large amounts of

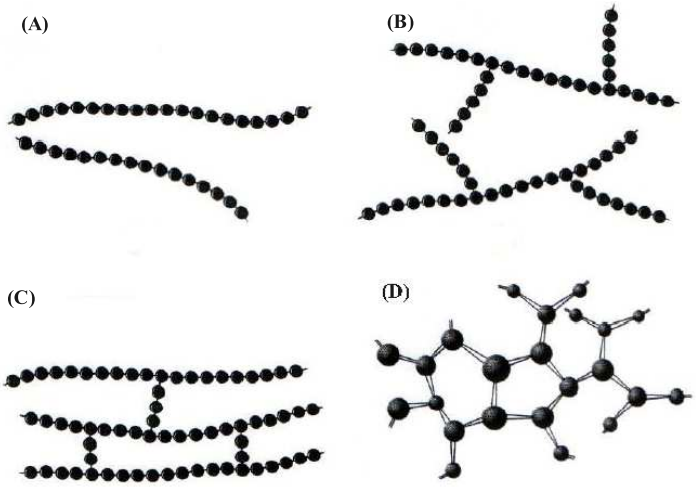

Figure 2.7: Polymer chains to different structural characteristics:(A) Linear, (B) Branched, (C) Cross linked, (D) network

empty space [6].

Cross linked polymers

In cross linked polymers (Figure 2.7.C), adjacent linear chains are joined one to another at various positions by covalent bonds. The process of cross linking is achieved either during synthesis or by a non reversible chemical reaction that is usually carried out at an elevated temperature. This cross linking is accomplished by additive atoms or molecules that are covalently bonded to the chains. Some materials can only have a few cross links, such as permanent press materials where the fabric contour is locked into place with cross links. Many of the rubber elastic materials are cross linked. In case of rubbers, it is called vulcanization.

- Network polymers

Trifunctional monomer units, having three active covalent bonds, form three-dimensional networks instead of the linear chain framework assumed by bifunctional monomers. Polymers composed of trifunctional units are called *network polymers* (D). A polymer that is highly cross linked may be classified as a network polymer. These materials have distinctive mechanical and thermal properties. The mechanical properties of a polymer are also affected by temperature. The glass transition temperature, T_g, different for each

polymer, is the temperature at which an amorphous solid, such as glass or a polymer, becomes brittle on cooling, or soft on heatings: below the glass transition temperature, amorphous solids are in a glassy state, above it, they are soft and rubbery. (*Note*: the glass transition is a property of only the amorphous portion of a semi-crystalline solid, the crystalline portion remains crystalline during the glass transition [6].
The T_g will vary depending on the chemical composition of the polymer, the molecular weight and the percentage of areas affected by amorphous sites. Since an implanted polymer device is capable of supporting a greater load at temperatures below its T_g, the majority of polymers used clinically has a T_g higher than the body temperature.

Polymers used in orthopedics are of viscoelastic nature, so their physical properties change with the rate of load application and depend on time. An increase in the molecular weight implies an increase in the intrinsic viscosity of the polymer, which leads to a lower deformability (ie, less flow) by applying a load. In general, polymers with high or medium molecular weight, and as such very viscous, have a slower biodegradation than those with lower molecular weight and lower viscosity.

2.4.1 Degradation and erosion

Polymer degradation and erosion play a role for all polymers. The distinction between degradable and non-degradable polymers is, therefore, not clean-cut and is in fact arbitrary, as all polymers degrade. It is the relation between the time-scale of degradation and the time-scale of the application that seems to make the difference between degradable and non-degradable polymers. We usually assign the attribute *degradable* to materials which degrade during their application, or immediately after it. *Non-degradable* polymers are those that require a substantially longer time to degrade than the duration of their application. Many different definitions for degradation and erosion exist in the current literature and sometimes vary markedly from one another. In general, the process of degradation describes the chain scission process during which polymer chains are cleaved to form oligomers and finally to form monomers. Erosion designates the loss of material owing to monomers and oligomers leaving the polymers [60].

All polymers are susceptible to degradation [11], but the conditions under which this occurs and the kinetics of the reactions are extremely variable.

The processes of degradation can be divided into two types:

1. those which involve the absorption[5] of some kind on energy to cause disruption of primary covalent bonds to form free radicals, which then cause the propagation of molecular degradation by secondary reaction;

2. those in which there are hydrolytic mechanisms where the depolymerization process can be seen as the reverse of polycondensation.

The conditions under which the first of these general processes takes place include elevated temperatures, electromagnetic radiations, (i.e. γ-rays, X-rays or ultra-violet radiations), mechanical stress at elevated temperatures giving thermo-mechanical degradation and ultrasonic vibration. Clearly, the physiological environment within the human body does not offer any of these conditions to an implanted polymer; hence, the optimistic statement that most polymers should be stable upon implantation [9]. Once implanted the devices are immersed in an aqueous environment and therefore subject to degradation due to hydrolysis. Hydrolysis, on the other hand, is quite feasible in the aqueous extra-cellular fluid but there are conditions that have to be met so that the process can take place:

- the polymer has to contain hydrolytically unstable bonds;

- for any significant degradation to occur, the polymer should be hydrophilic[6], otherwise the medium producing hydrolysis will have very limited opportunities for gaining access to the hydrolysable bonds;

- the hydrolysis has to take place at a physiological pH (around 7.4).

Each degradation process involves initiation, propagation and termination stages. During initiation, energy is absorbed from external sources, causing the breaking of a covalent bond (either the primary chain bond or a cross-link) and the formation of active radicals. Thus, thermal degradation occurs when the vibrational, rotational or translational energy exceeds the activation energy required to break a carbon-carbon bond on increasing the temperature.

[5]Absorption: the uptake of water , other fluids, or dissolved chemicals by a cell or an organism.

[6]Hydrophile refers to a physical property of a molecule that can transiently bond with water (H_2O) through hydrogen bonding

Radiative degradation of synthetic polymers largely involves either ultra-violet or high-energy radiation. As discussed by Shalaby [51], the radiative degradation caused by ultra-violet light is called *photolysis* and the one caused by high-energy radiation is called *radiolysis*. The ability to degrade of the polymers increases as the wavelength decreases or the energy increases [9].

The effects of these degradation processes will naturally vary, but generally there will be a change in average molecular weight, molecular-weight distribution, crystallinity and mechanical properties. Chain scission will generally result in reduced strength and creep resistance, while cross-linking will be associated with an increased modulus of elasticity.

The processes involved in the erosion of a degradable polymer are complicated. Water enters the polymer bulk, which might be accompanied by swelling. The intrusion of water triggers the chemical polymer degradation, leading to the creation of oligomers and monomers. Progressive degradation changes the microstructure of the bulk through the formation of pores, via which oligomers and monomers are released. Concomitantly, the pH inside pores begins to be controlled by degradation products, which typically have some acid-base functionality. Finally oligomers and monomers are released, leading to the weight loss of polymer devices [1].

All degradable polymers share the property of eroding upon degradation. Degradation and erosion are the decisive performance parameters of a device made of such materials. To classify degradable polymers a distinction is made between surface (or heterogeneous) and bulk (or homogeneous) eroding materials [28], which is illustrated in Figure 2.8.

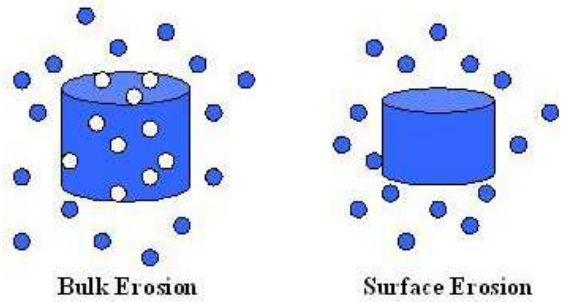

Figure 2.8: Illustration of surface erosion and bulk erosion.

During an application, surface eroding polymers lose material from the

surface only (*Surface erosion*). They get smaller but keep their original geometric shape. For bulk eroding polymers, degradation and erosion are not confined to the surface of the device. Therefore, the size of a device will remain constant for a considerable portion of time during its application [42]. The advantage of surface eroding polymers is the predictability of the erosion process [15]. This is desiderable when using such polymers for drug delivery, where the release of drugs can be related directly to the rate of polymer erosion [16]. Whether a polymer favors either surface erosion or bulk erosion makes it suitable for different kinds of applications.

The knowledge of the erosion mechanism is most important for the successful application of a degradable polymer. In tissue engineering, surface properties or porosity determine the performance of implantable scaffolds [10].

2.5 Biodegradable polymers

Over the past 40 years, polymer scientists, working closely with those in the medical device and clinical fields, have made tremendous advances in understanding and applying biodegrable polymers to more sophisticated applications. Currently, applications for these promising biomaterials cover a broad range of clinical and scientific disciplines, including sutures and fracture-fixation devices to support tissue regeneration [66], as drug delivery systems in the pharmaceutical industry, and, with recent scientific advances, as scaffolds in the field of tissue engineering [7]. Although the specific materials' requirements will differ depending to the nature of the application, it is a fundamental requirement that the polymer displays adequate biocompatibility. This implies that, for permanent implant applications, the material should not degrade within the physiological environment, nor should it have any adverse effect on the tissue, and that for short-term intentionally degradable prostheses, the rate of degradation and the release of degradation products should be physiologically tolerable [14].

Biodegradable polymers, belonging to the aliphatic polyester family, currently represent the most attractive group of polymers that meet the various medical and physical demands for safe clinical applications. This is mainly due to their high biocompatibility, acceptable degradation rates, and versatility regarding physical and chemical properties [45]. Two of the most

significant members of the aliphatic polyester family are the poly(α-hydroxy acids): polyglicolide (PGA) and polylactide (PLA) [4]. High molecular weight PGA and PLA were first introduced in the 1950s, however, they were initially discarded and research was abandoned into the polymerization of other α-hydroxy acids because of their poor thermal and hydrolytic stabilities, which did not allow them to be used as regular plastics for long-term industrial use [32]. Nevertheless, this instability has proven to be of immense importance, enabling PGA, PLA, and other aliphatic polyesters to be developed as synthetic biodegradable polymers for medical use.

The degradation of biodegradable devices follows a predictable pattern. The degradation rate of the polymer depends on many factors such as its starting molecular weight, its crystalline structure, composition and porosity of the device, loading conditions and the local vasculature. Within degradation process, firstly loss of molecular weight occurs, followed by loss of strength and finally mass. The initial phase of degradation has chemical nature. The biological process and removing of the device occur later. Because of this type of degradation, these materials lose their functional strength before healing tissue is completed . The initial phase of degradation is hydrolysis. The water molecules penetrate into the material implanted, causing the split of the monomer's molecular bonds. This condition leads to the cleavage of long chains of polymer into shorter ones, reducing the total molecular weight. This process is also influenced by the porosity of the implant. As the device loses its integrity and becomes fragmented, its biological removal takes place.

2.5.1 Poly-lactic acid

Poly lactic acid (PLA) is one of the most significant members of the aliphatic polyester family and has been the focus of significant research over the past 40-50 years. It is produced from the lactide monomer by ring-opening polymerization, as shown below.

Lactic acid is a small hydrophobic molecule with three atoms of carbon, which plays an important role in cellular energy production.
PLA is a highstrength, high-modulus polymer that can be made from annually renewable resources to yield articles for use in industrial packaging, in the agricultural field, or in the biomedical field as a suture material and in various orthopedic fixation devices [43]. Poly lactic acid is easily processed

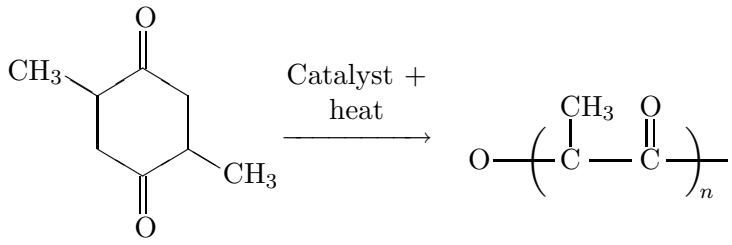

Lactide **Polylactide**

on standard plastics equipment to yield molded parts, films or fibers [21]. Crystalline PLA is soluble in chlorinated solvents and benzene at elevated temperatures [17], whereas the amorphous PLA is soluble in most organic solvents.

Due to the chirality of the central carbon and the methyl group, lactic acid has two enantiomers (Figure 2.9), hence, when polymerized, PLA exists as two optical isomers, poly-L-lactide (PLLA) and poly-D-lactide (PDLA). The poly-DL-lactide (PDLLA) is the synthetic blend of D-lactide and L-lactide [32]. The D-form is produced rapidly, but the L-isomer is the biologically

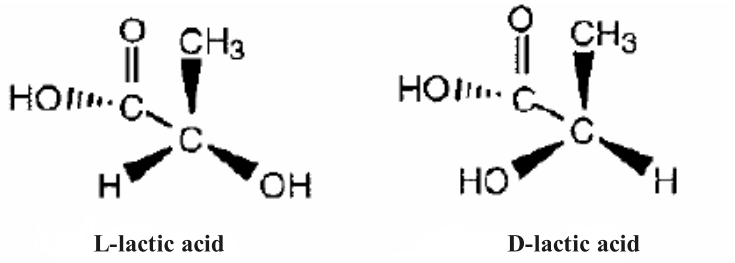

Figure 2.9: L- and D- enantiomers of lactic acid. Note the difference in location of the hydroxyl group in the chiral carbon.

active form (it interacts with the organism). PLLA shows a semicrystalline structure that consists of left handed helical chains. It possesses an high tensile strength and low elongation, making it suitable for load-bearing applications such as orthopedic devices and hard tissue scaffolds. In this case, the degradation rate of mechanical properties of the strength loss and tissue healing rates determines the strength of the healing tissue, and hence the ability of that tissue to support loading after complete degradation of the implant [14].

PDLA has a right handed helical crystalline structure. Contrariwise,

PDLA shows an amorphous structure and the characteristics of the copolymers are intermediate between those of the two monomers [6], poly(DL-lactide) is an amorphous polymer exhibiting a random distribution of both isomeric forms of lactic acid, and accordingly is unable to arrange into an organized crystalline structure. This material has lower tensile strength, higher elongation and a much more rapid degradation time, making it more attractive as a drug delivery system. The glass transition temperature of poly(lactic acid), T_g, is located around 60°C, with small dependence on the molecular weight, copolymerization and degree of crystallinity. When implanted, the material will usually be at a temperature slightly lower than T_g. Therefore, understanding the glass transition dynamics is most important because conformational dynamics will affect the behavior of the polymer at physiological temperatures, including structural relaxation that yields the inherent viscoelastic behavior. PLA is degraded by simple hydrolysis of the ester bond. This reaction occurs spontaneously and does not require the presence of catalytic enzymes [56]. This kind of hydrolysis is generally regarded as a "bulk hydrolysis" process: the polymer retains its volume for a considerable among of time throughout degradation, followed by a loss of molecular weight, of mechanical strength and finally of mass [32].

Chapter 3

Mechanical behavior of solid polymers

In this chapter basic concepts of continuum mechanics will be introduced. The aim is to understand the constitutive modelling of the polymer object of this thesis and that will be discussed in the next chapter.

3.1 Introduction

Mechanics is the study of bodies in motion. In general, a body in motion undergoes some combination of rigid motion (the distance between two particles does not change) and stretching (the distance between two particles changes). The motion influences the development of forces in the body.

Within mechanics of solid materials, the construction of a model consists in general of three steps: (i) kinematics (it is the study of body configuration changes); (ii) equilibrium (it is the study of the body equilibrium conditions, relative either to the whole body or to body subset); (iii) constitutive relation (it is the study of the relations taking into account the physical and phenomenological nature of the body).

3.2 Kinematics

As said before, the kinematics is the study of body configurations and of their changes in time.

We consider a material body $\boldsymbol{B}$ as a set of material particles and assume

that at any time instant t the body $\boldsymbol{B}$ can be identified with a closed subset, Ω, of the tridimensional real space $\mathcal{R}^3$ ($\boldsymbol{B} \equiv \Omega \subset \mathcal{R}^3$). If we identify $\boldsymbol{B}$ with a set Ω, in general indicated as *body configuration*, we may associate any material point $X \in \Omega \subset \mathcal{R}^3$:

$$X \in \boldsymbol{B} \rightarrow \boldsymbol{X} \in \Omega \subset \mathcal{R}^3 \tag{3.1}$$

As a consequent of this "body identification", we can treat the material body as a continuum.

If we concentrate on two time instants, t_0 (*initial time instant*) and t_1 (*current time instant*), with t_1 a generic time instant after t_0, at time t_0 we can identify $\boldsymbol{B}$ with a subset $\Omega_0 \in \mathcal{R}^3$, indicated as *initial or reference configuration*, such that at the same instant we may identify the generic material point $X \in \boldsymbol{B}$ with a corresponding point $\boldsymbol{X} \in \Omega_0$. At time t, we can identify $\boldsymbol{B}$ with a new subset $\Omega \in \mathcal{R}^3$, indicated as *current configuration*, such that at the same time instant we may identify the generic material point $X \in \boldsymbol{B}$ with a corresponding point $\boldsymbol{x} \in \Omega$.

Using Relation 3.1 we may also construct a map between the reference and current configuration, indicated, in general, as *change of configuration* or *deformation map* $\boldsymbol{\varphi}$:

$$\boldsymbol{x} = \boldsymbol{\varphi}(\boldsymbol{X}) \tag{3.2}$$

More precisely, we can define the map $\boldsymbol{\varphi}$ as:

$$\boldsymbol{\varphi} : \boldsymbol{X} \in \Omega_0 \subset \mathcal{R}^3 \rightarrow \boldsymbol{x} \in \Omega \subset \mathcal{R}^3 \tag{3.3}$$

where $\boldsymbol{X}$ is the reference position vector and $\boldsymbol{x}$ is the current position vector.

The main requirement on the deformation map is that it has to respect the body continuity, i.e., in respect to the body boundary and to the body interior. In the former case, we may assign the body configuration on a portion of the boundary, indicated as $\partial\Omega_0^{\boldsymbol{\varphi}}$, for example, $\boldsymbol{x} = \boldsymbol{X}$ for all time instant on $\partial\Omega_0^{\boldsymbol{\varphi}}$. In the second case, the body continuity in respect to the body interior can be expressed through the following conditions: (i) the map $\boldsymbol{\varphi}$ is a function; (ii) it is continuous and differentiable with continuous derivatives (class C^2); (iii) $\boldsymbol{\varphi}$ is invertible. Through the invertibility requirements, we can also write:

$$\boldsymbol{X} = \boldsymbol{\varphi}^{-1}(\boldsymbol{x}) \tag{3.4}$$

If we compare the Relations (3.4) and (3.2), in the description of motion we can assume as indipendent variable either $\boldsymbol{X}$ or $\boldsymbol{x}$. The choise of $\boldsymbol{X}$ as

indipendent variable results in the so-called *material description*, which is of particular convenience in solid mechanics; the choise of $\boldsymbol{x}$ as independent variable results in the so-called *spatial description*, which is more convenience in fluid mechanics.

The gradient of the deformation map, also called as *deformation gradient*, $\mathbf{F}$, can be defined as:

$$\boldsymbol{F} = \nabla \boldsymbol{x} \boldsymbol{\varphi} \tag{3.5}$$

and if we take $\boldsymbol{x} \equiv \boldsymbol{\varphi}$, $\boldsymbol{F}$ can be written as:

$$\boldsymbol{F} = \frac{\partial \boldsymbol{x}}{\partial \boldsymbol{X}} \tag{3.6}$$

Hence, we can say that, through the map $\boldsymbol{\varphi}$, an infinitesimal vector $\mathrm{d}\boldsymbol{X}$ with origin in $\boldsymbol{X}$, is transformed in a vector, $\mathrm{d}\boldsymbol{x}$, with origin in $\boldsymbol{x}$, as follows:

$$d\boldsymbol{x} = \boldsymbol{F} d\boldsymbol{X} \tag{3.7}$$

The deformation gradient is a second-order tensor since it maps vectors into vectors, it operates on vectors defined in the reference configuration and it returns vectors in the current configuration.

The deformation gradient contains all the informations on the stretch of a generic fiber, as well as all the information on the angle change between two fibers. If we consider an infinitesimal vector $\mathrm{d}\boldsymbol{X}$, with origin in $\boldsymbol{X}$ and expressed as $\mathrm{d}\boldsymbol{X} = \boldsymbol{N} dX$ with $\boldsymbol{N}$ unit vector, and if we consider $\mathrm{d}\boldsymbol{x}$ the vector with origin in $\boldsymbol{x}$, obtained from $\mathrm{d}\boldsymbol{X}$ through the deformation map $\boldsymbol{\varphi}$ (Eq. 3.7), we can define the *stretch* of the vector $\mathrm{d}\boldsymbol{X}$ as the elongation of the vector through $\boldsymbol{\varphi}$:

$$\lambda = \frac{\parallel d\boldsymbol{x} \parallel}{\parallel d\boldsymbol{X} \parallel} \tag{3.8}$$

so, the square of the stretch begins:

$$\lambda^2 = \frac{d\boldsymbol{x} \cdot d\boldsymbol{x}}{d\boldsymbol{X} \cdot d\boldsymbol{X}} \tag{3.9}$$

and through mathematical steps, we obtain:

$$\lambda^2 = \boldsymbol{C}\boldsymbol{N} \cdot \boldsymbol{N} = \lambda^2(\boldsymbol{N}) \tag{3.10}$$

where $\boldsymbol{C}$ is the *right Cauchy-Green deformation* tensor, defined as:

$$\boldsymbol{C} = \boldsymbol{F}^T \boldsymbol{F} \tag{3.11}$$

accordingly:

$$\lambda = \sqrt{\boldsymbol{CN} \cdot \boldsymbol{N}} \tag{3.12}$$

so, given $\boldsymbol{F}$ and hence $\boldsymbol{C}$, we can compute the elongation of any fiber as function of the direction $\boldsymbol{N}$.

Through a similar reasoning, if we consider two infinitesimal vectors $\mathrm{d}\boldsymbol{X}_1$ and $\mathrm{d}\boldsymbol{X}_2$, with origin in $\boldsymbol{X}$, if θ_0 is the angle between them and θ is the angle between $\mathrm{d}\boldsymbol{x}_1$ and $\mathrm{d}\boldsymbol{x}_2$ (infinitesimal vectors with origin in $\boldsymbol{x}$), the difference $\gamma = \theta - \theta_0$ represents the angle variation. Also this quantity can be expressed in terms of $\boldsymbol{F}$:

$$\gamma = \frac{d\boldsymbol{x_1} \cdot d\boldsymbol{x_2}}{\parallel d\boldsymbol{x_1} \parallel \parallel d\boldsymbol{x_1} \parallel} = \frac{\boldsymbol{FN_1} \cdot \boldsymbol{FN_2}}{\parallel \boldsymbol{FN_1} \parallel \parallel \boldsymbol{FN_2} \parallel} \tag{3.13}$$

However, in the undeformed configuration $\boldsymbol{F} = \boldsymbol{C} = \boldsymbol{I}$, while it is expected that the strain to be zero in undeformed configuration, so, $\boldsymbol{F}$ and $\boldsymbol{C}$ are inappropriate strain measures. On the basis of this reasoning, a plausible strain measure could be the so-called *Lagrangian* or *Green strain* tensor $\boldsymbol{E}$, defined as:

$$\boldsymbol{E} = \frac{1}{2}(\boldsymbol{C} - \boldsymbol{I}) = \frac{1}{2}(\boldsymbol{F}^T\boldsymbol{F} - \boldsymbol{I}) \tag{3.14}$$

Since $\boldsymbol{C}$ is a second order tensor, there exists three scalar *invariants*, defined as:

$$\begin{aligned} I_{\boldsymbol{C}} &= tr(\boldsymbol{C}) \\ II_{\boldsymbol{C}} &= \frac{1}{2}\left[tr(\boldsymbol{C})^2 - tr(\boldsymbol{C}^2)\right] \\ III_{\boldsymbol{C}} &= det(\boldsymbol{C}) \end{aligned} \tag{3.15}$$

The scalar quantities $I_{\boldsymbol{C}}$, $I_{\boldsymbol{C}}$ and $I_{\boldsymbol{C}}$ are called invariants, since they do not change when we change the coordinate system.

An other strain measure also could be the so-called *Eulerian* or *Almansi strain* tensor $\boldsymbol{e}$:

$$\boldsymbol{e} = \frac{1}{2}(\boldsymbol{I} - \boldsymbol{B}^{-1}) \tag{3.16}$$

where the tensor $\boldsymbol{B}$ is the so-called *left Cauchy-Green deformation* tensor, defined as:

$$\boldsymbol{B} = \boldsymbol{F}\boldsymbol{F}^T \tag{3.17}$$

The deformation map affects not only the length of lines, but also volumes and areas. If we consider a parallelepiped, that has an infinetisimal

volume dV and dv, in the reference configuration and in the current configuration, respectively, the volume change can be written in terms of $\boldsymbol{F}$ as:

$$\frac{dv}{dV} = det(\boldsymbol{F}) = J \tag{3.18}$$

So, if a solid body is incompressible the volume change is null and $det(\boldsymbol{F}) = 0$.

Similarly, if we have consider a parallelepiped with area dA and da in the reference configuration and in the current configuration, respectively, the area change is given by

$$\frac{da}{dA} = det(\boldsymbol{F}) \parallel \boldsymbol{F}^{-T}\boldsymbol{N} \parallel \tag{3.19}$$

where $\boldsymbol{N}$ is an unit vector.

The deformation gradient $\boldsymbol{F}$ can be subject to the so-called *polar decomposition*. In particular we can rewrite $\boldsymbol{F}$ as a product of an orthogonal tensor $\boldsymbol{R}$ times a pure stretch tensor $\boldsymbol{U}$ or as a product of a different pure stretch tensor $\boldsymbol{V}$ and of the same orthogonal tensor $\boldsymbol{B}$:

$$\boldsymbol{F} = \boldsymbol{R}\boldsymbol{U} = \boldsymbol{V}\boldsymbol{R} \tag{3.20}$$

$\boldsymbol{R}$ represents a rotation, while $\boldsymbol{U}$ is indicated as the *material* or *right stretch tensor*, and $\boldsymbol{V}$ is indicated as the *spatial* or *left stretch tensor*. $\boldsymbol{R}$ acts on a vector in the reference configuration and it changes the vector direction without changing the vector length; $\boldsymbol{U}$ acts on a vector in the reference configuration and it changes the vector length without changing the vector direction; finally, $\boldsymbol{U}$ acts on a vector in the current configuration and it changes the vector length without changing the vector direction.

Displacement gradient

The change of configuration can be described by introducing the displacement field $\boldsymbol{u}$, defined as the difference between the current and the reference configurations:

$$\boldsymbol{u}(\boldsymbol{X}) = \boldsymbol{x}(\boldsymbol{X}) - \boldsymbol{X} \tag{3.21}$$

So, the current position vector $\boldsymbol{x}$ can be expressed as the sum of the reference position vector and of the displacement vector:

$$\boldsymbol{x} = \boldsymbol{\varphi}(\boldsymbol{X}) = \boldsymbol{X} + \boldsymbol{u}(\boldsymbol{X}) \tag{3.22}$$

In the small displacement filed, we can define a small displacement gradient $\nabla \boldsymbol{u}$ as

$$\| \nabla \boldsymbol{u} \| = \boldsymbol{\varepsilon} \qquad \text{with} \qquad \boldsymbol{\varepsilon} \ll 1 \tag{3.23}$$

In this contest, one can show that within an error of order $O(\varepsilon)$: the tensors $\boldsymbol{E}$ and $\boldsymbol{\varepsilon}$ coincide, as well as the tensors $\boldsymbol{C}$ and $\boldsymbol{B}$ coincide; the displacement gradient corresponding to a rigid deformation is skew.

So, a deformation map characterized by a small displacement gradient filed can be indicated as a *small deformation map* or symply we can talking about of *small deformation.*

3.3 Equilibrium

Equilibrium introduces proper quantities measuring internal forces, i.e., actions exchanged between neighborhood body subsets.

If we consider a body $\boldsymbol{B}$ in a configuration Ω, we postulate that the interaction between the external world and the body can be described through two force field: (i) a surface force field $\boldsymbol{t}$, with dimension of force by unit area and defined on a portion of the current boundary surface, $\partial\Omega^{\boldsymbol{t}}$; (ii) a volume force field, $\boldsymbol{b}$, with dimension of force by unit volume and defined on the current configuration Ω. Furthermore, we postulate that, the interaction between any portion of the body $\boldsymbol{P}$ internal to the body, and the remaining part of the body $\Omega/\boldsymbol{P}$, can be described through a surface force filed, indicated also as *traction force* field, with dimension of force by unit area defined on $\partial\boldsymbol{P}$. These interaction forces are assumed to be function of the local outward normal to $\boldsymbol{P}$, and, accordingly, we indicate this field with $\boldsymbol{t_n}$, where the subscript highlights the dependency form thr normal $\boldsymbol{n}$.

The *static equlibrium axioma* for a deformable body postulates that "a deformable body is in equilibrium if and only if the force resultant $\boldsymbol{r}(\boldsymbol{P})$ and the force momentum $\boldsymbol{m}(\boldsymbol{P})$ on each portion of the body are zeros" [3], i.e., a body $\boldsymbol{B}$ in a configuration Ω is in equilibrium if and only if:

$$\begin{aligned} \boldsymbol{r}(\boldsymbol{P}) &= \int_{\boldsymbol{P}} \boldsymbol{b} dv + \int_{\partial \boldsymbol{P}} \boldsymbol{t_n} da = 0 \qquad \forall \boldsymbol{P} \subseteq \Omega \\ \boldsymbol{m}(\boldsymbol{P}) &= \int_{\boldsymbol{P}} (\boldsymbol{x} \times \boldsymbol{b}) dv + \int_{\partial \boldsymbol{P}} (\boldsymbol{x} \times \boldsymbol{t_n}) da = 0 \qquad \forall \boldsymbol{P} \subseteq \Omega \end{aligned} \tag{3.24}$$

where $\boldsymbol{x}$ is the current position vector and the resultant momentum $\boldsymbol{m}$ is computed with respect to a generic origin $\mathbf{o}$.

The stress tensor

Through the *action-reaction principle* or *first Cauchy theorem*, which involves the traction force vector $\boldsymbol{t}_n$ (for more details see [3]), we can introduce the *second Cauchy theorem*, valid for any point internal to the body in a configuration Ω:

$$\boldsymbol{t_n} = \boldsymbol{\sigma n} \tag{3.25}$$

where $\boldsymbol{\sigma}$ is a second order tensor known as *Cauchy stress tensor*. Knowing $\boldsymbol{\sigma}$ in a point, it is possible to compute the stress vector $\boldsymbol{t_n}$ acting on any surface of normal $\boldsymbol{n}$ of a body $\boldsymbol{B}$. It is equivalent to say that $\boldsymbol{\sigma}$ contains all the information relative to the local state of stress.

It is sometimes convenient to decompose the traction vector $\boldsymbol{t_n}$, acting on a plane of unit normal $\boldsymbol{n}$, into a component normal to the plane and a component contained in the palne as:

$$\boldsymbol{t_n} = \sigma \boldsymbol{n} + \tau \boldsymbol{m} \tag{3.26}$$

where σ is the magnitude of the *normal traction component*, τ is the magnitude of the *shearing traction component*, $\boldsymbol{m}$ is a unit vector indicating the direction of the in-plane component.

The directions that maximize the normal component σ of the traction vector $\boldsymbol{t_n}$ can be computed formulating the problem as follows:

$$\text{find} \quad \max_{\boldsymbol{n}} (\boldsymbol{\sigma n} \cdot \boldsymbol{n}) \qquad \text{subject} \quad \text{to} \quad \boldsymbol{n} \cdot \boldsymbol{n} = 1 \tag{3.27}$$

To compute a solution, we need to rewrite it as an unconstrained problem, through the use of a Lagrangian formulation:

$$\mathcal{L}(\boldsymbol{n}, p) = \boldsymbol{\sigma n} \cdot \boldsymbol{n} - p(\boldsymbol{n} \cdot \boldsymbol{n} - 1) \tag{3.28}$$

with p a Lagrangian multiplier. The necessary condition for an extremum is that the derivative of the Lagrangian with respect to its arguments be equal to zero. In particular, taking the derivative of the Lagrangian with respect to $\boldsymbol{n}$, we get

$$\boldsymbol{\sigma n} = p\boldsymbol{n} \tag{3.29}$$

and to obtain a solution such that $\boldsymbol{n} \neq \boldsymbol{0}$, we need to require that:

$$det[\boldsymbol{\sigma} - p\boldsymbol{I}] = 0 \tag{3.30}$$

Through mathematical steps, we obtain the so-called *characteristic equation*:

$$-p^3 + Ip^2 + IIp + III = 0 \tag{3.31}$$

with:

$$\begin{aligned} I_{\boldsymbol{\sigma}} &= tr(\boldsymbol{\sigma}) \\ II_{\boldsymbol{\sigma}} &= \frac{1}{2}\left[tr(\boldsymbol{\sigma})^2 - tr(\boldsymbol{\sigma}^2)\right] \\ III_{\boldsymbol{\sigma}} &= det(\boldsymbol{\sigma}) \end{aligned} \tag{3.32}$$

where the scalar $I_{\boldsymbol{\sigma}}$, $II_{\boldsymbol{\sigma}}$ and $III_{\boldsymbol{\sigma}}$ are the so-called *Invariants* of the tensor $\boldsymbol{\sigma}$, since they do not change when we change the coordinate system. Through the balance of the angular momentum (3.24), we can demonstrate that the tensor $\boldsymbol{\sigma}$ is symmetric, i.e., its matrix representation has only six indipendent components, instead of nine.

Alternative representations for the stress are those that take into account the reference configuration and are known as *Piola-Kirchhoff stress tensors*. All the equilibrium considerations presented so far were relative to the current configuration Ω. However, thanks to the invertibility of the map $\boldsymbol{x} = \boldsymbol{\varphi}(\boldsymbol{X})$ and relating to the current configuration Ω to the reference configuration Ω_0, we can also write equilibrium equations relative to the current configuration Ω in terms of geometrical quantities relative to the reference configuration Ω_0; equilibrium equations relative to the reference configuration Ω_0 in terms of geometrical quantities relative to the reference configuration Ω_0. The *first Piola-Kirchhoff stress* tensor $\boldsymbol{P}$ is defined as:

$$\boldsymbol{P} = J\boldsymbol{\sigma}\boldsymbol{F}^{-T} \tag{3.33}$$

The tensor $\boldsymbol{P}$ represents the stress tensor relative to the current configuration per unit area in the refernece configuration, hence relative to forces normal to vectors relative to the reference configuration.

The balance of linear momentum relative to the current configuration, but expressed in terms of geometrical quantities relative to the reference configuration, can be rewrite. It returns the symmetry condition on the first Piola-Kirchhoff stress tensor, expressed as:

$$\boldsymbol{P}\boldsymbol{F}^T = \boldsymbol{F}\boldsymbol{P}^T \tag{3.34}$$

and it allows to introduce the *second Piola-Kirchhoff stress* tensor, $\boldsymbol{\Sigma}$, defined as:

$$\boldsymbol{\Sigma} = J\boldsymbol{F}^{-1}\boldsymbol{\sigma}\boldsymbol{F}^{-T} \tag{3.35}$$

The traction vector, acting in the reference configuration per unit area in the reference configuration, is now defined as $\boldsymbol{T_N}$:

$$\boldsymbol{T_N} = \boldsymbol{\Sigma N} \tag{3.36}$$

So, the tensor $\boldsymbol{\Sigma}$ represents the stress tensor relative to the reference configuration per unit area in the reference configuration.

3.4 Constitutive relations

A body response strongly depends on the nature of the constituent material. The strain and stress measures describe the macroscopic nature of the material constituting the body and they are called *constitutive relations*. Clearly, constitutive laws represent an idealization of the real world, hence they describe an ideal material, and many different idealizations are possible.

Since the polymer under investigation shows a purely viscoelastic response, to limit the discussion, we only focus on two particular constitutive models: hyperelastic and viscoelastic model.

3.4.1 Hyperelastic material

A material is said to be *Green elastic* or *hyper-elastic* if there exist a scalar *free-energy potential* (or *strain-energy potential*), U, determined entirely by the current state of deformation, such that the internal work density associated to a virtual change in deformation state is equal to the first variation of the potential U.

Assuming the strain $\boldsymbol{\varepsilon}$ as a measure for the local state of deformation, we have:

$$U = U(\boldsymbol{\varepsilon}) \tag{3.37}$$

such that the internal work density associated to a virtual strain field, $W^{int}_{\delta\boldsymbol{\varepsilon}} = \boldsymbol{\sigma} : \delta\boldsymbol{\varepsilon}$, is equal to the first variation of the potential $U(\boldsymbol{\varepsilon})$, that is:

$$W^{int}_{\delta\boldsymbol{\varepsilon}} = \boldsymbol{\sigma} : \delta\boldsymbol{\varepsilon} = dU(\boldsymbol{\varepsilon}) \tag{3.38}$$

with the first variation $\mathrm{d}U(\boldsymbol{\varepsilon})$ given in a more explicit format as follows:

$$dU(\boldsymbol{\varepsilon}) = \frac{\partial U(\boldsymbol{\varepsilon})}{\partial \boldsymbol{\varepsilon}} : \delta\boldsymbol{\varepsilon} \tag{3.39}$$

where the symbol δ highlights the fact that the quantity is evaluated in the direction of a virtual quantity. As a consequence, the density of internal work computed in going from an initial strain, $\boldsymbol{\varepsilon}_i$ to a final strain, $\boldsymbol{\varepsilon}_f$, depends only on such initial and final strains and not on the specific path followed to go from $\boldsymbol{\varepsilon}_i$ to $\boldsymbol{\varepsilon}_f$.

Comparison of Equation 3.38 and 3.39 results in:

$$\boldsymbol{\sigma} = \frac{\partial U}{\partial \boldsymbol{\varepsilon}} \tag{3.40}$$

hence $\boldsymbol{\sigma} = \boldsymbol{\sigma}(\varepsilon)$, taht is an hyper-elastic material.

The free energy can be though as representing the energy stored in a material during a deformation process, and should be in general a positive monotonic function. Moreover, the existence of a scalar function $U = U(\boldsymbol{\sigma})$ from which we may compute the stress underlines the *conservative nature* of the hyper-elastic model.

Isotropic material

A material is said *isotropic* if has the same response in all the directions as well as infinite symmetry planes. As a consequnce, the free-energy should be invariant for any change of the reference system, implying that U is a function of the strain only through its invariants:

$$U(\boldsymbol{\varepsilon}) = U(I_{\boldsymbol{\varepsilon}}, II_{\boldsymbol{\varepsilon}}, III_{\boldsymbol{\varepsilon}}) \tag{3.41}$$

where

$$\begin{aligned} I_{\boldsymbol{\varepsilon}} &= tr(\boldsymbol{\varepsilon}) \\ II_{\boldsymbol{\varepsilon}} &= \frac{1}{2}\left[tr(\boldsymbol{\varepsilon})^2 - tr(\boldsymbol{\varepsilon}^2)\right] \\ III_{\boldsymbol{\varepsilon}} &= det(\boldsymbol{\varepsilon}) \end{aligned} \tag{3.42}$$

The corresponding stress is:

$$\boldsymbol{\sigma} = \frac{\partial U}{\partial \boldsymbol{\varepsilon}} = \sum_{a=1}^{3} \frac{\partial U}{\partial I_a} \frac{\partial I_a}{\partial \boldsymbol{\varepsilon}} \tag{3.43}$$

If we now limit the discussion to the case of a *linear isotropic material*, the stress-strain relation should be linear. Therefore, the strain-energy may at most be a quadratic dependency on the strain, hence:

$$U(\boldsymbol{\varepsilon}) = U(I_{\boldsymbol{\varepsilon}}, II_{\boldsymbol{\varepsilon}}) \tag{3.44}$$

leaving out the dependency from $III_{\boldsymbol{\varepsilon}}$. In a more explicit format we can write:

$$U(\boldsymbol{\varepsilon}) = C_1(tr(\boldsymbol{\varepsilon})^2 + C_2(\boldsymbol{\varepsilon}^2) \tag{3.45}$$

where C_1 and C_2 are material constants.

Among the most common functions of strain energy, the most relevant for our analysis are: the Mooney-Rivlin function, the Neo-Hookean function (a submodel of the Mooney-Rivlin function) and the Polynomial function.

- *Mooney-Rivlin and Neo-Hookean strain energy function*

Mooney and Rivlin proposed a strain energy function U as an infinite series in powers of $(I_{\boldsymbol{\varepsilon}} - 3)$ and $(II_{\boldsymbol{\varepsilon}} - 3)$ of the form:

$$U(I_{\boldsymbol{\varepsilon}}, II_{\boldsymbol{\varepsilon}}) = \sum_{ij=0}^{n\to\infty} C_{ij}(I_{\boldsymbol{\varepsilon}} - 3)^i (II_{\boldsymbol{\varepsilon}} - 3)^i \tag{3.46}$$

Eequation (3.46) shows a series of powers which are usually truncated in the first terms. Then, taking only the first term of equation (3.46), the neo-Hookean model is obtained:

$$U = C_{10}(I_{\boldsymbol{\varepsilon}} - 3) \tag{3.47}$$

- *Polynomial strain energy function*

$$U = \sum_{i+j=1}^{N} C_{ij}(I_{\boldsymbol{\varepsilon}} - 3)^i (II_{\boldsymbol{\varepsilon}} - 3)^j \tag{3.48}$$

Such strain-energy functions will be used in the next chapter to modelling the polymer response under investigation.

3.4.2 Viscoelastic material

The behaviour of materials of low relative molecular mass is usually discussed in terms of two particular types of ideal material: the elastic solid and the viscous liquid. The former has a definite shape and is deformed by external forces into a new equilibrium shape; on removal of these forces it reverts instantaneously to its original form. The solid stores all the energy that it obtains from the external forces during the deformation, and this energy is available to restore the original shape when the forces are removed.

By contrast, a viscous liquid has no definite shape and flows irreversibly under the action of external forces.

One of the most interesting features of polymers is that a given polymer can display all the intermediate range of properties between an elastic solid and a viscous liquid depending on the temperature and the experimentally chosen time-scale. This form of response is termed viscoelasticity.

In the following we consider a simple case, i.e., an isotropic linear viscoelastic model, detailling the time-continuous version of the model.

Some phenomena in viscoelastic materials are: (i) if the stress is held constant, the strain increases with time (creep); (ii) if the strain is held constant, the stress decreases with time (relaxation); (iii) the effective stiffness depends on the rate of application of the load; (iv) if cyclic loading is applied, hysteresis occurs, leading to a dissipation of mechanical energy; (v) acoustic waves experience attenuation; (vi) rebound of an object following an impact is less than 100%; (vii) during rolling, frictional resistance occurs.

All materials exhibit some viscoelastic response. Synthetic polymers, wood, and human tissue as well as metals at high temperature display significant viscoelastic effects. In some applications, even a small viscoelastic response can be significant. Some examples of viscoelastic materials include amorphous polymers, semicrystalline polymers, biopolymers, metals at very high temperatures, and bitumen materials. Cracking occurs when the strain is applied quickly and outside of the elastic limit.

Let us see in detail the three main features of a visco-elastic response.

Hysteresis

Hysteresis is a strongly nonlinear phenomenon which occur in many systems, it represents the history dependence of physical systems. In mechanics, hysteresis can be defined as the dependence of the strain of a material on the instantaneous value and on the previous history of the stress; for example, the elongation is less at a given value of tension when the tension is increasing than when it is decreasing (Figure 3.1).

Creep

When subjected to a step constant stress, viscoelastic materials experience a time-dependent increase in strain. This phenomenon is known as viscoelastic creep.

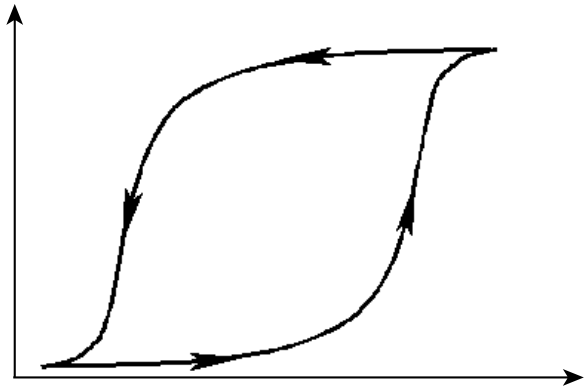

Figure 3.1: Loop of hysteresis.

At a time t_0, a viscoelastic material is loaded with a constant stress that is maintained for a sufficiently long time period. The material responds to the stress with a strain that increases until the material ultimately breaks. When the stress is maintained for a shorter time period, the material undergoes an initial strain until a time t_1, after which the strain immediately decreases (discontinuity) at times $t > t_1$ to a residual strain. The responses to two levels of stress for linear elastic and linear viscoelastic materials are compared in Figure 3.2. In the former case the strain follows the pattern of the loading programme exactly and in exact proportionality to the magnitude of the stresses applied. For the most general case of a linear viscoelastic solid, the total strain e is the sum of three essentially separate parts: e_1 (the immediate elastic deformation), e_2 (the delayed elastic deformation) and e_3 (the Newtonian flow, which is identical with the deformation of a viscous liquid obeying Newton's law of viscosity).

Because the material shows linear behaviour the magnitudes of e_1, e_2 and e_3 are exactly proportional to the magnitude of the applied stress, so that a creep compliance $J(t)$ can be defined, which is a function of time only:

$$J(t) = \frac{e(t)}{\sigma} = J_1 + J_2 + J_3 \tag{3.49}$$

where J_1, J_2 and J_3 correspond to e_1, e_2 and e_3. Linear amorphous polymers show a significant J_3 above their glass transition temperatures, when creep may continue until the specimen ruptures, but at lower temperatures J_1 and J_2 dominate. Crosslinked polymers do not show a J_3 term, and to a very good approximation neither do highly crystalline polymers.

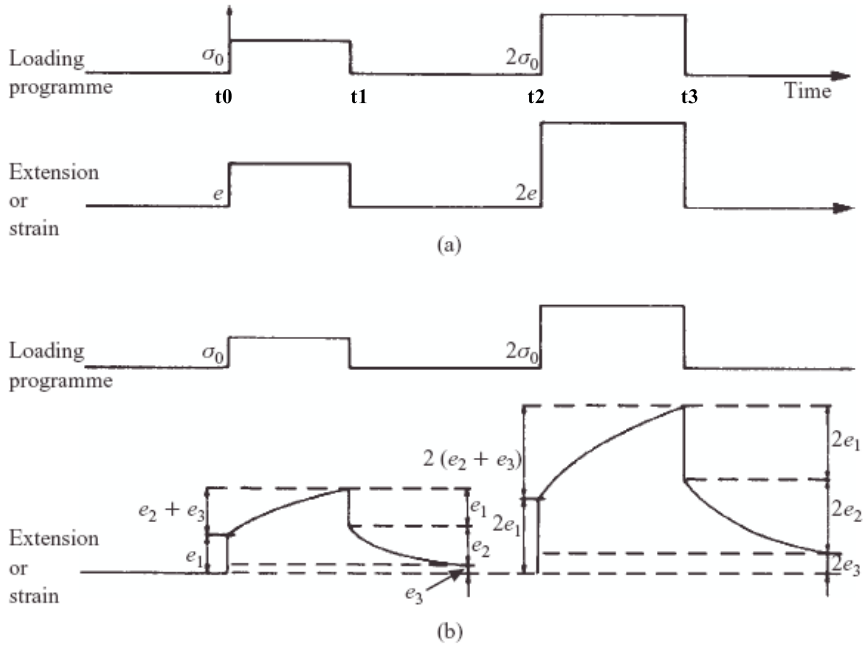

Figure 3.2: (a) Deformation of an elastic solid; (b) deformation of a linear viscoelastic solid.

The initial elastic deformation is sometimes called the *unrelaxed* response to distinguish it from the *relaxed* response observed at times long enough for the various relaxation mechanisms to have occurred. The maximum insight into the nature of creep is obtained by plotting the logarithm of creep compliance against the logarithm of time over a very wide time-scale (Figure 3.3). This diagram shows that at very short times the compliance (typically 10^{-9} Pa^{-1}) is that for a glassy solid and is independent of time; in contrast, at very long times the compliance (typically 10^{-5} Pa^{-1}) is that for a rubber-like solid and is again time independent. At intermediate times the compliance lies between these extremes and is time dependent, so that the behaviour is viscoelastic.

Creep function and Boltzmann superposition principle

Boltzmann proposed that:

1. the creep is a function of the entire past loading history of the specimen
2. each loading step makes an independent contribution to the final defor-

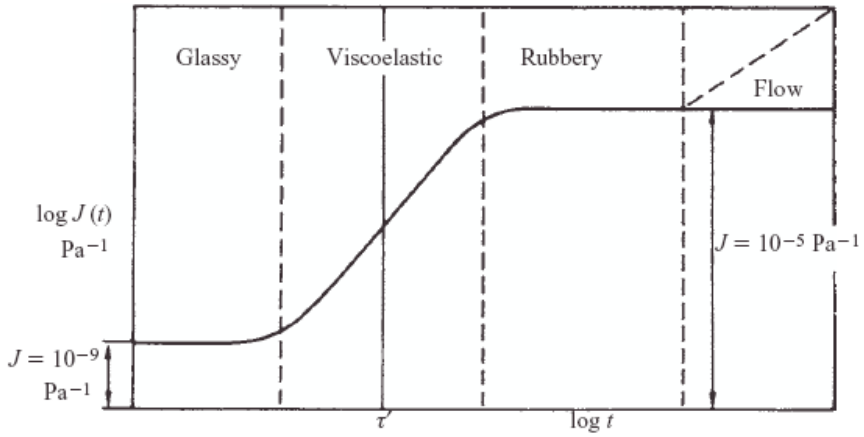

Figure 3.3: (a) The creep compliance $J(t)$ as a function of time t; τ' is the characteristic time (the retardation time).

mation, so that the total deformation can be obtained by the addition of all the contributions.

Figure 3.4 illustrates the creep response to a multistep loading programme, in which incremental stresses $\Delta\sigma_1, \Delta\sigma_2, \ldots$ are added at times $\tau_1, \tau_2, \ldots$ respectively. The total creep at time t is then given by

$$e(t) = \Delta\sigma_1 J_1(t-\tau_1) + \Delta\sigma_2 J_2(t-\tau_2) + \Delta\sigma_3 J_3(t-\tau_3) + \ldots \qquad (3.50)$$

where $J(t-\tau)$ is the creep compliance function. The summation of (3.50) can be generalized in integral form as

$$e(t) = \int_{-\infty}^{t} J(t-\tau)d\sigma(t) \qquad (3.51)$$

It is usual to separate out the instantaneous elastic response in terms of the unrelaxed modulus G_u, giving

$$e(t) = \frac{\sigma}{G_u} + \int_{-\infty}^{t} J(t-\tau)\frac{d\sigma(\tau)}{d\tau}d\tau \qquad (3.52)$$

where σ represents the total stress at the end of the experiment. Note that the integral extends from $-\infty$ to t, which implies that all previous elements of loading history must be taken into account and, in principle, the user must know the history of each specimen since its manufacture. In fact, when creep levels are low enough for linearity to apply, the deformation effectively levels off at sufficiently long times, so that only comparatively recent history is relevant.

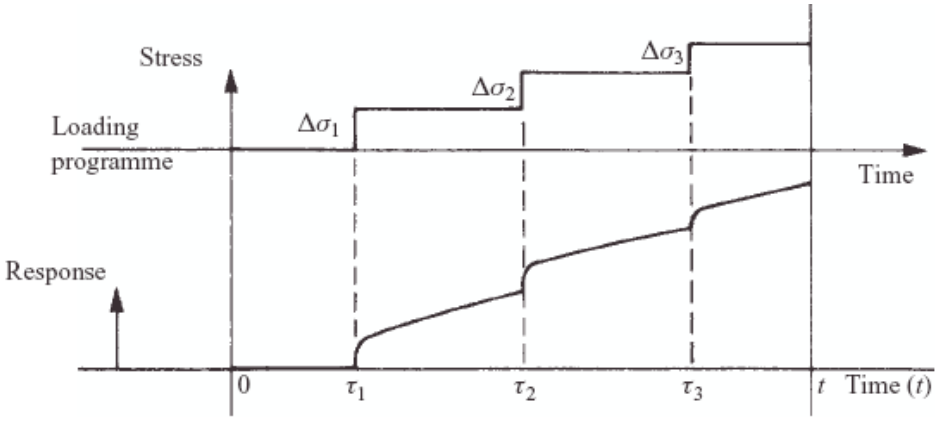

Figure 3.4: The creep behaviour of a linear viscoelastic solid.

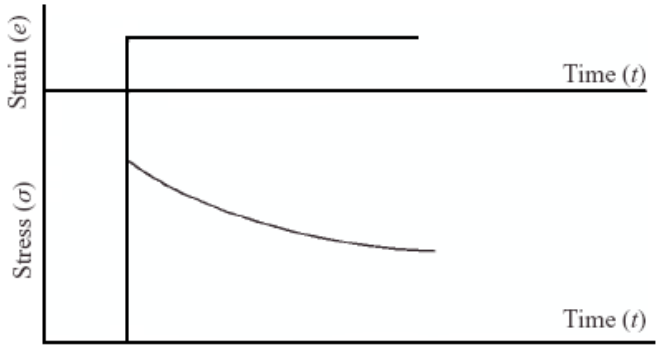

Figure 3.5: Stress relaxation (idealized)

Stress relaxation

Can be defined as the time-dependent decrease in stress of a material under sustained strain.

When an instantaneous strain is applied to an ideal elastic solid a finite and constant stress will be recorded. For a linear viscoelastic solid subjected to a nominally instantaneous strain the initial stress will be proportional to the applied strain and will decrease with time (Figure 3.5), at a rate characterized by the relaxation time τ. Making the assumption of linear viscoelastic behaviour we can define the stress relaxation modulus $G(t) = \sigma(t)/e$. Where there is no viscous flow, the stress decays to a finite value (Figure 3.5), to give an equilibrium or relaxed modulus G_r at finite time. As with

creep, we see that there are regions of glassy, viscoelastic, rubberlike and flow behaviour; similarly, changing temperature is equivalent to changing the time-scale. The relaxation time τ is of the same general magnitude as the retardation time τ', but the two are identical only for the simpler models [72].

Stress relaxation behaviour can be represented in an exactly complementary fashion using the Boltzmann superposition principle. Consider a stress relaxation programme in which incremental strains Δe_1, Δe_2, Δe_3, etc. are added at times τ_1, τ_2, τ_3, etc., respectively. The total stress at time t is then given by

$$\sigma(t) = \Delta e_1 G(t - \tau_1) + \Delta e_2 G(t - \tau_2) + \Delta e_3 G(t - \tau_3) + \dots \tag{3.53}$$

where $G(t-\tau)$ is the stress relaxation modulus. Equation (3.53) may be generalized in an identical manner in which Equation (3.54) leads to Equations (3.50) and (3.54) to give

$$\sigma(t) = [G_r] + \int_{-\infty}^{t} G(t - \tau)\frac{\mathrm{de}(\tau)}{\Delta\tau}\mathrm{d}t \tag{3.54}$$

where G_r is the equilibrium or relaxed modulus. Viscoelastic materials, such as amorphous polymers, semicrystalline polymers, and biopolymers, can be modeled in order to determine their stress or strain interactions as well as their temporal dependencies. These models, which include the Maxwell model, the Kelvin-Voigt model, and the Standard Linear Solid Model, are used to predict a material's response under different loading conditions. Viscoelastic behavior is comprised of elastic and viscous components modeled as linear combinations of springs and dashpots, respectively. The spring should be visualized as representing the elastic or energetic component of the response, while the dashpot represents the conformational or entropic component. Each model differs in the arrangement of these elements.

The elastic components, as previously mentioned, can be modeled as springs of elastic constant E, given the formula:

$$\sigma = E\varepsilon \tag{3.55}$$

where σ is the stress, E is the elastic modulus of the material, and ε is the strain that occurs under the given stress, similar to Hooke's Law.

The viscous components can be modeled as dashpots such that the stress-strain rate relationship can be given as

$$\sigma = \eta\frac{d\varepsilon}{dt} \tag{3.56}$$

where η is the viscosity of the material.

The relationship between stress and strain can be simplified for specific stress rates. For high stress states/ short time periods, the time derivative components of the stress-strain relationship dominate. A dashpots resists changes in length, and in a high stress state it can be approximated as a rigid rod. Since a rigid rod cannot be stretched past its original length, no strain is added to the system. Conversely, for low stress states/longer time periods, the time derivative components are negligible and the dashpot can be effectively removed from the system - an "open" circuit. As a result, only the spring connected in parallel to the dashpot will contribute to the total strain in the system.

Maxwell model

The Maxwell model can be represented by a purely viscous damper and a purely elastic spring connected in series, as shown in the Figure 3.6.

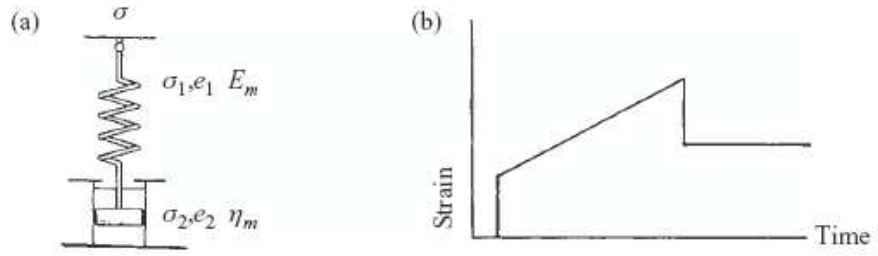

Figure 3.6: (a) The Maxwell unit; (b) creep and recovery behaviour

The model can be represented by the following equation:

$$\frac{d\varepsilon_{Total}}{dt} = \frac{\sigma}{\eta} + \frac{1}{E}\frac{d\sigma}{dt}. \tag{3.57}$$

Under this model, if the material is put under a constant strain, the stresses gradually *relax*. When a material is put under a constant stress, the strain has two components: (i) an elastic component occurs instantaneously, corresponding to the spring, and relaxes immediately upon release of the stress; (ii) a viscous component that grows with time as long as the stress is applied. The Maxwell model predicts that stress decays exponentially with time, which is accurate for most polymers. One limitation of this model is that it does not predict creep accurately. The Maxwell model

for creep or constant-stress conditions postulates that strain will increase linearly with time. However, polymers for the most part show the strain rate to be decreasing with time.

Kelvin-Voigt model

The Kelvin-Voigt model, also known as the Voigt model, consists of a Newtonian damper and Hookean elastic spring connected in parallel, as shown in the Figure 3.7. It is used to explain the stress relaxation behaviors of polymers.

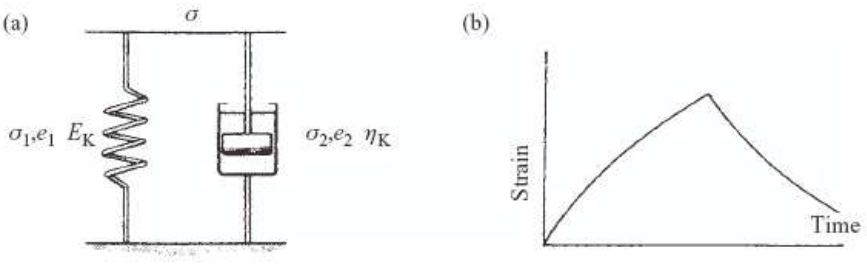

Figure 3.7: (a) The Kelvin-Voigt unt; (b) creeo and recovery behaviour

The constitutive relation is expressed as a linear first-order differential equation:

$$\sigma(t) = E\varepsilon(t) + \eta\frac{d\epsilon(t)}{dt} \tag{3.58}$$

This model represents a solid undergoing reversible, viscoelastic strain. Upon application of a constant stress, the material deforms at a decreasing rate, asymptotically approaching the steady-state strain. When the stress is released, the material gradually relaxes to its undeformed state. At constant stress (creep), the model is quite realistic as it predicts strain to tend to $\sigma/\ E$ as time continues to infinity. Similar to the Maxwell model, the Kelvin-Voigt model also has limitations. The model is extremely good with modelling creep in materials, but with regards to relaxation the model is much less accurate.

Standard Linear Solid Model

The Standard Linear Solid Model effectively combines the Maxwell Model and a Hookean spring in parallel. A viscous material is modeled as a spring

and a dashpot in series with each other, both of which are in parallel with a lone spring (Figure 3.8).

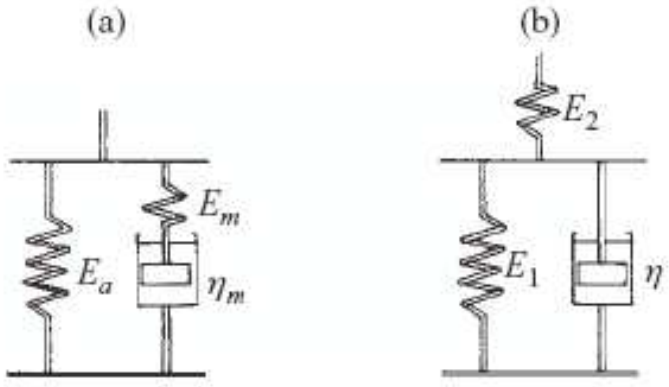

Figure 3.8: Three element model: (a) is known as the standard linear solid

For this model, the governing constitutive relation is:

$$\frac{d\varepsilon}{dt} = \frac{\frac{E_2}{\eta}\left(\frac{\eta}{E_2}\frac{d\sigma}{dt} + \sigma - E_1\varepsilon\right)}{E_1 + E_2} \tag{3.59}$$

Under a constant stress, the modeled material will instantaneously deform to some strain, which is the elastic portion of the strain, and after that it will continue to deform and asymptotically approach a steady-state strain. This last portion is the viscous part of the strain. Although the Standard Linear Solid Model is more accurate than the Maxwell and Kelvin-Voigt models in predicting material responses, mathematically it returns inaccurate results for strain under specific loading conditions and is rather difficult to calculate.

Generalized Maxwell Model

The Generalized Maxwell also known as the Maxwell-Weichert model is the most general form of the models described above. It takes into account that relaxation does not occur at a single time, but at a distribution of times. Due to molecular segments of different lengths with shorter ones contributing less than longer ones, there is a varying time distribution. The Weichert model shows this by having as many spring-dashpot Maxwell elements as are necessary to accurately represent the distribution. The Figure 3.9 represents a possible Weichert model.

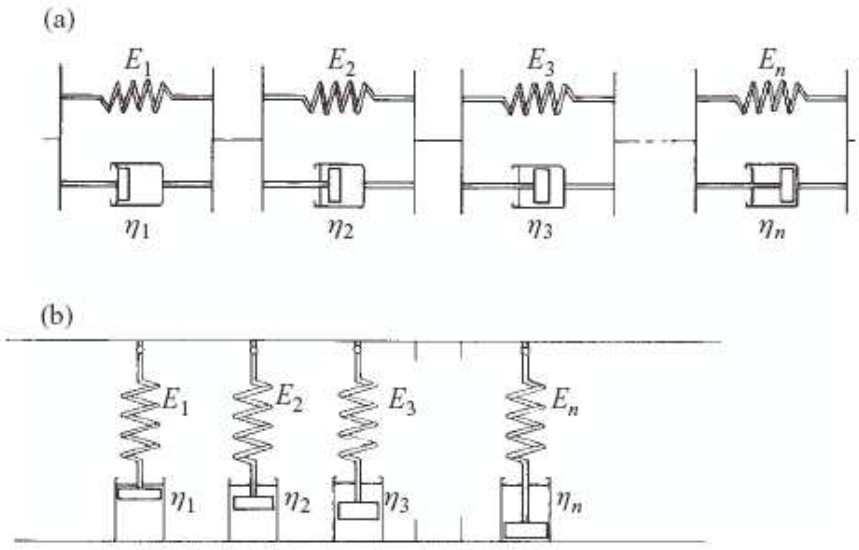

Figure 3.9: Schematic of Maxwell-Weichert Model

3.4.3 Prony series

In order to determine the time dependent stress - strain state in a linear viscoelastic material, under an arbitrary loading process, the deformation history must be considered. The time dependent constitutive equations of a solid viscoelastic material include these history effects. The load (stress) and displacement (strain) history, the loading rate (displacement rate), and time of load application on the specimen are all needed to determine the constants in the constitutive equations. A common form for these constitutive equations employs a Prony series, i.e., a series of the form

$$\sum_{i=1}^{N} k_i e^{\frac{-t}{\tau_i}} \tag{3.60}$$

where k_1 is the i-th Prony constant and τ_i is the Prony retardation time constant.

Creep and relaxation tests are most commonly used to determine the viscoelastic material properties. In ideal relaxation and creep tests, the displacements or loads are applied to the specimen instantly. In the real test, especially for a large structural component, limitations of the testing equipment result in a relatively low strain rate and long period of loading. The response during the period of loading is typically ignored, and only the

data obtained during the period of constant displacement or constant load are used to determine the material properties. Ignoring this long loading period and the strain rate effects in the data reduction introduces additional errors in the determination of the material properties.

The viscoelastic model can also be formulated in differential form. This is becoming popular recently since the differential models can be effectively incorporated into finite element algorithms. When using these internal variable methods, each Prony series term is associated with a material internal state variable. In the discrete finite element model, each term in the Prony series adds a substantial number of global variables. Thus, a short Prony series, which can accurately represent the material, is desirable. Nonlinear regression methods can help with determining a short and accurate Prony series.

Chapter 4

Constitutive modelling of the poly-L-lactic acid

In this chapter we will discuss the work I have done in the laboratory of structural mechanics of the University of Pavia. The purpose of said work was to study a constitutive model for a biodegradable polymer whose use, in these last years, has been aimed at building endovascular devices, like stents. The subject of this work is the poly-L-lactic acid (PLLA). After a brief introduction of its chemical properties, we will examine its mechanical response at fixed degradation levels.

First, we well develop the concept within the theory of elasticity and later we will expand it to account for the nonlinear response under finite deformations. The parameters used for the constitutive model are the ones found in literature, due to the impossibility to conduct appropriate mechanical tests. For a better understanding of the work done, a little section of this chapter is devoted to a particular text taken as reference [56].

4.1 Introduction to material

Mechanical behavior of polymers show a viscoelastic nature due to common microstrutural characteristics among them. When an external force is applied to a material, internal forces are produced by distortion of its physical structure. Viscoelastic phenomena in polymers are related to the movement of flexible thread-like long chain molecules. The conformational changes of these long molecules happen at different time and space scale,

ranging from gross long-range contour rearrangement to the atomic level reorientation of bonds in the chains.

From a macroscopic standpoint, viscoelastic materials show three characteristics (as seen in the previous chapter): (i) stress relaxation, which is a time dependent decrease in load for a constant deformation; (ii) creep, which is a time-dependent increase in deformation under the action of a constant load; (iii) hysteresis, associated with dissipative system, on which the work done by deformation is not fully recoverable but converted to heat energy.

4.1.1 Statistical model of the PLLA network

Before proceeding with the development of a constitutive model for degradable polymeric solids, we should briefly resume some concepts about the structure of a polymeric network.

The basic structure of polymer molecules consists of flexible chains that can adopt a very large number of conformations. Usually, these chains are connected to one another by cross-linkages, but most of the structure consists of the intervening polymer chains each comprising a sufficiently high number of bonds between crosslinks. Upon application of external stimuli, the long chains are able to rearrange into other conformations, in particular into more extended ones that allow sufficiently large deformations. Uncoiling takes place and chains tend to become aligned parallel to the axis of elongation. The ability to recover from large deformations is related to the ability of the chains to return to their initial configurations [56].

PLLA is a semicrystalline polymer that degrades through hydrolytic scission of the ester groups and its degradation time is much slower than that of PDLA, requiring more than 2 years to be completely absorbed.

The statistical theory for rubber elasticity, based on assumptions seen before, yields the definition of the stored energy function, for polymeric materials, given by

$$U = \frac{\rho RT}{2M_w}(\lambda_1^2 + \lambda_2^2 + \lambda_3^2 - 3) \tag{4.1}$$

where λ_i are the principal stretches, ρ the density, R the universal gas constant, T the absolute temperature, and M_w is the molecular weight of the portion of a molecule lying between successive junction points [67].

4.2 Reference framework

In the framework taken as start point for my work, PLLA fibers were obtained from PLLA pellets and produced by wet-spinning technique [22] [56]. The main polymer's features provided were:

- intrinsic viscosity of the melt in chloroform at 25°C

$$\eta = 5.45\text{x}10^{-4} M_{\nu}^{0.73};$$

- viscometric molecular weight $M_{\nu} = 60.654$ g/mol ;
- glass transition temperature $\mathrm{T}_g = 58°\mathrm{C}$;
- melting temperature $\mathrm{T}_m = 180°\mathrm{C}$;
- crystallization temperature range form 90°C to 110°C;
- crystalline fraction $x_c \approx 51\%$.

Mechanical testing included ramp increases in displacement at a constant rate of 100μm/min and consecutively ramp displacement up to 300μm. The results showed that strain induced chain alignment, which rendered the sample slightly stiffer for the second test.

The controlled force mode was investigated with other samples; tests with prescribed ramps in force of 1.0 N/min were conducted consecutively. The main results obtained by these tensile experiments were: (i) a delayed recovery after the instantaneous release of either strain or stress, and (ii) a dependency of the response of the material on the rate at which it was loaded. The same deformation yielded higher stresses if the material was deformed faster, and the response was not instantaneous, as the fiber took a few minutes (about 10) to recover its initial shape.

Furthermore, creep, stress relaxation tests and cyclic load tests were performed to study the response of the polymer.

Samples subject to cyclic ramp in stress showed mechanical hysteresis. The responses obtained by creep tests showed these typical features: an instantaneous increase in strain, and a continued straining in time at a non-constant rate. The instantaneous increase in strain was thought as an instantaneous elastic response and the total creep curve was a combination of elastic and viscous effects. After that the stress was released to zero, the

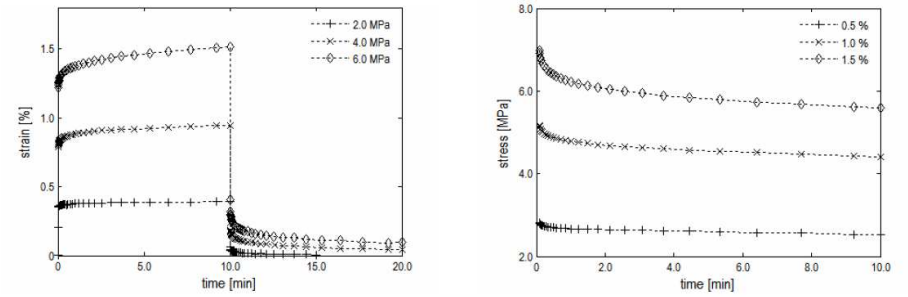

Figure 4.1: Experimental data from non-degraded PLLA creep and stress relaxation tests

test response showed instantaneous strain recovery, followed by a delayed recovery.

The stress relaxation test was characterized by an instantaneous increase in strain and then held fixed for 10 minutes. The results were an instantaneous jump in stress followed by a gradual decrease of the stress required to maintain the constant strain ε_0 over time. The responses of both experiments are showed in Figure 4.1.

Since the response of PLLA at very high strain rates looks like it is insensitive to strain rate of loading (5%/min and 10%/min), experimental testing were used to obtain a time independent instantaneous elastic response (IER) (Figure 4.2), hence, in order to better fit the experimental data, hyperelastic models were used.

The responses before strain of 5%, which comprised both tests, seemed to concord, and the validity of an IER independent of strain rate seemed to hold. The strain steps applied to the samples during stress relaxation tests (Figure 4.1, right graphic) were up to 3%, hence, for data reduction purposes, the range 0% to 5% had been chosen as validity range for the constitutive equations employed to describe the IER of PLLA.

Experimental data obtained from uniaxial extension tests, in the reference framework, are showed in Figure 4.3.

4.3 Constitutive modelling of the non-degraded PLLA

Starting from considerations and results seen in the reference framework of the previous section, we will now move onto the constitutive modelling for

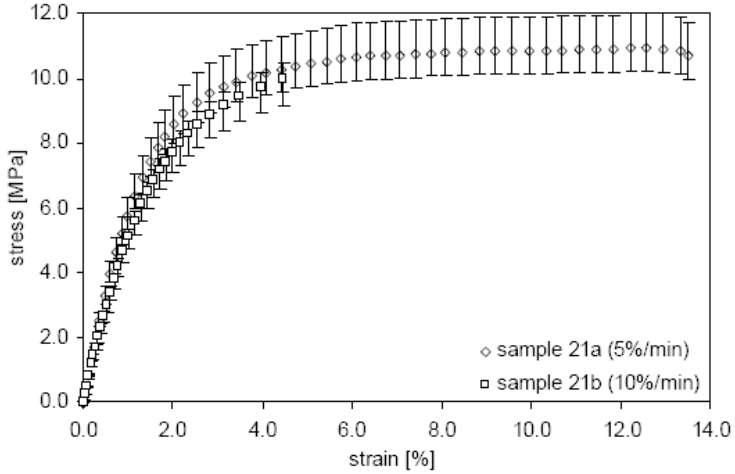

Figure 4.2: Non degraded PLLA instantaneous elastic response. Intense strain softening is observed after some deformation is achieved. Two regime are distinguished: an initial increase followed by deformation with little increase in stress.

the polymer. Hyperelastic and viscoelastic model will be used to reproduce the trend of the experimental curves.

The plots were obtained with the **Matlab** program. Other programs like **Maple** were sometimes used to find numerical solutions of some problems.

4.3.1 Hyperelastic models

The first choices for hyperelastic models were the Neo-Hookean and the Mooney-Rivlin models, with the corresponding stored energy function given by equations:

$$U^{NH} = \frac{G}{2}(I_{\boldsymbol{C}} - 3) \tag{4.2}$$

$$U^{MR} = \frac{C_1}{2}(I_{\boldsymbol{C}} - 3) + \frac{C_2}{2}(II_{\boldsymbol{C}} - 3). \tag{4.3}$$

where G is the shear modulus and C_1 and C_2 are constants that describe the material properties; $I_{\boldsymbol{C}}$ and $II_{\boldsymbol{C}}$ are the first and second invariants of the Cauchy-Green stretch tensor given by:

$$I_{\boldsymbol{C}} = \lambda^2 + \frac{2}{\lambda}; \qquad II_{\boldsymbol{C}} = \frac{1}{\lambda^2} + 2\lambda \tag{4.4}$$

and λ is the axial stretch related to strain(ε) by the relation $\lambda = 1 + \varepsilon$. To simulate the material response to a simple tensile test, an uniaxial extension

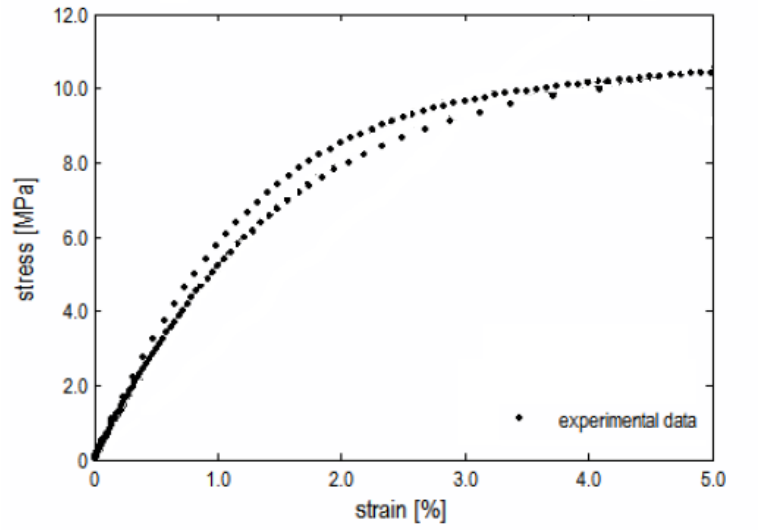

Figure 4.3: Experimental data from uniaxial test on PLLA non-degraded [56].

was considered and the corresponding motion is given by

$$x_1 = \frac{1}{\sqrt{\lambda}} X_1, \qquad x_2 = \frac{2}{\sqrt{\lambda}} X_2, \qquad x_1 = \lambda X_3, \tag{4.5}$$

where $(X_1, X_2, X_3,)$ and (x_1, x_2, x_3) represent the coordinate of a material particle in the undeformed and deformed configurations, respectively.

The deformation gradient $\mathbf{F}$ corresponding to the motion above has this matrix representation:

$$\mathbf{F} = \begin{pmatrix} 1/\sqrt{\lambda} & 0 & 0 \\ 0 & 1/\sqrt{\lambda} & 0 \\ 0 & 0 & \lambda \end{pmatrix} \tag{4.6}$$

The left and right Cauchy-Green stretch tensor have the same matrix representation with respect to the above defined coordinate system:

$$(\mathbf{B}) = (\mathbf{C}) = \begin{pmatrix} 1/\lambda & 0 & 0 \\ 0 & 1/\lambda & 0 \\ 0 & 0 & \lambda^2 \end{pmatrix} \tag{4.7}$$

The Cauchy stress in a Neo-Hookean and a Mooney-Rivlin body undergoing uniaxial extension have the following matrix representations, respectively:

$$\boldsymbol{\sigma}^{NH} = \begin{pmatrix} -p + G/\lambda & 0 & 0 \\ 0 & -p + G/\lambda & 0 \\ 0 & 0 & -p + G\lambda^2 \end{pmatrix} \tag{4.8}$$

$$\boldsymbol{\sigma}^{MR} = \begin{pmatrix} -p + C_1/\lambda - C_2\lambda & 0 & 0 \\ 0 & -p + C_1/\lambda - C_2\lambda & 0 \\ 0 & 0 & -p + C_1\lambda^2 - C_2/\lambda \end{pmatrix} \tag{4.9}$$

Assuming that the lateral surface of the fiber is traction free and with the enforcement of incompressibility, it is possible to derive the Lagrange multiplier p. If the traction is directed in z direction, the σ_{xx} and σ_{yy} components of the stress tensors are zero, then p becomes:

$$p^{NH} = \frac{G}{\lambda}; \qquad p^{MR} = \frac{C_1}{\lambda} - C_2\lambda \tag{4.10}$$

So the Cauchy stress tensors only have a single non-zero component in z direction, and replacing the (4.10) in the (4.8) and (4.9) we obtain:

$$\sigma_z^{NH} = G\left(\lambda^2 - \frac{1}{\lambda}\right) \tag{4.11}$$

$$\sigma_z^{MR} = C_1\left(\lambda^2 - \frac{1}{\lambda}\right) + C_2\left(\lambda - \frac{1}{\lambda}^2\right) \tag{4.12}$$

Because we are under a large displacement conditions, it is necessary to use the Piola-Kirchoff stress tensor given by:

$$\mathbf{P} = \frac{\partial U}{\partial \mathbf{F}} \tag{4.13}$$

thus the corresponding Neo-Hookean and Mooney-Rivlin stress tensors are:

$$P_z^{NH} = G\left(\lambda - \frac{1}{\lambda^2}\right) \tag{4.14}$$

$$P_z^{MR} = C_1\left(\lambda - \frac{1}{\lambda^2}\right) + C_2\left(1 - \frac{1}{\lambda^3}\right) \tag{4.15}$$

The stress-strain curves obtained from this models are showed in Figure 4.4.

From a comparison with the experimental data found in the reference framework (Figure 4.3), these models are not useful to describe the PLLA response under uniaxial extension. The Neo-Hookean model fails to describe the strain softening behavior of the material and the Mooney-Rivlin material stored energy function is only able to do so with negative C_1. So,

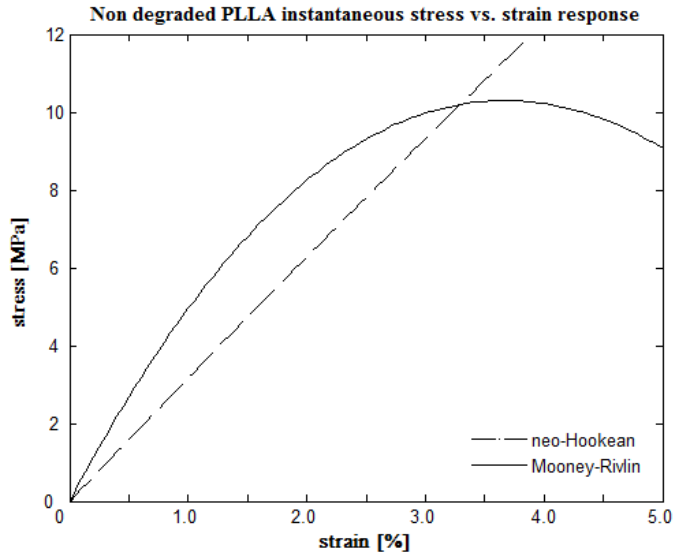

Figure 4.4: Non-degraded PLLA instantaneous stress vs. strain response; Noe-Hookean and Mooney-Rivlin Model.

with the purpose of better describing the experimental data of the reference framework, a higher order stored energy function was considered, such as the extension of the Mooney-Rivlin material, i.e.

$$U = C_1 e^{-(I_C - 3)}(I_{\boldsymbol{C}} - 3) + C_2 \ln[1 + a(I_{\boldsymbol{C}} - 3)] \tag{4.16}$$

The axial stress P_z is given by $\partial U / \partial I_C$.

$$P_z = 2\left[C_1 e^{-(\lambda^2 + 2/\lambda - 3)}\left(4 - \lambda^2 - \frac{2}{\lambda}\right) + \frac{aC_2}{1 + a(\lambda^2 + 2/\lambda - 3)}\right]\left(\lambda - \frac{1}{\lambda^2}\right) \tag{4.17}$$

and the consequent plot stress vs. strain is showed in Figure 4.5. This stored energy function shows a trend that is very similar to that of the data of the reference framework. Furthermore, this stored energy function shows acceptable phenomenological characteristics beyond 5%strain: as the state of deformation increases, the rate of change of stored energy decreases.

4.3.2 Viscoelastic model

The viscoelastic model used here was introduced by Fung [76] and its concept was a multiplicative separation between the relaxation function and the instantaneous elastic response. For simplicity, a two term Prony series

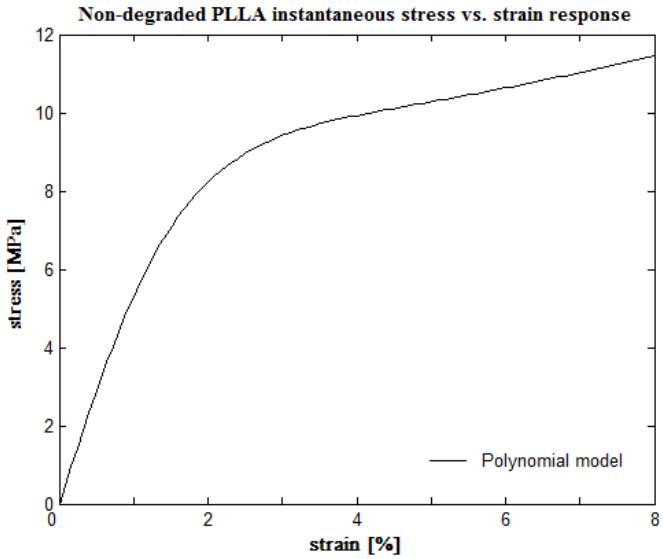

Figure 4.5: Non-degraded PLLA instantaneous stress vs. strain response; polynomial second order model

was chosen to represent the relaxation function:

$$G(t) = k_0 + k_1 e^{-\frac{t}{\tau_1}} + k_2 e^{-\frac{t}{\tau_2}} \tag{4.18}$$

where $k_0 = 1 - k_1 - k_2$, so that $G(0) = 1$, k_1, k_2, τ_1, τ_2 are positive constants that describe the stress relaxation of non-degraded PLLA.

The stress response of the viscoelastic model with the IER (4.17) and with the relaxation function (4.18) is given by

$$P(t) = \int_{-\infty}^{t} G(t-s) \frac{dP_z}{d\lambda} \frac{d\lambda}{ds} ds \tag{4.19}$$

where $P(t)$ is the Piola stress, $\lambda = \lambda(t)$ is the uniaxial stretch history and $G(t)$ is the relaxation function.

Stress relaxation analysis were performed with the following ideal strain history:

$$\varepsilon(t) = \begin{cases} 0 \quad , & t < 0 \\ \dfrac{\varepsilon_0}{T} t \quad , & t \in [0, T] \\ \varepsilon_0 \quad ; & t > T \end{cases} \tag{4.20}$$

where ε_0 is the step in strain and T the rise time. A constant rate increase to ε_0 occurs during the rise time interval and as $T \to 0$, the ramp history

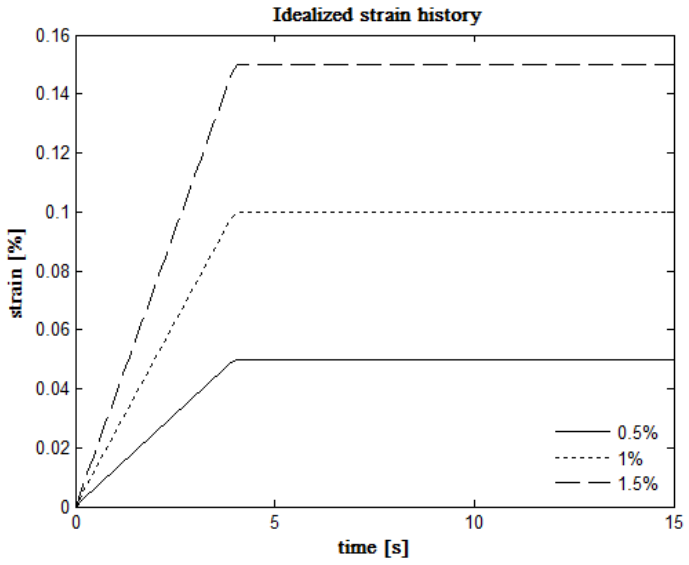

Figure 4.6: Strain history for stress relaxation tests.

approaches the step strain history (Figure 4.6). The response obtained with the constants k_1 and τ_1 and the strain history (4.20) is showed in Figure 4.7.

Analyzing this response and comparing it to the experimental stress relaxation data in Figure 4.1 (right graphic) we could say that this viscoelastic model describes, within certain accuracy, the viscoelastic response of material.

The constants used in the models are summarized in Table 4.1.

4.4 Model for degradable polymeric solids

Based on a general framework that describes the response of dissipative systems, Rajagopal et al. [26] developed a model for polymeric solids undergoing strain-induced degradation, due to scission of the polymer chains. The thermodinamic based model was obtained through the incorporation of an appropriate form for the rate of dissipation

$$\xi := \boldsymbol{\sigma} \cdot \mathbf{D} - \rho\dot{\psi} \geq 0$$

where $\boldsymbol{\sigma} \cdot \mathbf{D}$ is the stress power and $\dot{\psi}$ the rate of increase of the Helmholtz potential. Following the framework of Rajagopal and coworkers [24] [25],

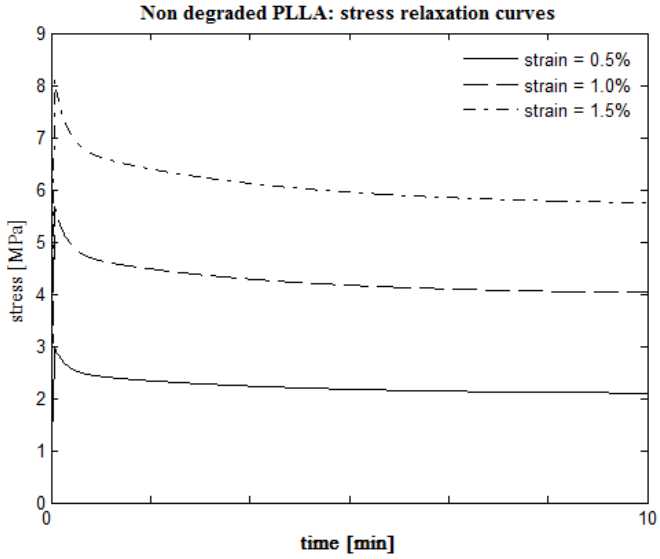

Figure 4.7: Non-degraded PLLA viscoelastic stress relaxation response after 10 minute

the specification of constitutive forms for the Helmholtz potential and for the rate of entropy production yielded a constitutive model.

Rajagopal et al. [26] said that "it is common practice in developing constitutive theories of this sort to stipulate the constitutive equation for the stress in terms of the derivatives of ψ as well as for the reaction rate and choose coefficients such that the inequality above is met, thus satisfying the second law of thermodynamics". The development of a model for degradable polymeric solids following such phenomenological approach is the main concern of this section.

Equation (4.1) and the stored energy of a Neo-Hookean hyperelastic material (Eq. 4.2) are similar but were obtained from different reasonings. Hence, there is a an obvious relationship between the properties of the polymeric network (through M_w) and its macroscopic shear modulus G, i.e. as the size of the segments between crosslinks decreases the network becomes stiffer and the modulus G increases.

Since the connection between hyperelastic materials and the simplest statistical model for molecular networks has been made, the statistical theory of rubber elasticity and non-linear elasticity became closely related.

Other works [65][23] showed that changes in chain conformation, scission and subsequent crosslinking lead to softening and permanent set on removal

Constitutive model	**Material constants [MPa]**	**[s^{-1}]**
Neo-Hookean	G = 106.64	
Mooney-Rivlin	C_1 = -2545	
	C_2 = 2739	
Polynomial	C_1 = 17.999	
	C_2 = 0.17047	
	a = 477.28	
Viscoelastic	k_1 = 0.17659	τ_1 = 11.852
	k_2 = 0.13822	τ_2 = 198.56

Table 4.1: Material constant of the hyperelastic model for the description of the IER of non-degraded PLLA

of the load. On the other hand, the events that occur to the polymer bulk upon scission follow these stages:

1. a reduction in molecular weight resulting directly from the chemical reaction occurs;
2. a loss of mechanical properties directly related with the decrease amount of effective crosslinked segments occurs;
3. a loss in mass that is perceived as dissolution and erosion of oligomers and monomers [32] occurs.

The proposed model tries to describe scission and loss of mechanical properties that occur during the short and medium term period.

4.4.1 Model for degradable PLLA

For simplicity's sake we assume that the properties of the material depend on the extent of scission and consequent molecular weight reduction. Such dependence is captured by introducing a degradation parameter d that expresses the fraction of broken bonds in a polymeric chain and quantifies the degree of local degradation of a given particle at place $\mathbf{x}$ and at time t in a representative volume:

$$d = d(\mathbf{x}, t) \tag{4.21}$$

We assume that d has values between zero and unity, hence it will always be > 0; $1 - d$ is a measure of the fraction of intact crosslinks in a representative

volume element of the body; the value $d = 0$ represents the specimen in the virgin state and $d = 1$ corresponds to the state of maximum possible degradation, i.e. a network without any remaining crosslinked segments.

A rate equation governing the degradation process is assumed:

$$\frac{\partial d}{\partial t} = \mathcal{D}(d, \mathbf{F}, \boldsymbol{\sigma}). \tag{4.22}$$

where $\dot{d}(t)$ is assumed to be dependent on the extent of degradation (d), the state of deformation ($\mathbf{F}$) and the stress ($\boldsymbol{\sigma}$). Rajagopal et al. [26], following a constitutive framework that maximizes the rate of dissipation, obtained a governing equation for strain-induced degradation:

$$\frac{\partial d}{\partial t} = (1 - d)\mathcal{B}(D) \tag{4.23}$$

where $\mathcal{B}$ is a function that depends on the deformation gradient $\mathbf{F}$ (4.6) and D can be seen as *driving forces* that depend on $\mathbf{F}$ through. Equation (4.23) governs the rate of increase of degradation in a material that undergoes strain-induced scission and that shows an elastic behavior at fixed levels of degradation (hence, $\xi = 0$ when $\partial d/\partial t = 0$).

The constitutive models of interest for the description of the degradable PLLA are such that their response is made to depend on the degradation parameter and assumes the general form

$$\boldsymbol{\sigma} = \boldsymbol{\sigma}(\mathbf{F}, d). \tag{4.24}$$

Hence, the material properties become functions of d, i.e. they are no longer a set of material constants, but a set of material functions, $C_i = C_i(d)$.

Degradable materials at fixed degradation

We assume that a non-degraded body is an incompressible, isotropic and hyperelastic solid. The hyperelastic models studied in the previous sections will now be reviewed by the addition of the degradation parameter d.

The first model considered was that of Neo-Hookean, characterized by a strain energy and a uniaxial Piola stress of Equations 4.2 and 4.14 respectively, that now become:

$$U^{NH}(d) = \frac{G(d)}{2}(I_{\boldsymbol{C}} - 3) \tag{4.25}$$

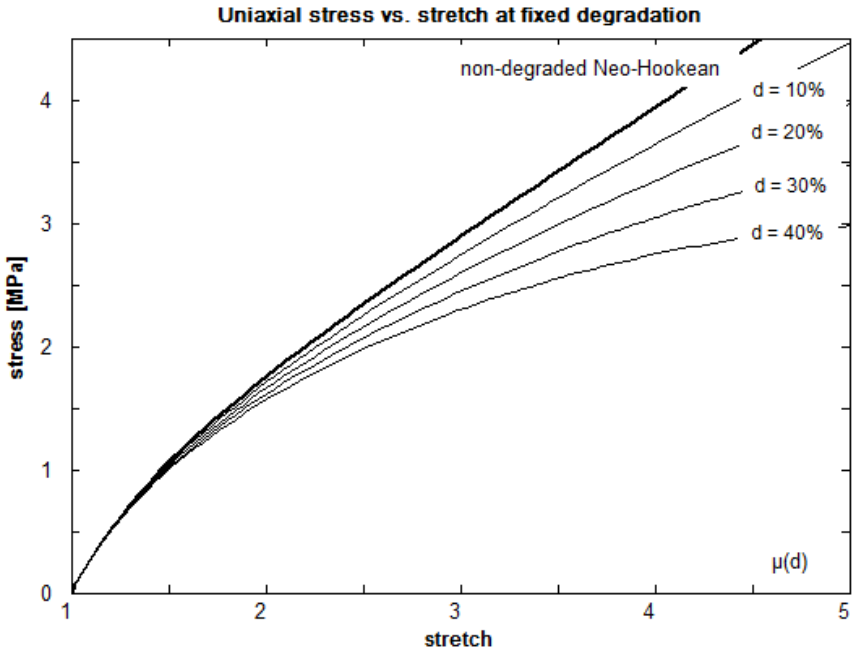

Figure 4.8: Uniaxial stress vs. stretch a different levels of degradation of a degradable material that in the virgin state responds as a Neo-Hookean material.

$$P^{NH}(d) = G(d)\left(\lambda - \frac{1}{\lambda^2}\right). \tag{4.26}$$

The shear modulus G is now a material function dependent on the degradation. The form of material property reduction with the amount of degradation, in agreement with [26], has been chosen to be the simplest possible, i.e. a linear decrease in d, and takes the following form:

$$G(d) = G_0(1 - \beta d) \tag{4.27}$$

where G_0 is the shear modulus of the non-degraded body and $\beta < 1$ is a constant related with the maximum state of degradation. When the maximum degradation is achieved, the shear modulus is given by $G(d = 1) = G_0(1-\beta)$. When the degradation is complete, $\beta = 1$ and the material fails, hence the (4.27) becomes:

$$G(d) = G_0(1 - d) \tag{4.28}$$

The stress vs. stretch response of the Neo-Hookean-like materials is shown in Figure (4.8). Note that for stretch values higher than 2%, the slope of the curves decreases slightly.

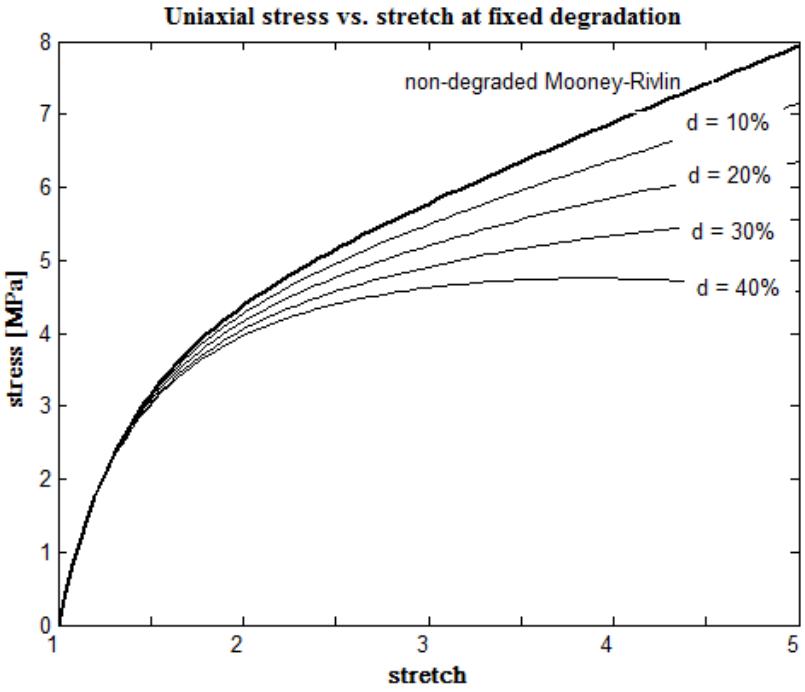

Figure 4.9: Uniaxial stress vs. stretch response at different levels of degradation of a degradable polymer that in the virgin state responds as a Mooney-Rivlin material (with $C_2^0 = 3C_1^0$).

A similar procedure can be applied to the Mooney-Rivlin material, whose stored energy function is given in (4.3). The two material functions, $C_1(d)$ and $C_2(d)$ similarly as in (4.27), are given by

$$C_1(d) = C_1^0(1 - \beta_1 d); \qquad C_2(d) = C_2^0(1 - \beta_2 d) \tag{4.29}$$

where C_1^0 and C_2^0 are the respective non-degraded material constants at $d = 0$, and β_1 and β_2 are related to the maximum degradable modulus at $d \to 1$. In Figure 4.9 note that if $C_2 = 0$, the response would be the same of the previous of Neo-Hookean.

The third non-degraded model considered was the polynomial model that better fitted the experimental data of the reference framework. The IER was described by the Equation (4.17) with a stored energy function given by the Equation (4.16). A degradable material that describes the degradable instantaneous elastic response of PLLA is given by

$$U(d) = C_1(d)e^{-(I_{\boldsymbol{C}}-3)}(I_{\boldsymbol{C}} - 3) + C_2(d)\ln[1 + a(I_{\boldsymbol{C}} - 3)] \tag{4.30}$$

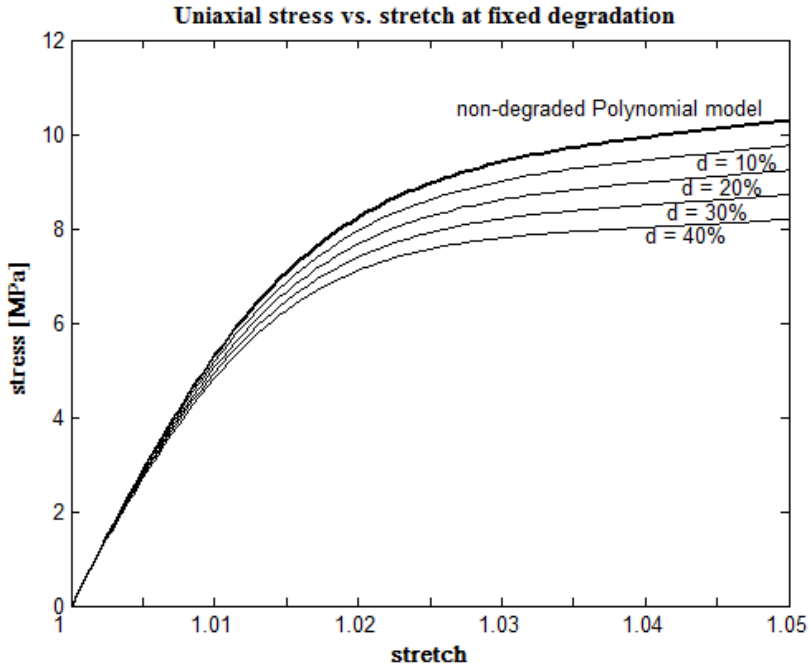

Figure 4.10: Uniaxial stress vs. stretch at different levels of degradation of a degradable material that in the virgin state responds as a hyperelastic material.

where both the material properties C_1 and C_2 degrade. The coefficient a was set to be constant because closely related to the mode of degradation of C_2. The stress-strain curves of the model are shown in Figure 4.10.

In both responses, Figures 4.8 and 4.9, the IER of degraded PLLA is characterized by a step increase in stress in the low strain region followed by a mild increase in stress with strain. Note the similarity of the curves at each level of degradation.

The next step of this modelling was to consider how even the simplest model among those seen varies over time. In the next section we will see an extension of the Neo-Hokkean model in the time domain.

Time dependent response of the Neo-Hookean-like material

Let us consider a motion that is similar to (4.5); however, in this case such motion is time dependent, hence its governing equations become:

$$x_1 = \frac{1}{\sqrt{\lambda(t)}} X_1, \qquad x_2 = \frac{2}{\sqrt{\lambda(t)}} X_2, \qquad x_1 = \lambda(t) X_3 \tag{4.31}$$

Either the deformation gradient **F** and the left and right Cauchy-Green stretch tensors **B** and **C** depend on the time. Due to the properties of this motion, the degradation occurs homogeneously, i.e. is independent of position, thus $d = d(t)$, and the corresponding rate of degradation is:

$$\frac{\mathrm{d}}{\mathrm{dt}}d(t) = C(1 - d(t))[(I_{\boldsymbol{C}} - 3)^2 + (II_{\boldsymbol{C}} - 3)^2]^{1/2} \tag{4.32}$$

where C is a constant that describes this particular mode of strain-induced degradation and it can be expressed as

$$C = \frac{1}{\tau_d} \tag{4.33}$$

where τ_d can be thought as a half time of degradation per unit deformation.

The invariants I_C and II_C are time dependent and the forms are

$$I_{\boldsymbol{C}} = \lambda(t)^2 + \frac{2}{\lambda(t)}; \qquad II_{\boldsymbol{C}} = 2\lambda(t) + \frac{1}{\lambda(t)^2} \tag{4.34}$$

By replacing the (4.34) in the (4.32) we obtain the following form of the rate degradation:

$$\frac{\mathrm{d}}{\mathrm{dt}}d(t) = C(1-d(t))\frac{(\lambda(t)-1)^2}{\lambda(t)^2}(\lambda(t)^4+4\lambda(t)^3+8\lambda(t)^2+4\lambda(t)+1)^{1/2} \tag{4.35}$$

The Cauchy stress of Equation (4.11) now becomes

$$\sigma_z^{NH}(t) = G_0(1 - d(t))\left(\lambda(t)^2 - \frac{1}{\lambda(t)}\right) \tag{4.36}$$

This relationship is nonlinear and can be solved for any two of the following three quantities, $\lambda(t)$, $\sigma_z(t)$, or $d(t)$. For the case in which a stress $\sigma_z(t)$ is imposed, the stretch $\lambda(t)$ is obtained as one solution of (4.36), and from it the corresponding increase of degradation is obtained with (4.35).

With time, as the material degrades, the stress necessary to maintain a given constant stretch decreases, i.e. *stress relaxation* occurs (Figure 4.11). As we can see, the rate of decay is exponential, with τ_d dependent on the applied stretch. For larger stretches, the initial required stress is larger, but it relaxes faster.

When the material is fully degraded, the shear modulus and the required stress decay to zero. Higher initial stretching leads to a greater rate of degradation, and thus a shorter time to effective material breakdown.

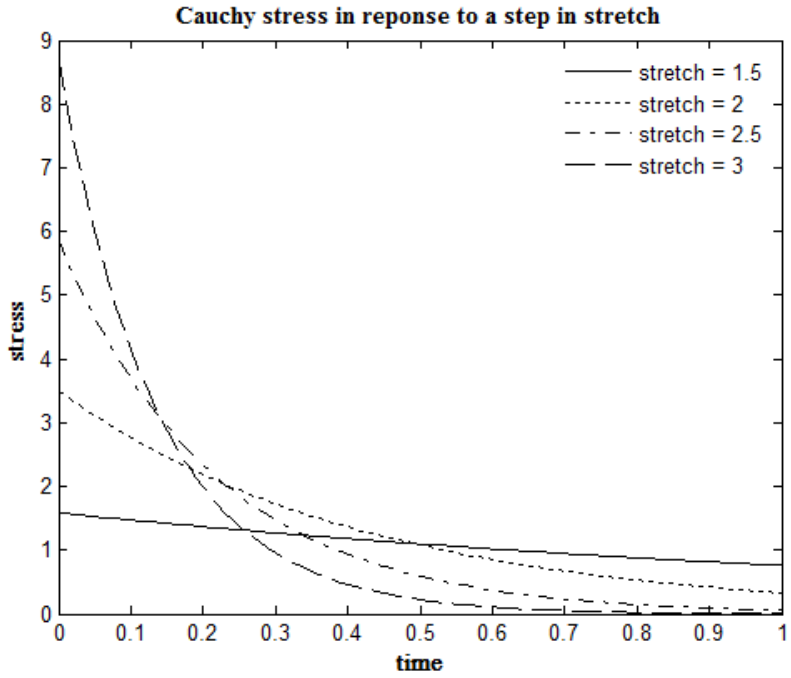

Figure 4.11: Non dimensional Caucgy stress required to maintain a constant stretch.

Degradation due to a constant stretch increases steeply during the initial stage of degradation. This rate is directly related to the amount of stretch, i.e. more stretch will lead to a faster degradation. The degradation tends asymptotically to its maximum value of unity as time tends to infinity (Figure 4.12)

Under constant loads, the stretch increases over time (Figure 4.13), i.e. the body exhibits creep-like behavior. As the stress increases, the impact of degradation is greater. The amount of degradation increases progressively where the effects of greater softening lead to greater stretches. Finally, the modulus of the material approaches zeros (Figure 4.14) and the stretch increases dramatically (Figure 4.13).

Under cyclic stretches, the material shows mechanical hysteresis as observed in the stress vs. stretch plot (Figure 4.16). The cyclic stretch $\lambda(t)$ and the stress vs. time response are shown in Figure 4.15 and Figure 4.17 respectively. As we can see, hysteresis is dependent on the stretching rate, with the area spanned by the hysteresis loop increasing as the rate of stretch decreases. The effects of degradation are indistinguishable in the first stages

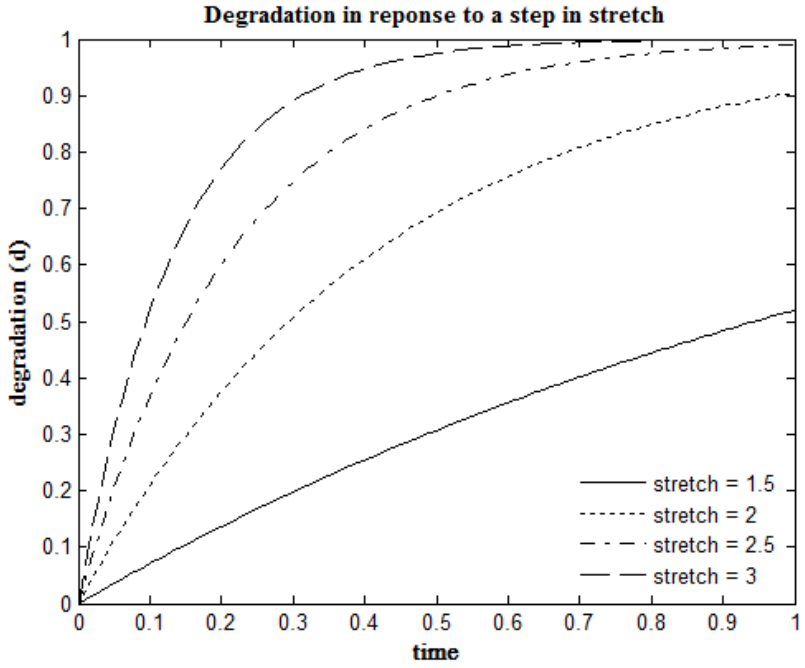

Figure 4.12: Degradation for several constant stretches.

of stretching, but as degradation proceeds the curves deviate from each other. Note that no permanent set is induced due to degradation, i.e. when the material is back to the original configuration at $t = 0$, no stress is still present (Figure 4.17); hence, degradation did not induce permanent set.

Since now, we have seen a degradable material that is hyperelastic at fixed degradation and that shows stress relaxation, creep and hysteresis as it degrades. These phenomena, although superficially similar to viscoelastic behavior, arise from different mechanisms, i.e. irreversible chain scission instead of conformational relaxations. The response of PLLA is than clearly one of a viscoelastic material, hence viscoelastic models should be used to describe its response.

Viscoelastic model for degradable PLLA

In the last sections we have already seen a possible constitutive model for viscoelastic materials, but now we shall integrate it with the degradation parameter d. We have seen that the viscoelastic model is determined by two material properties, the instantaneous elastic response and the relaxation

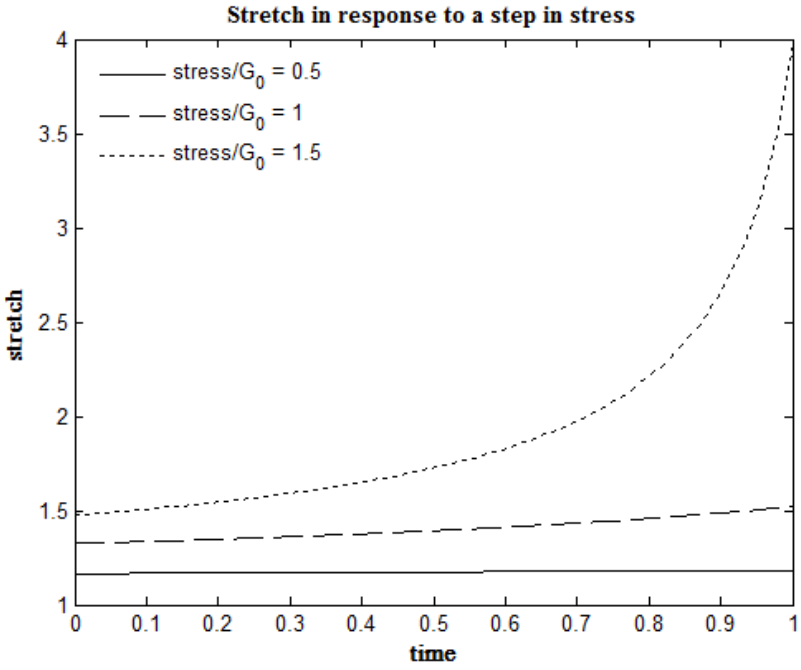

Figure 4.13: Stretch for several constant applied stresses.

function. For simplicity, we chose the Neo-Hookean hyperelastic solid for the former (strain energy function with the form of the (4.2) and uniaxial stress given by (4.11)) and a one term Prony's series for the latter:

$$G(t,d) = k_0(d) + k_1(d)e^{-t/\tau_1(d)} \tag{4.37}$$

where G is the shear modulus of the associated IER (4.36) and τ_1 the relaxation time. Like in (4.18), the relaxation function is restricted by $G(0) = 1$, hence $k_0 = 1 - k_1$ and the stress decay was normalized by $k_1 + k_0$.

As the material degrades, it is not just the relaxation that is expected to be faster, i.e. the relaxation time decreases with degradation

$$\tau_1(d) = \tau_1^0(1 - \beta d), \tag{4.38}$$

but its residual modulus is also influenced, i.e.

$$\tau_0(d) = 1 - k_1(d) = 1 - k_1^0(1 - \beta_1 d) \tag{4.39}$$

where k_1^0 and τ_1^0 are material constants that characterize the relaxation function of the non degraded material, $k_1(d)$ and $\tau_1(d)$ material functions

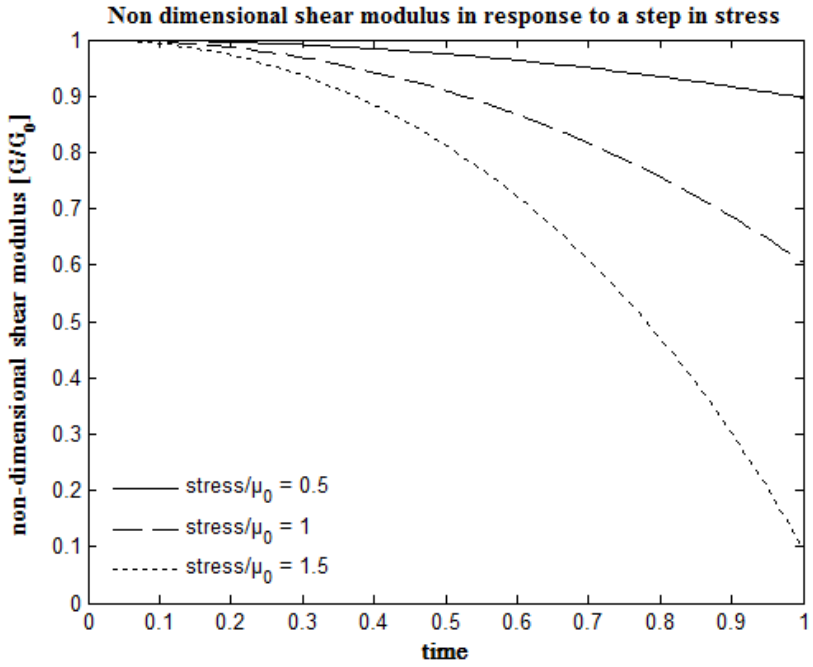

Figure 4.14: Shear modulus of the material under several applied constant stresses.

that characterize the degraded material. As seen in the previous cases, β and β_1 are constants that define the values of the material functions at the stage of maximum degradation. In this case, for simplicity, they are considered to be equal to the unity, hence the properties approach zero as $d \rightarrow 1$.

If we make each propertie degrade simultaneously, the stress relaxation response to steps in strain in (4.20) is shown in Figure (4.18).

Viscoelastic model that composes the degradable material shows the following characteristics: (i) as the material degrades, the stress levels achieved with similar strain histories decrease, (ii) the amount of stress decay increases with degradation, and (iii) the material relaxes faster.

This expected behavior shows acceptable phenomenological characteristics:

- as the number of effective crosslinks is reduced with increasing degradation, the ability for the network to withstand load is decreased;

- either the initial and the residual moduli k_0 and k_1 respectively decrease;

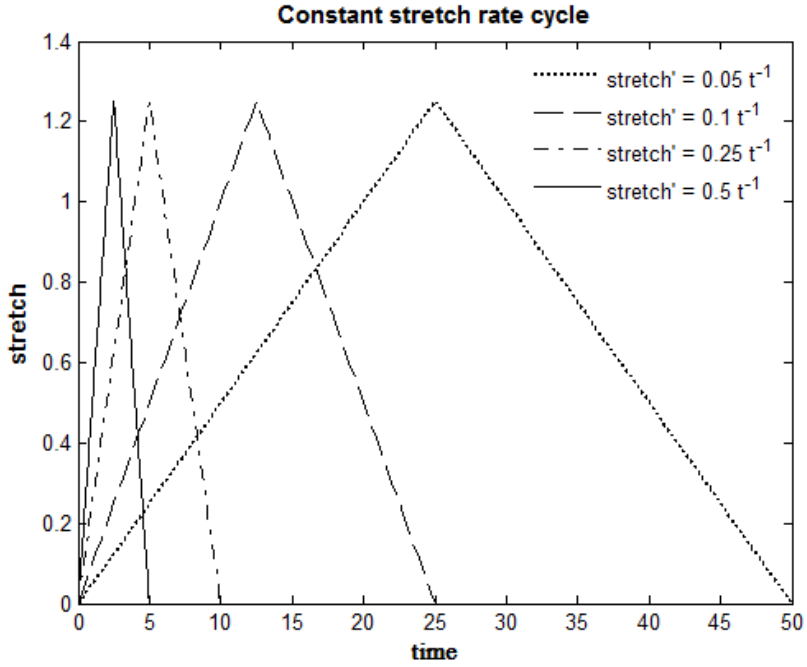

Figure 4.15: Cycle in strtch.

- smaller and less constrained chains allow faster conformational relaxations and hence a faster relaxation towards the residual modulus.

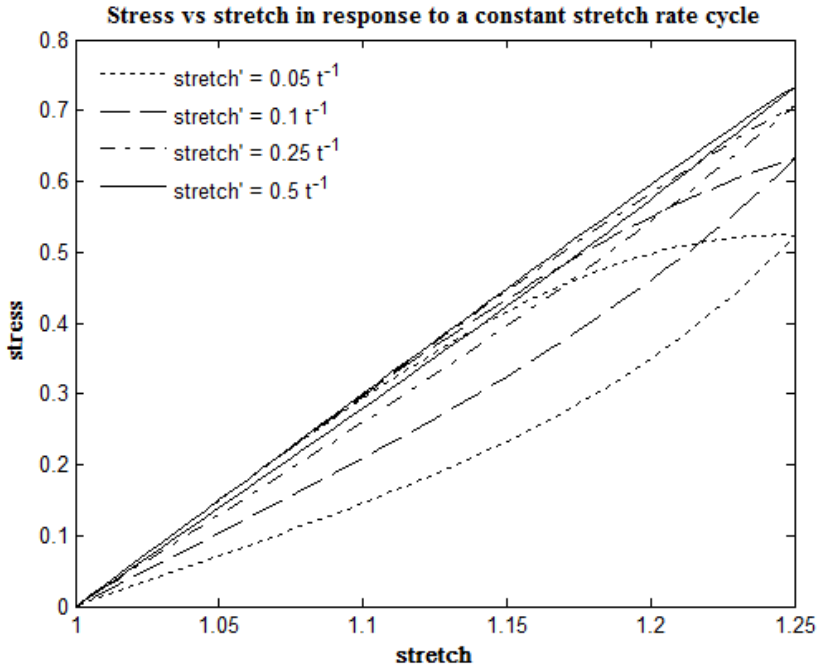

Figure 4.16: Non-dimensional Cauchy stress vs. stretch for several stretching rates.

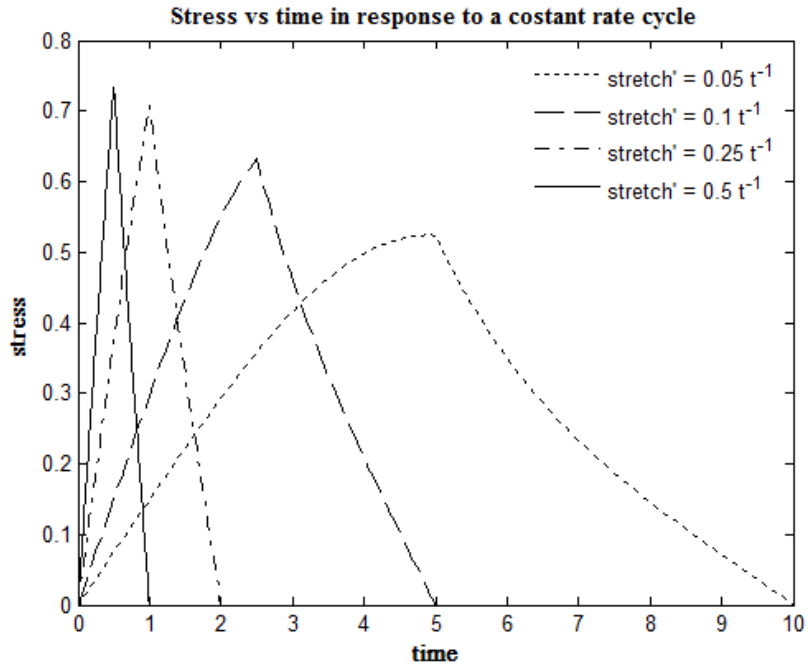

Figure 4.17: Non-dimensional Cauchy stress vs. time for cycles in stretch with constant stretching rate.

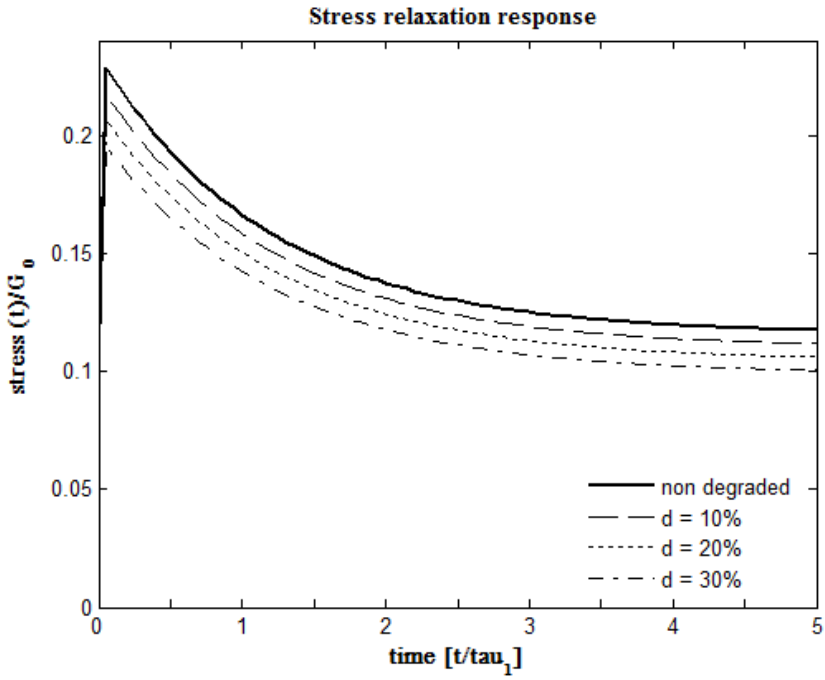

Figure 4.18: Stress relaxation response to steps in strain of the degradable viscoelastic material

Chapter 5

Constitutive modelling with Abaqus

The purpose of this chapter is to conduct an analysis on the kind of the constitutive models that Abaqus is able to implement. The first step was to find a correspondence between what has already been done with Matlab and what could be done with Abaqus.

5.1 Short introduction to Abaqus

Abaqus is based on the finite element stiffness method, with mixed stress-displacement formulations included. It is specifically designed to do advanced structural analysis on very large linear models or highly nonlinear response models.

Abaqus provides a broad range of possible material behaviors. A material is defined by choosing the appropriate behaviors for the purpose of an analysis. Some material behaviors in Abaqus require the presence of other material behaviors, and some exclude the use of other ones. For example, viscoelasticity requires the definition of hyperelastic material.

Material data are often specified as functions of independent variables such as temperature. In some cases a material property can be defined as a function of variables calculated by Abaqus; for example, to define a work-hardening curve, stress must be given as a function of equivalent plastic strain. Material properties can also be dependent on "field variables" but these variables must often be specified through user-defined subroutines .

Based on the behavior of the studied material until now, we will only focus on the hyperelastic and viscoelastic behaviors that Abaqus allows to implement.

5.2 Hyperelastic model in Abaqus

In Abaqus all hyperelastic models are based on the assumption of isotropic behavior throughout the deformation history. Hence, the strain energy potential can be formulated as a function of the strain invariants.

Hyperelastic materials are described in terms of a strain energy potential, which defines the strain energy stored in the material per unit of reference volume (volume in the initial configuration) as a function of the strain at that point in the material. There are several forms of strain energy potentials available in Abaqus to model approximately incompressible isotropic elastomers: the Arruda-Boyce form, the Marlow form, the Mooney-Rivlin form, the Neo-Hookean form, the Ogden form, the polynomial form, the reduced polynomial form, the Yeoh form, and the Van der Waals form. The reduced polynomial and Mooney-Rivlin models can be viewed as particular cases of the polynomial model; the Yeoh and Neo-Hookean potentials, in turn, can be viewed as special cases of the reduced polynomial model.

Generally, when data from multiple experimental tests are available, the Ogden and Van der Waals forms are more accurate in fitting experimental results. If limited test data are available for calibration, the Arruda-Boyce, Van der Waals, Yeoh, or reduced polynomial forms provide reasonable behavior. When only one set of test data (uniaxial, equibiaxial, or planar test data) is available, the Marlow form is recommended. In this case a strain energy potential is constructed that will reproduce the test data exactly.

The mechanical response of a hyperelastic material is defined by choosing a strain energy potential to fit the particular material. Generally, for this kind of material models available in Abaqus, we can either directly specify material coefficients or provide experimental test data and Abaqus automatically determines appropriate values of the coefficients.

It happens more often that the same experimental data can be fully fitted by different constitutive models. In these cases, Abaqus provides the values of the coefficients for each model. A similar situation happened with

polynomial model used with Matlab, and given by:

$$U(d) = C_1(d)e^{-(I_C-3)}(I_{\boldsymbol{C}} - 3) + C_2(d)\ln[1 + a(I_{\boldsymbol{C}} - 3)] \tag{5.1}$$

The model defined above was not present among the models provided by Abaqus. To implement it, the stress-strain data, obtained with Matlab, were tranferred to Abaqus. The better fit was obtained through the polynomial model and the corresponding model was:

$$U = C_{10}(I_{\boldsymbol{C}}-3)+C_{20}(I_{\boldsymbol{C}}-3)^2+C_{01}(II_{\boldsymbol{C}}-3)+C_{02}(II_{\boldsymbol{C}}-3)^2+C_{11}(I_{\boldsymbol{C}}-3)(II_{\boldsymbol{C}}-3) \tag{5.2}$$

The value of the coefficients provided by Abaqus are summarized in Table 5.1, and the hyperelastic response is showed in Figure 5.1.

Constitutive model	**Material constants [MPa]**
Polynomial	C_{10} = -2799.13757
	C_{01} = 2913.45638
	C_{02} = 27122.1027
	C_{20} = -515.453003
	C_{11} =-21168.3635

Table 5.1: Material constant of the polynomial hyperelastic model provided by Abaqus

This step was clearly crucial, because the viscoelastic model, developed by Matlab, kept into account the IER of the polynomial hyperelastic model in (5.1).

5.3 Viscoelastic model

In Abaqus, the elastic response of viscoelastic materials can be specified by defining either the instantaneous response or the long-term response of such materials. To define the instantaneous response, the experiments have to be performed within time spans much shorter than the characteristic relaxation times of these materials. Contrariwise, when the long-term elastic response is used, data from experiments have to be collected after time spans much longer than the characteristic relaxation times of these materials. Long-term elastic response is the default elastic material behavior setted by abaqus to calibrate the model coefficients.

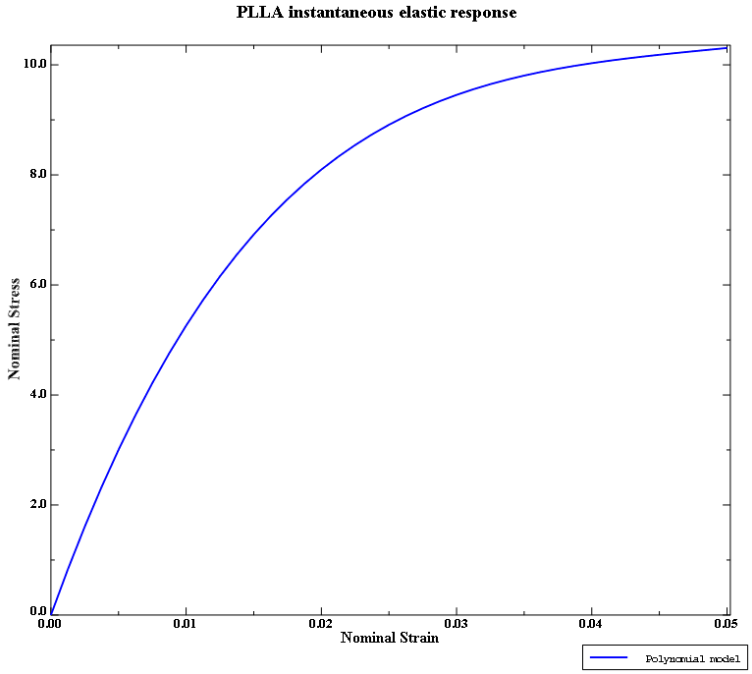

Figure 5.1: Normal stress-strain response of the polynomial model provided by Abaqus with the value coefficients in Table 5.1.

The time domain viscoelastic material model describes isotropic rate-dependent material behavior for materials in which dissipative losses primarily caused by viscous (internal damping) effects and must be modeled in the time domain; it assumes that the shear (deviatoric) and volumetric behaviors are independent in multiaxial stress states and can be used only in conjunction with linear elastic behavior, hyperelastic behavior of rubberlike materials, to define the elastic material properties. Olso, the model can be used in large-strain problems and can be calibrated using time-dependent creep test data, time-dependent relaxation test data, or frequency-dependent cyclic test data.

Time domain viscoelasticity is available in Abaqus for small-strain applications where the rate-independent elastic response can be defined with a linear elastic material model and for large-strain applications where the rate-independent elastic response must be defined with a hyperelastic model.

5.3.1 Small strain

Consider a shear test at small strain, in which a time varying shear strain, $\gamma(t)$, is applied to the material. The response is the shear stress $\tau(t)$. Abaqus defines the viscoelastic material model as

$$\tau(t) = \int_0^t G_R(t-s)\dot{\gamma}(s)ds \tag{5.3}$$

where G_R is the time-dependent "shear relaxation modulus" that characterizes the material's response. This constitutive behavior can be illustrated by considering a relaxation test in which a strain γ is suddenly applied to a specimen and then held constant for a long time. The experiment starts at $t = 0$; when the strain is suddenly applied the shear relaxation modulus can be expressed as

$$\tau(t) = \int_0^t G_R(t-s)\dot{\gamma}(s)ds = G_R(t)\gamma \quad (\text{since} \quad \dot{\gamma} = 0 \quad \text{for} \quad t > 0) \tag{5.4}$$

where γ is the fixed strain. The viscoelastic material model is "long-term elastic" in the sense that, after having been subjected to a constant strain for a very long time, the response settles down to a constant stress; i.e., $G_R(t) \to G_\infty$ as $t \to \infty$. The shear relaxation modulus can be written in dimensionless form:

$$r_R(t) = \frac{G_R(t)}{G_0}, \tag{5.5}$$

where $G_0 = G_R(0)$ is the instantaneous shear modulus, so that the expression for the stress takes the form

$$\tau(t) = G_0 \int_0^t g_R(t-s)\dot{\gamma}(s)ds \tag{5.6}$$

The dimensionless relaxation function has the limiting values $g_R(0) = 1$ and $g_R(\infty) = G_\infty/G_0$

5.3.2 Large strain

The equation for the stress can be transformed by using integration by parts:

$$\tau(t) = G_0 \left(\gamma - \int_0^t \dot{g_R}(s)\gamma(t-s)ds\right) \tag{5.7}$$

It is convenient to write this equation in the form

$$\tau(t) = \tau_0(t) - \left(\int_0^t \dot{g_R}(s)\tau_0(t-s)ds\right) \tag{5.8}$$

where $\tau_0(t)$ is the instantaneous shear stress at time t. This form allows a straightforward generalization to nonlinear elastic deformations by replacing the linear elastic relation $\tau_0 = G_0\gamma$ with the nonlinear elasticity relation $\tau_0 = \tau_0\gamma$. This generalization yields a linear viscoelasticity model, in the sense that the dimensionless stress relaxation function is independent of the magnitude of the deformation.

In the above equation the instantaneous stress, τ_0, applied at time $t - s$ influences the stress, τ, at time t. Therefore, to create a proper finite-strain formulation, it is necessary to map the stress that existed in the configuration at time $t - s$ into the configuration at time t. In Abaqus this is done by means of a mixed push-forward transformation with the relative deformation gradient $\mathbf{F}_{t-s}(t)$:

$$\mathbf{F}_{t-s}(t) = \frac{\partial \mathbf{x}(t)}{\partial \mathbf{x}(t-s)} \tag{5.9}$$

To ensure that the stress remains symmetric, Abaqus uses the integral form:

$$\boldsymbol{\tau} = \boldsymbol{\tau_0} - SYM\left[\int_0^t \frac{G_R(s)}{G_0}\mathbf{F}_t^{-1}\cdot\boldsymbol{\tau}_0(t-s)\cdot\mathbf{F}_t(t-s)ds\right] \tag{5.10}$$

where $\boldsymbol{\tau}$ is the deviatoric part of the Piola-Kirchhoff stress.

5.3.3 Numerical implementation

Abaqus assumes that the viscoelastic material is defined by a Prony series expansion of the dimensionless relaxation modulus:

$$g_R(t) = 1 - \sum_{i=1}^{N}\overline{g}_i^P\left(1 - e^{-t/\tau_i^G}\right) \tag{5.11}$$

where N, $\overline{g}_i^P$, and τ_i^G, are material constants. Substitution in the small-strain expression for the shear stress yields

$$\tau(t) = G_0\left(\gamma - \sum_{i=1}^{N}\gamma_i\right) \tag{5.12}$$

where

$$\gamma_i = \frac{\overline{g}_i^P}{\tau_i^G}\int_0^t e^{-s/\tau_i^G}\gamma(t-s)ds \tag{5.13}$$

The γ_i are interpreted as state variables that control the stress relaxation, and

$$\gamma^{cr} = \sum_{i=1}^{N}\gamma_i \tag{5.14}$$

is the creep strain: the difference between the total mechanical strain and the instantaneous elastic strain (the stress divided by the instantaneous elastic modulus).

The Prony series expansion, in combination with the finite-strain expression for the shear stress, produces the following large-strain shear model:

$$\boldsymbol{\tau} = \boldsymbol{\tau}_0 - \sum_{i=1}^{N} \boldsymbol{\tau}_i \tag{5.15}$$

where

$$\boldsymbol{\tau}_i = SYM\left[\frac{\overline{g}_i^P}{\tau_i^G}\int_0^t e^{-s/\tau_i^G}\mathbf{F}_t^{-1}(t-s)\cdot\boldsymbol{\tau}_0(t-s)\cdot\mathbf{F}_t(t-s)ds\right] \tag{5.16}$$

The $\boldsymbol{\tau}_i$ are interpreted as state variables that control the stress relaxation.

The above equations are used to model the time-dependent shear and volumetric behavior of a viscoelastic material. The relaxation parameters can be defined in one of four ways: direct specification of the Prony series parameters, inclusion of creep test data, inclusion of relaxation test data, or inclusion of frequency-dependent data obtained from sinusoidal oscillation experiments. To implement our viscoelastic model (Section 4.3.2), the Prony series parameters ($\overline{g}_i^P$ and τ_i) in Table 4.1 were used. Creep and stress relaxation normalized responses are shown in Figures (5.2) and (5.3) respectively. These responses are obtained by providing a short-time interval for the polynomial IER, and a sufficiently long-time interval to simulate the long-term responses of the creep and stress relaxation functions.

Material data are often specified as functions of independent variables such as temperature. In some cases, a material property can be defined as a function of variables calculated by Abaqus; for example, to define a work-hardening curve, stress must be given as a function of equivalent plastic strain. Material properties can also be dependent on "field variables" but such variables must often be specified through an user-defined subroutine.

The following step was the study of the kinds of "damage" Abaqus was able to simulate. The range of possible choices was not very wide and only one could satisfy the desidered requirements for our material. The "damage" should reflect the depreciation in the material properties, due to the degradation process, i.e., stress softening should occur. Thus, the damage model that could better represent this relaxation process is the "Mullins effect".

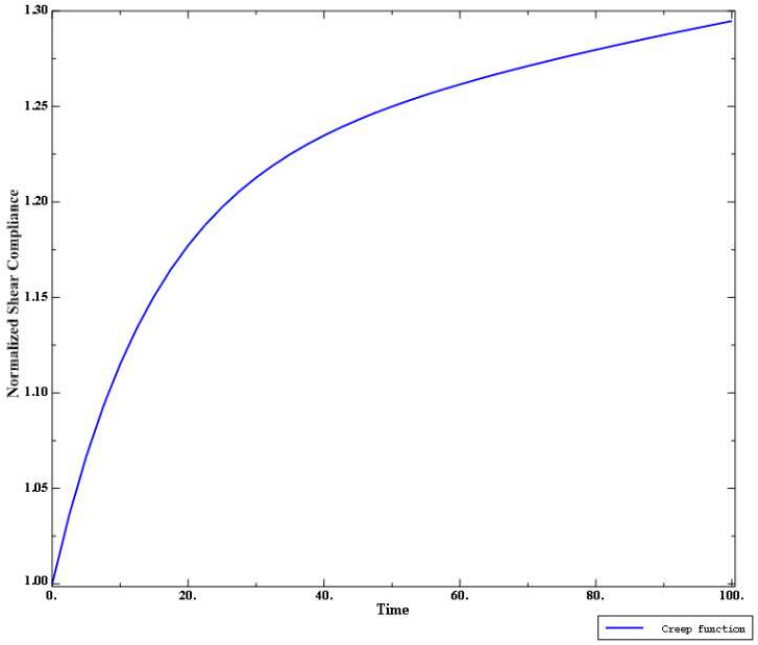

Figure 5.2: Normalized creep function obtained by Abaqus for the PLLA non-degraded.

5.4 Damage models

The damage models provided by Abaqus are:

1. Ductile damage
2. Forming limit diagram damage
3. Forming limit stress diagram damage
4. Johnson-Cook damage
5. Maximum or quadratic nominal strain damage
6. Maximum or quadratic nominal stress damage
7. Marciniak-Kuczynsky damage
8. M-S forming limit diagram damage
9. Shear damage
10. Hashin damage
11. Mullins effect

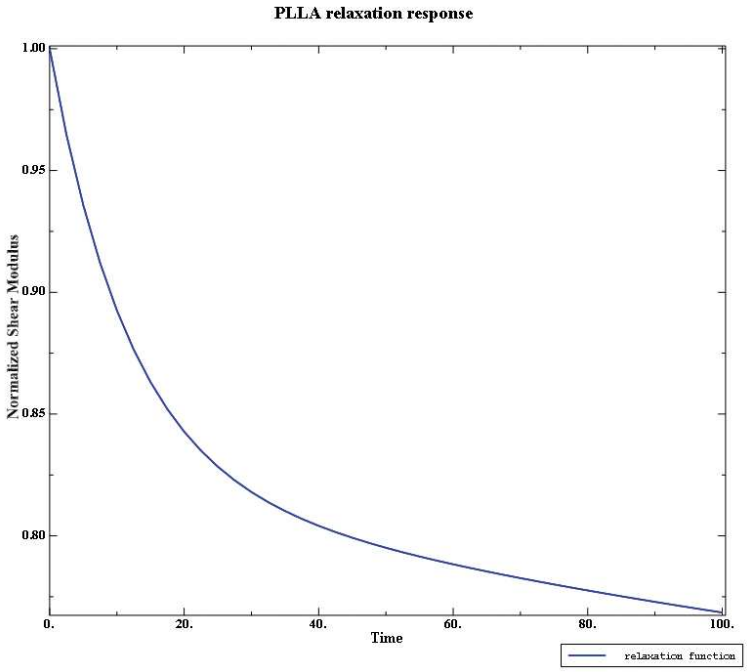

Figure 5.3: Normalized stress relaxation function obtained by Abaqus for the PLLA non-degraded.

For each damage model mentioned above, Abaqus required a *damage initiation criteria* and an associated *damage evolution*. Once an initiation criterion is met, Abaqus applies the associated damage evolution law to determine the material degradation. When a damage initiation is met, material damage begins. Abaqus uses the damage evolution definition associated with the initiation criterion to evaluate the extent of the damage.

All models, except for the Mullins effect, are specific for metallic or simple elastic materials. Contrariwise, the Mullins effect is intended for modeling stress softening of filled rubber elastomers. Thus, it was the model on which we focused the study of the damage.

5.4.1 Mullins effect in rubberlike material

The Mullins effect model is intended for modelling stress softening of filled rubber elastomers under quasi-static cyclic loading, a phenomenon referred to in the literature as Mullins effect. It provides an extension to the isotropic hyperelastic models and it is based on the theory of incompressible isotropic elasticity modified by the addition of a single variable, referred to

as the damage variable. The Mullins effect assumes that only the deviatoric part of the material response is associated with damage.

Material behavior

The real behavior of filled rubber elastomers under cyclic loading conditions is quite complex. Certain idealizations have been made for modelling purposes. In essence, these idealizations result in two main components to the material behavior: the first component describes the response of a material point (from an undeformed state) under monotonic straining, and the second component is associated with damage and describes the unloading-reloading behavior.

When an elastomeric test specimen is subjected to simple tension from its virgin state, unloaded, and then reloaded, the stress required on reloading is less than that on the initial loading for stretches up to the maximum stretch achieved during the initial loading. This stress softening phenomenon is known as the Mullins effect and reflects damage incurred during previous loading. This type of material response is depicted qualitatively in Figure 5.4.

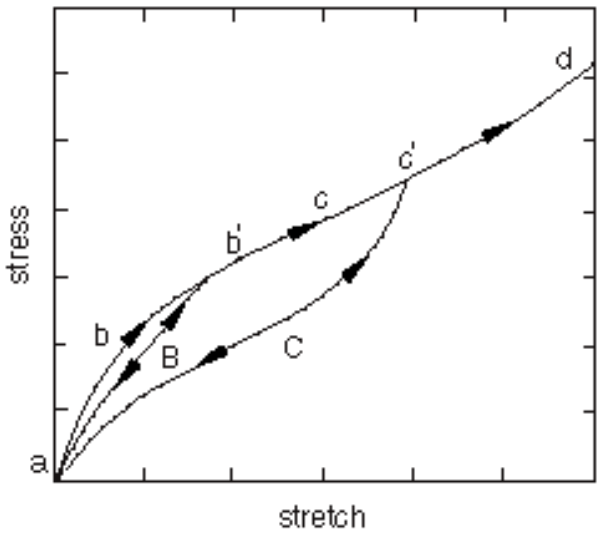

Figure 5.4: Idealizeed response of a Mullins effect model.

This figure and the accompanying description is based on work by Ogden and Roxburgh [35], which forms the basis of the model implemented in Abaqus.

This is an ideal representation of Mullins effect, since in practice there is some permanent set upon unloading and/or viscoelastic effects such as hysteresis appear. Points such as b' and c' may not exist in reality in the sense that unloading from the primary curve followed by reloading to the maximum strain level attained earlier usually results in a stress that is somewhat lower than the stress corresponding to the primary curve. In addition, the cyclic response for some filled elastomers shows evidence of progressive damage during unloading from and subsequent reloading to a certain maximum strain level. Such progressive damage usually occurs during the first few cycles, and the material behavior soon stabilizes to a loading/unloading cycle that is followed beyond the first few cycles.

Stress softening is interpreted as being due to damage at the microscopic level. As the material is loaded, the damage occurs by the severing of bonds between filler particles and the rubber molecular chains. Different chain links break at different deformation levels, thereby leading to continuous damage with macroscopic deformation. An equivalent interpretation is that the energy required to cause the damage is not recoverable.

5.4.2 Primary hyperelastic behavior

As we have seen in the last section, hyperelastic materials are described in terms of a strain energy potential function $U(\mathbf{F})$ where $\mathbf{F}$ is the deformation gradient tensor. To account for Mullins effect, Ogden and Roxburgh propose a material description that is based on an energy function of the form $U(\mathbf{F}, \eta)$, where the additional scalar variable, η, represents damage in the material. The damage variable controls the material properties in the sense that it enables the material response to be governed by an energy function on unloading and subsequent submaximal reloading different from that on the primary (initial) loading path from a virgin state. Because of the above interpretation of η, it is no longer appropriate to think of U as the stored elastic energy potential. Part of the energy is stored as strain energy, while the rest is dissipated due to damage. The area between the loading and unloading-curves, in Figure (5.4), represents the energy dissipated by damage as a result of deformation until the point c', while the part outside represents the recoverable strain energy.

By dividing the strain energy function in deviatoric and volumetric parts

as $U = U_{dev} + U_{vol}$, the damage variable η is defined by Abaqus as:

$$\eta = 1 - \frac{1}{r} erf\left(\frac{U_{dev}^m - \tilde{U}_{dev}}{m + \beta U_{dev}^m}\right) \tag{5.17}$$

where U_{dev}^m is the maximum value of $\tilde{U}_{dev}$ at a material point during its deformation history; r, β and m are material parameters and $erf(x)$ is the error function defined as

$$erf(x) = \frac{2}{\sqrt{\pi}} \tag{5.18}$$

When $\tilde{U}_{dev} = U_{dev}^m$, corresponding to a point on the primary curve, $\eta = 1$. For all intermediate values of $\tilde{U}_{dev}$, η varies monotonically between 1.0 and η_m.

While the parameters r and β are dimensionless, the parameter m has the dimensions of energy. The material parameters may be specified directly or may be computed by Abaqus based on curve-fitting of unloading-reloading test data. These parameters are subject to the restrictions $r > 1$, $\beta \geq 0$, and $m \geq 0$ (the parameters β and m cannot both be zero). The parameters r, β, and m do not have direct physical interpretations in general. The parameter m controls whether damage occurs at low strain levels. If $m = 0$, there is a significant amount of damage at low strain levels. On the other hand, a nonzero m leads to little or no damage at low strain levels. The qualitative effects of varying the parameters r and β individually, while holding the other parameters fixed, are shown in Figure 5.5. The left figure

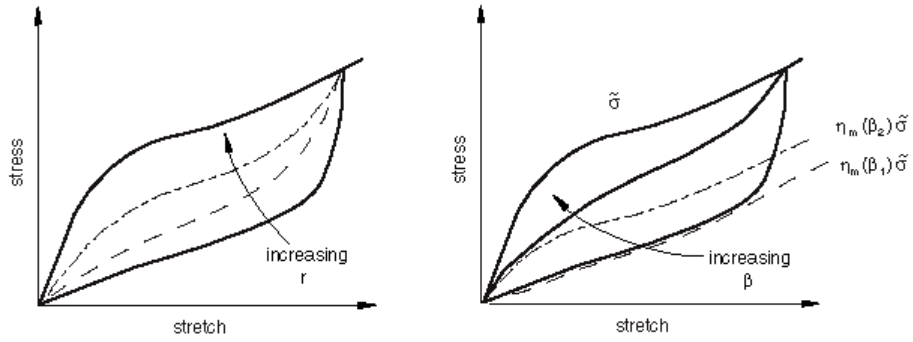

Figure 5.5: Qualitative dependence of damage on material properties.

shows the unloading-reloading curve from a certain maximum strain level for increasing values of r. It suggests that the parameter r controls the amount of damage, with decreasing damage for increasing r. The figure on the right

shows the unloading-reloading curve from a certain maximum strain level for increasing values of β. The figure suggests that increasing β also leads to lower amounts of damage. The dashed curves represent the asymptotic response at two different values of β (β_1 and β_2). For fixed values of r and m, η_m is a function of β. In particular, if $m = 0$,

$$\eta_m = 1 - \frac{1}{r} erf\left(\frac{1}{\beta}\right) \tag{5.19}$$

The above relation is approximately true if U^m_{dev} is much greater than m.

Using test data to calibrate the parameters

Experimental unloading-reloading data from different strain levels can be specified for up to three simple tests: uniaxial, biaxial, and planar. Abaqus will then compute the material parameters using a nonlinear least-squares curve fitting algorithm. It is generally best to obtain data from several experiments involving different kinds of deformation over the range of strains of interest in the actual application and to use all these data to determine the parameters. It is also important to obtain a good curve-fit for the primary hyperelastic behavior if the primary behavior is defined using test data. The strain data should be given as nominal strain values (change in length per unit of original length). The stress data should be given as nominal stress values (force per unit of original cross-sectional area). For each set of test input, the data point with the maximum nominal strain identifies the point of unloading. This point is used by the curve-fitting algorithm to compute U^m_{dev} for that curve.

When nominal stress-strain data are used to calibrate the Mullins effect model, the resulting response will capture the overall stiffness characteristics, while ignoring effects such as hysteresis, permanent set, or progressive damage.

Cyclic loading tests were performed with Matlab to implement the Mullins effect in respect to the PLLA, with the purpose to obtain stress-strain data. However, no suitable results were obtained because the data did not match the conditions required by Abaqus. The stress-strain values obtained using the hyperelastic model (5.2) and cyclic strains from 5% to 25% were inadequate to calibrate the Mullins effect parameters, since the resulting stresses were too small.

Hence, the obvious conclusions are that the models provided by Abaqus are not adequate to model the degradation of the analyzed polymer. To develop a suitable model of degradation through Abaqus, the only way is to create specific subroutines for the material of interest.

Chapter 6

Preliminary chemical tests on PLLA films

In this chapter we shall describe some preliminary tests we have performed on PLLA films at the Department of Chemistry of the University of Pavia. Similar PLLA films were subjected to degradation under tension inside a purpose-made degradation chamber. Tests of PLLA films were conducted in order to study the evolution of their degradation with time.

6.1 Materials and methods

Molecular weight strongly influences the chemical-mechanical response of a polymer, as widely discussed in Chapter 2. As a first step, we chose a polymer whose molecular weight is about the same as the polymers' used to build biodegradable stents. The polymers found on the market, and that meet the requirements, had molecular weight whose values are shown in Table 6.1 and were in form of pellets.

Polymer	$\mathbf{M}_W$
A	99,000 ÷ 152,000
B	50,400 ÷ 67,400

Table 6.1: Molecular weight of the analyzed polymers

The following tests were performed on each polymer: a little amount of material was put in distilled water in order to make sure that they were not soluble in this environment, otherwise tests in saline environment would not be possible. The results demonstrated that both polymers were not soluble in distilled water.

The solubility of polymer materials was tested in several solvents (tetrahydrofuran, dichloromethane, methanol) and the result was that both polymers were easily soluble in dichloromethane forming a transparent and viscous solution. Once the polymers were in solution, the next step was to convert them into films. For each polymer, 200mg of material were dissolved in dichloromethane and left to evaporate on a glass dish (called "Petri capsule") with a diameter of 5cm. Films almost homogeneous and with the same thickness were obtained through evaporation. Both films were transparent but their consistencies were different: polymer A, with higher molecular weight, was more elastic; contrariwise, polymer B was less elastic and more glassy.

Several stripes about 3cm long, 1cm wide and 1/10 mm thick were cut from each film. The next thing to do was to decide the value of the load we should apply to the films. Some literature-based studies told us that fibers whose molecular weight is not dissimilar from the one examined (about 1mm thick and subject to loads of about 100g for about 1 year) didn't show any appreciable change, either in molecular weight or fiber elongation. In order to obtain any appreciable change in a short span of time, so that we could make some qualitative assessments, we decided to subject the 1/10mm thick films to loads of about 100g. The density of lead allows for high weight with small volumes. Since we could only test the films in small test-tubes (2cm diameter, 18cm length), we had to use lead weights. Some stainless steel clamps were purpose-made to clip each individual film and attach them to the little weights with a fastener. Stainless steel was chosen because it is a compound that does not release any ions in solution, so that the surrounding environment is not contaminated.

The analysis procedure was characterized by the following steps:

1. firstly, for each film, weight and length between the clamps were measured;

2. the stripes were clamped between the clips and attached to the little weights;

Code	$\boldsymbol{\Delta T}$ [h][a]	$\mathbf{W}_0^c$ [mg]	$\mathbf{W}_f^c$ [mg]	$\mathbf{L}_0^b$ [cm]	$\mathbf{L}_f^b$ [cm]
A_{01}	24	26,0	18,3	1,9	4,5
A_{02}	24	21,6	19,8	1,8	4,8
A_{03}	24	20,3	23,3	1,8	4,8
A_{04}^f	24	44,4	40,4	2,0	2,1
A_{05}^f	96	52,0	46,8	2,3	2,4
A_{06}^f	168	60,6	53,1	2,6	2,8
B_{03}^e	120	15,5	14,9	1,8	1,8
B_{04}^d	42	44,8	/	1,9	/
B_{05}^d	42	36,0	/	1,9	/
B_{06}^d	42	43,9	/	2,0	/

Table 6.2: Experimental results on loaded PLLA films. (a) In isotonic saline solution (0.9% sodium chloride at 37°C), (b) length between the clamps; (c) total weight (clamps included), (d) rupture of films after 5-10min, (e) load free films, (f) double thickness.

3. the films were inserted in test tubes containing saline solution and kept at a temperature of 37°C;

4. a few days away from one another, the films were removed from saline solution, washed with deionized water and they were left to air-dry with the purpose to remove residual saline solution;

5. finally, the samples were re-weighed, the stretch was measured and infrared analysis was performed.

The results obtained for each sample are summarized in Table 6.2

Where ΔT is the time the films spent in solution, W_0^c is the original weight of the films and clamps as a whole, W_f^c is the final weight of films after the degradation, L_0^b is the initial length and L_f^b is the final length.

In order to evaluate the chemical degradation of the polymers, the films were analyzed through infrared spectroscopy.

Infrared spectroscopy exploits the fact that molecules have specific frequencies at which they rotate or vibrate corresponding to discrete energy levels (vibrational modes). These resonant frequencies are determined by the shape of the molecular potential energy surfaces, the masses of the atoms and the associated vibronic coupling. In order for a vibrational mode in a molecule to be IR active, it must be associated with changes in the permanent dipole. The resonant frequencies can be related to the strength of the bond, and the mass of the atoms at either end of it. Thus, the frequency of the vibrations can be associated with a particular bond type (Figure 6.1).

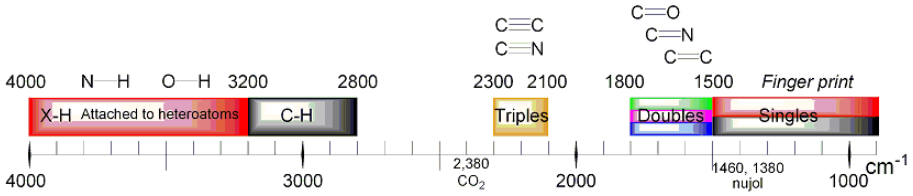

Figure 6.1: Summary of absorptions of bonds in organic molecules

Simple diatomic molecules have only one bond, which may stretch. More complex molecules have many bonds, and vibrations can be conjugated, leading to infrared absorptions at characteristic frequencies that may be related to chemical groups. For example, the atoms in a CH_2 group, commonly found in organic compounds, can vibrate in six different ways. The infrared spectrum of a sample is collected by passing a beam of infrared light through the sample. Examination of the transmitted light reveals how much energy was absorbed at each wavelength. From this, a transmittance or absorbance spectrum can be produced, showing at which IR wavelengths the sample absorbs. Analysis of these absorption characteristics reveals details about the molecular structure of the sample. This technique works almost exclusively on samples with covalent bonds.

6.1.1 Results

Clearly, the results obtained must be regarded as indicative because of the experimental conditions under which the tests were performed. However, some qualitative considerations can be made.

The IR results are reported in Figures 6.2, 6.4 and 6.5.

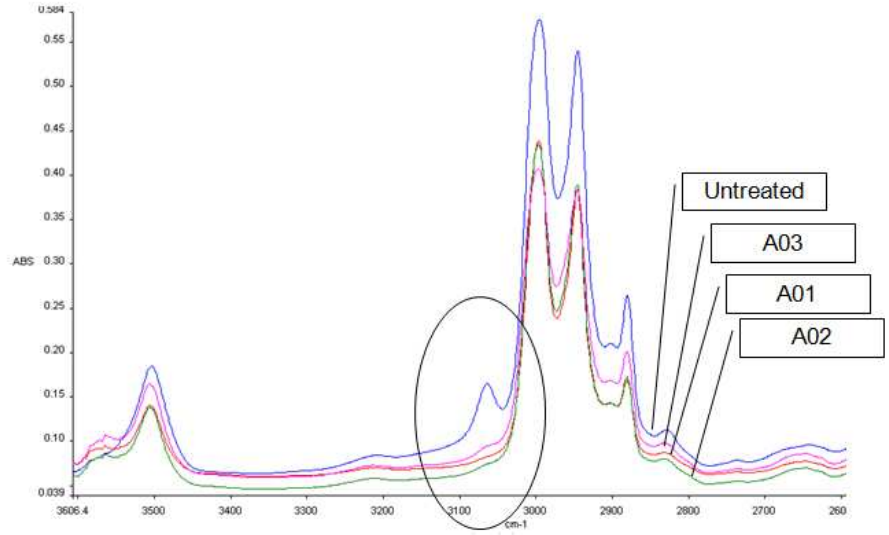

Figure 6.2: IR spectroscopy on the treated samples A_{01}, A_{02}, A_{03} and the non-treated sample.

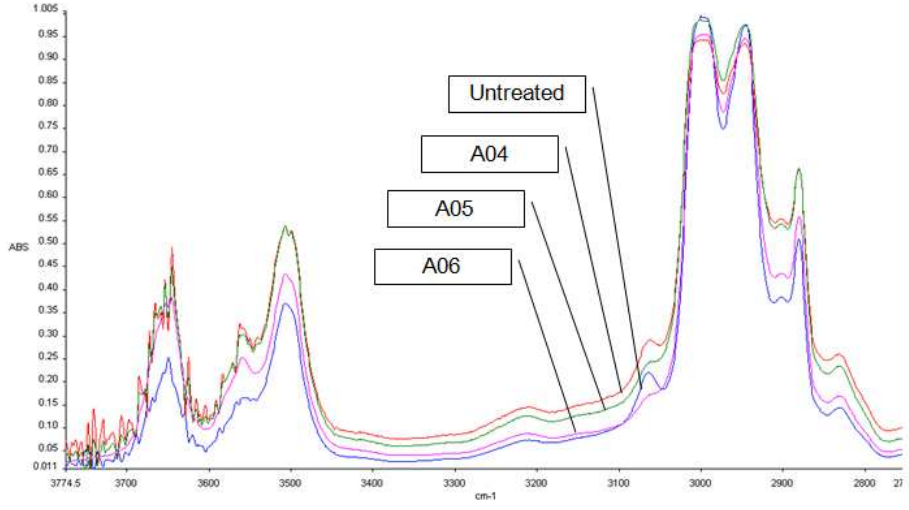

Figure 6.3: IR spectroscopy on the treated A_{04}, A_{05}, A_{06} and the non-treated sample. The samples have a double thickness than the set of samples A_{01}, A_{02} and A_{03}.

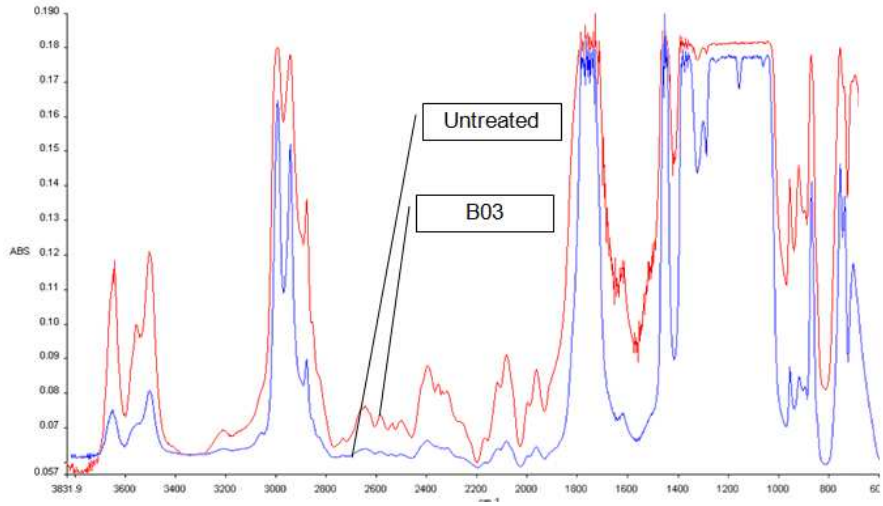

Figure 6.4: IR spectroscopy on the treated sample B^e_{03}.

After a day, no changes had occurred at molecular level. Samples A_i, removed from solution after just one day, did not show any changes at molecular level and they all share a similar pattern.

As we can see, the untreated sample's pattern presents a peak that disappears in the range of 3100-3064cm^{-1} (as highlighted in Figure 6.2). Such disappearance can be attributed to molecular reorganization of the polymer chains due to stretch, rather than degradation.

Sample B^e_{03}, was left in solution for five days, load free. It shows an appreciable chemical degradation compared to the untreated sample. Relative band intensity shows that chemical degradation in the range 3400-3700cm^{-1} is higher than chemical degradation in the range 2800-3100cm^{-1}.

The chemical degradation is more visible in Figure 6.5, in which peaks are normalized. The starting material (blue line) presents sharper peaks at 2900-3000 cm^{-1} with respect to the treated sample (red line). The peaks broadening in the latter film indicate the presence of C−C and C−H bonds with different molecular mobility (i.e., higher chain disorder). Moreover, in the range 3450-3700 cm^{-1}, an evident increase of OH and COOH vibrations show a chemical degradation of polymeric ester groups to give OH and COOH moieties (Figure 6.6).

All of these chemical modifications are compatible with chain breaking and thus lowering of the polymer molecular weight.

It should be noted that the films we have analyzed were not subjected to

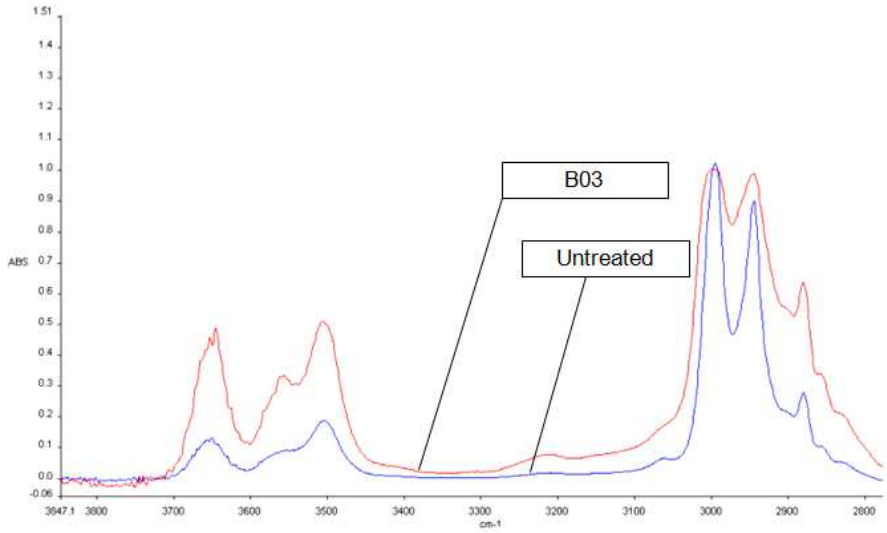

Figure 6.5: Zoom on IR spectroscopy of the treated sample B^{e}_{03}.

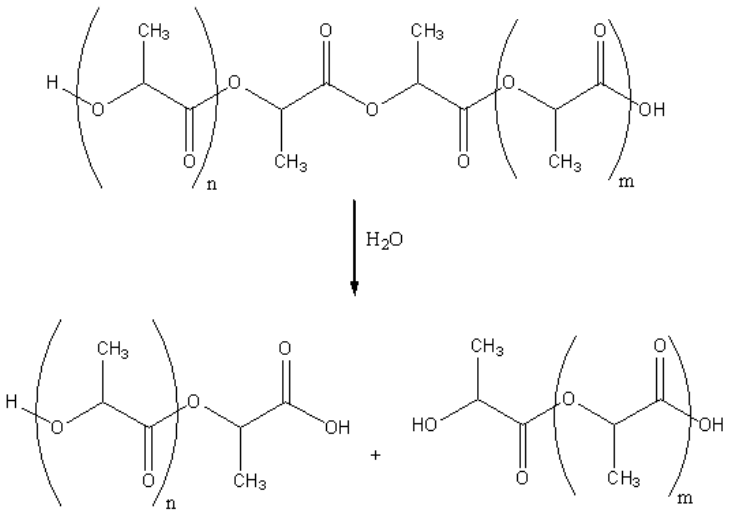

Figure 6.6: Chain breaking

any other kind of processing in order to increase their load resistance, resulting in an excessive elongation. Generally, polymers employed in industrial field undergo specific treatments allowing crosslinking between the chains, increasing their elasticity and resistance, as widely discussed in Chapter 2.

Conclusions

The purpose of this work was to study the mechanical response of a particular degradable polymer that, in these last years, was employed in the medical field for endovascular devices, such as stents. This framework is based on data found in literature and the reading key of the results obtained is phenomenological. The scission of the molecular chains due to external factors such as environment and external applied forces (or strain induced), results in the reduction of mechanical properties of material. Degradation was captured with the introduction of a local scalar measure describing the extent of bond scissions. We have chosen degradable hyperelastic-like and degradable viscoelastic-like materials to illustrate the model. At fixed levels of degradation these models showed hyperelastic and viscoelastic response, respectively. When degradation occurs due to the presence of deformations, the response of the body shows creep, stress relaxation and hysteresis, but these phenomena arise from internal entropy producing the same mechanical responses as the classical viscoelastic behavior.

Through a finite element code, Abaqus, it is possible to characterize a wide range of materials, realize complex geometries (such as those of the stent) and to implement boundary conditions as close as possible to real situations. While the program is not able to provide a model suitable for implementing the PLLA degradation, user-defined subroutines can be specifically created for this purpose.

Preliminary tests conducted on the degradation of the material showed an actual loss of mass of PLLA films. The study by infrared spectroscopy also showed that small variations which can be seen, are necessarily tied up not to a real degradation of the material but to a rearrangement of the polymeric chains. Meaningful values of degradation can already be noticed after 3 days that the samples are left in solution.

An adequate experimental trend should use degradation and stress-strain

data as the start-point from which the coefficient values for the constitutive model of the material should be calibrated. Once a suitable constitutive model is implemented, we can draw appropriate conclusions.

Bibliography

[1] Gopferich A. Mechanism of polymers degradation and erosion. *Biomaterials*, 1996.

[2] Kumbakonam Ramamani Rajagopal A. S. Wineman. Mechanical response of polymers: An introduction, 2000.

[3] F. Auricchio. Mechanics of solid materials: theoretical and computational aspects, 2001.

[4] Chu C. Biodegradable polymeric biomaterials: an overview. *The Biomedical Engineering Handbook*, pages 43–87, 1995.

[5] M. Calnan. *Preventing Coronary Heart Disease: Prospects, Policies, and Politics*. Routleges, 1991.

[6] Di Bello Carlo. Biomateriali. introduzione allo studio dei materiali per uso biomedico, 2004.

[7] Vacanti Chaignaud B. E., Langer. The history of tissue engineering using synthetic biodegradable polymer scaffolds and cells. *Eds A. Atala and D.J.Mooney, year = 1997, pages = 1-14.*

[8] Agrawal CM. Reconstructing the human body using biomaterials. *JOM*, 50:31–35, 1998.

[9] Williams D. Review: Biodegradation of surgical polymers. *Journal of Materials Science*, 17:1233–1246, 1982.

[10] Williams DF. Mechanisms of biodegradation of implantable polymers. *Clin Mater*, 1992.

[11] Gilding D.K. *Fundamentale aspects of biocompatibility*, volume I. CRC Press, Boca Raton, 1981.

[12] FELDMAN Dorel. Polymer history, 1998. Designed monomers and polymers.

[13] Sebastian Pagni MD Edwin E. Quan, MD. Adaptive-outward and maladaptive-inward arterial remodeling measured by intravascular ultrasound in hyperhomocysteinemia and diabetes. *J Cardio Pharmacology and Therapeutics*, 11(1):65–77, 2006.

[14] Harrison J Goodship AE, Lawes TJ. The biology of fracture repaire. *Science basic to orthopaedics*, 1998.

[15] Langer R Gopferich A. Predicting drug release from cylindric polyanhydride matrix disd. *Eur J Pharmacol Biopharmacol*, 1995.

[16] Langer RS Gopferich A. Modeling of polymer erosion in three dimensions-rotationally symmetric devices. *AIChE J*, 1995.

[17] M.H. Hartmann. *High molecular weight polylactic acid polymers, in: Biopolymers from renewable resources*. Springer-Verlag, Berlin, 1998.

[18] Eeva-Maija Hietala. Poly-l d-lactide stents as intravascular devicesan experimental study, 2004. Academic dissertation.

[19] Dussaillant GR Popma JJ Pichard AD Salter LF et al Hoffmann R, Mints GS. Patterns and mechanisms of in stent-restenosis. a serial intravascular ultrasound study. *Circulation*, 94(12):47–54, 1996.

[20] Curcio A et al Idolfi C, Mongiardo A. Molecular mechanisms of instent restenosis and approach to therapy with eluting stents. *Trends Cardiovasc Med*, 13:142–148, 2003.

[21] M. Mang J.R. Dorgan, H. Lehermeier. Thermal and rheological properties of commercial-grade poly(lactic acid)s. *J. Polym. Environ*, 8:1–9, 2000.

[22] P. Waggoner et al. K.D. Nelson, A. Romero. Technique paper for wet-spinning poly(l-lactic acid) and poly(dl-lactide-coglycolide) monofilament fibers. *Tissue Eng.*, 9:1323–1330, 2003.

[23] A.R. Srinivasa K.R. Rajagopal. Mechanics of the inelastic behavior of materials-part 1, theoretical underpinnings. *J. Plasticity*, 4:945–967, 1998.

[24] A.R. Srinivasa K.R. Rajagopal. On the thermomechanics of materials that have multiple natural configurations - part i: Viscoelasticity and classical plasticity. *Agnew. Math. Phys*, 55:861–893, 2004.

[25] A.S. Wineman K.R. Rajagopal. A constitutive equation for nonlinear solids which undergo deformation induced microstructural changes. *J. Plasticity*, 8:385–395, 1992.

[26] A.S. Wineman K.R. Rajagopal, A.R. Srinivasa. On the shear and bending of a degrading polymer beam. *J. Plasticity*, 23:1618–1636, 2007.

[27] Wildling F et al Lammer J, Hausegger K. Common bile duct obstruction due to malignancy: tratment with plastic versus metal stents. *Radiology*, 201:167–172, 1996.

[28] Peppas N Langer R. Chemical and physical structure of polymers as carries for controlled release of bioactive agents: a review. *J Macromol Sci-Rev Macromol Chem Phys*, 1983.

[29] Fiset M Mantovani D Levesque J, Dubè D. Investigation of corrosion behaviour of magnesium alloy am60b-f under pseudophysiological conditions. *Mater Sci Forum*, 426-4(521-526), 2003.

[30] Azharu H Loshakove A. Mathematical formulation for computing the performance of self expanding helical stents. *Int J Med Inform*, 44, 1997.

[31] Robert S. Schwartz MD Heleen M.M et. al. Michael Lincoff, MD. Marked inflammatory sequelae to implantation of biodegradable and nonbiodegradable polymers in porcine coronary arteries. *Circulation*, 94:1690–1697, 1996.

[32] Tipton AJ Middleton JC. Synthetic biodegradable polymers as orthopeadic devices. *Biomaterials*, 21:2335–2346, 2000.

[33] Pichard AD et al Mintz GS, Popma JJ. Arterila remodeling after coronary angioplasty: a serial intravascular ultrasound study. *Circulation*, 94:35–43, 1996.

[34] Bennet MR. In-stent stenosis: Pathology and implications for development of drug eluting stents. *Heart*, 89:218–224, 2003.

[35] Ray W. Ogden. Mechanics of rubberlike solids, 2004.

[36] Manabe T Kobayashi K Okazaky Y, Gotoh E. Comparison of metal concentrations in rat tibia tissues with various metallic implants. *Biomaterials*, 25(59):13–20, 2004.

[37] Boffetta P. Carcinogenicity of trace elements with reference to evaluations made by the international agency for research on cancer. *Scand J Work Environ Health*, 19:67–70, 1993.

[38] Therese JR Paul E, Matthias S. The road to bioabsorbable stents: reaching clinical reality. *Cardiovascular Intervent Radiol*, 29:11–16, 2006.

[39] Deloose K et al Peeters P, Verbist J. Preliminary results after application of absorbable metal stents in patients with critical limb ischemia. *J Endovasc Ther*, 12:1–5, 2005.

[40] Manegol B Pescatore P, Meier W H. A sever complication of the new self-expanding spiral nitinol biliary stent. *Endoscopy*, 29:413–415, 1997.

[41] Talja M et al Petas A. A randomized study to compare biodegradable self-reinforced polyglycolic acid spiral stents to suprapubic and indewelling catheters after visual laser ablation of the prostate. *J Urol*, 157:173–176, 1997.

[42] Langer R. New methods of drug delivery. *Science*, 1990.

[43] Hirvensalo E et al Rokkanen PU, Bostman O. Bioabsorbable fixation in orthopeadic surgery and traumatology. *Biomaterials*, 21:2607–2613, 2000.

[44] Maier W Zeiher AM Meier B Rotter M, Pfiffner D. Interventional cardiology in europe 1999. *Eur Heart J*, 24(11):64–70, 2003.

[45] Li S. and Vert M. *Degradable Polymers principles and application.* Chapman and Hall, 1995.

[46] Karppanen H et al Saris NL, Mervaala E. Magnesium-an update on physiological, clinical and analyticl aspects. *Clin Chim Acta*, 294:1–26, 2000.

[47] Polistina RA Schmitt EE. Surgical sutures. *US Pat*, 3:297, 1954.

[48] MUdra H Blasini R Schuhlen H Klauss V et al Schoming A, Kastrati A. Four-year experience with palmaz-schatz stenting in coronary angioplasty complicated by dissection with threatened or present vessel closure. *Circulation*, 90(27):16–24, 1994.

[49] Behnke I et al Schranz D, Zartner P. Bioabsorbable metal stents for percutaneous treatment of critical recoarctation of the aorta in newborn. *Catheter Cardiovasc Interv*, 67:671–673, 2006.

[50] Ong AT Serruys PW, Kutryk MJ. Coronary-artery stents. *N Eng J Med*, 354:483–495, 2006.

[51] Shalaby. J polymer sci. macromol, 1979.

[52] Chen YL Su YY Lai ST Wu GJ et al Shih CC, Lin SJ. The cytotoxicity of corrosion products of nitinol stent wire on cultured smooth muscle cells. *J Biomed Mater Res*, 52:395–403, 2000.

[53] Mirkovich V Loffre F Kappenberg L Sigwart U, Puel J. Intravascular stents to prevent occlusion and restenosis after transluminal angioplasty. *N Engl J Med*, 316(701):706, 1987.

[54] Yachia D Slepian M. Urological stents: material, mechanical and functional classification. *Isis Medical Media Ltd*, pages 3–10, 1998.

[55] Bare B. Smeltzer, S. *Brunner and Suddarth's Textbook of Medical-Surgical Nursing*. Williams, Wilkins, 2004.

[56] Joao Filipe Da Silva Soares. *Constitutive Modeling for biodegradable polymers for applications in endovascular stents*. PhD thesis, Office of Graduate Studies of Texas AeM University, 2008.

[57] S CLARK Howard G. WALKER William F STACK, Richard. Bioabsorbable stent, 1991.

[58] Pietk A Staiger M. Biomater, 2006.

[59] Hayashi T. Biodegradable polymers for biomedical uses. *Prog Polym Sci*, 19:663–702, 1994.

[60] Longer R Tamada J. Erosion mechanism of hydrolytically degradable polymes. *Proc Nat Acad Sci USA*, 1993.

[61] Koon Hou Makb Tan Lay Poha, Tjong Vinaliaa and Freddy Boeya. Collapse pressures of biodegradable stents, 2002. The Journal of Invasive Cardiology.

[62] Phillips 3rd HR Stack RS Tanguay JF, Zidar JP. Current status of biodegradable stents. *Cardiol Clin*, 12:699–713, 1994.

[63] Moreno M Moore J Timmins L, Mayer C. Mechanical modeling of stent deployed in tapered atteries. *Annals of biomedical engineering*, 36:2042–2050, 2008.

[64] Scanlon Valerie C.; Sanders Tina. Anatomia e fisiologia, 2003.

[65] A.V. Tobolsky. Structure and properties of polymers, 1965. Interscience, New York.

[66] Rokkanen P Tormala P, Pohjonen T. Bioabsorbable polymers: material technology and surgical applications. *Proc Instn Mech Engrs*, 212:101–112, 1998.

[67] L.R.G. Treloar. Physics of rubber elasticity, 2nd, 1958. Clarendon Press, Oxford.

[68] Kyo E Igaky K et al Tsuji T, Tamai H. Biodegradable polymeric stents. *Curr Interv Cardiol Rep*, 3:10–17, 2001.

[69] et al Valimaa T, Laaksovirta T L G. Viscoelastic memory and self-expansion of self-reinforced bioabsorbale stents. *Biomaterials*, 23:3575–3582, 2002.

[70] Schwartz RS et al Van Der Giessen WJ, Lincoff Am. Marked inflammatory sequelae to implantation of biodegradable and non-biodegradable polymers in porcine coronary arteries. *Circulation*, 94:1690–1697, 1996.

[71] Vinalia T et al Venkatraman S, Poh TL. Collapse pressures of biodegradable stents. *Proc Instn Mech Engrs*, 212:101–112, 1998.

[72] Sweenwy Ward I. *An introduction to The mechanical properties of solid polymers*. Second edition, 2004.

[73] Ruffieux K et al Wintermantel E, Mayer J. Biomaterial: humane toleranze and integration. *Chirurg*, 70:847–857, 1999.

[74] Meyer LA et al Witte F, Kaese V. In vivo corrosion of four magnesium alloys and the associated bone response. *Biomaterials*, 26:3557–3563, 2005.

[75] Cittadini A Wolf FI. Chemistry an biochemistry of magnesium. *Mol Aspects Med*, 24:3–9, 2003.

[76] M. Anliker Y.C. Fung, N. Perrone. Stress-strain history relations of soft tissues in simple elongation. *Biomechanics, its foundations and objectives*, pages 181–201, 1972.

[77] Singer H et al Zartner P, Cesnjevar R. First successful implantation of a biodegradable metal stent into the left pulmonary artery of a preterm baby. *Catheter Cardiovasc Interv*, 66:590–594, 2005.